THERMAL PLASMA SYNTHESIS OF BORON CARBIDE

A THESIS SUBMITTED TO
THE GRADUATE SCHOOL OF NATURAL AND APPLIED SCIENCES
OF
MIDDLE EAST TECHNICAL UNIVERSITY

BY

SERTAÇ ALTINOK

IN PARTIAL FULFILLMENT OF THE REQUIREMENTS
FOR
THE DEGREE OF MASTER OF SCIENCE
IN
METALLURGICAL AND MATERIALS ENGINEERING

AUGUST 2018

Approval of the thesis:

THERMAL PLASMA SYNTHESIS OF BORON CARBIDE

submitted by **SERTAÇ ALTINOK** in partial fulfillment of the requirements for the degree of **Master of Science in Metallurgical and Materials Engineering Department, Middle East Technical University** by,

Prof. Dr. Halil Kalıpçılar
Dean, Graduate School of **Natural and Applied Science** _____

Prof. Dr. Cemil Hakan Gür
Head of Department, **Metallurgical and Materials Engineering** _____

Prof. Dr. Tayfur Öztürk
Supervisor, **Metallurgical and Materials Eng. Dept., METU** _____

Examining Committee Members:

Prof. Dr. C. Hakan Gür
Metallurgical and Materials Engineering Dept., METU _____

Prof. Dr. Tayfur Öztürk
Metallurgical and Materials Engineering Dept., METU _____

Assist. Prof. Dr. Mert Efe
Metallurgical and Materials Engineering Dept., METU _____

Assist. Prof. Dr. Simge Çınar
Metallurgical and Materials Engineering Dept., METU _____

Assist. Prof. Dr. Caner Şimşir
Manufacturing Engineering Dept., Atılım University _____

Date: 17/08/2018

I hereby declare that all information in this document has been obtained and presented in accordance with academic rules and ethical conduct. I also declare that, as required by these rules and conduct, I have fully cited and referenced all material and results that are not original to this work.

Name, Last Name : Sertaç Altınok

Signature :

ABSTRACT

THERMAL PLASMA SYNTHESIS OF BORON CARBIDE

Altınok, Sertaç

M.Sc., Department of Metallurgical and Materials Engineering
Supervisor: Prof. Dr. A. Tayfur Öztürk

August 2018, 113 pages

Boron carbide is of interest for many applications due to unique combination of superior properties. These properties also make its production quite challenging. The net-shape boron carbide products are obtained by sintering of powders at high temperatures. So as to decrease the sintering temperature, initial particle size should be reduced to nanometer sizes. In this study, thermal plasma synthesis of boron carbide nanoparticles was investigated. For this purpose, radio frequency inductively coupled plasma system was used, operated at 25 kW. Initial experiments were carried out with boron oxide as solid precursor with methane as carbon source. This has shown that the boron carbide can be synthesized with this approach, but, the fraction in the total resulting powder was very low. To increase the conversion efficiency, a new precursor was used. This was azeotrope mixture of trimethyl borate and methanol used as both boron and carbon sources, fed into the plasma in gas phase with the use of evaporator coupled with peristaltic pump. Pure boron carbide with an average particle size of 31 nm were successfully synthesized. This powder was obtained after methanol-washing of as-synthesized nanopowder. In order to further increase the efficiency, diisopropylamine (DIPA) and nitrogen gas were used as additives. With the use of these additives the resulting powder was 70% B_4C in the form of nanoparticles with an average size 51 nm.

Keywords: Boron Carbide, Thermal Plasma Synthesis, Trimethyl Borate, Liquid Precursor, Diisopropylamine.

ÖZ

BOR KARBÜRÜN ISIL PLAZMA İLE SENTEZİ

Altınok, Sertaç

Yüksek Lisans, Metalurji ve Malzeme Mühendisliği Bölümü
Tez Yöneticisi: Prof. Dr. A. Tayfur Öztürk

Ağustos 2018, 113 sayfa

Bor karbür, sahip olduğu üstün özellikler nedeni ile birçok uygulama için cazip bir malzemedir. Bu özellikler aynı zamanda bor karbür üretimini zorlaştırmaktadır. Son ürün olarak bor karbür, tozların yüksek sıcaklıkta sinterlenmesi ile elde edilmektedir. Sinterlemenin makul sıcaklıklarda yapılması ancak parçacık boyutunun nanometre seviyesine azaltılması ile mümkün olabilmektedir. Bu çalışmada, bor karbürün nanoparçacık olarak sentezlenmesi hedeflenmiştir. Bu amaçla 25 kW gücünde endüksiyon ısıl plazma reaktörü kullanılmıştır. Başlangıçta üretim plazmaya katı parçacık olarak bor oksit ve karbon kaynağı olarak metan gazı beslemek sureti ile yapılmıştır. İşlem başarılı olmuş ancak sentezlenen bor karbür elde edilen ürünün çok az bir kısmını oluşturmuştur. Takiben başlangıç malzemesi olarak, trimetil borat-methanol eşkaynar (TMB-M) çözeltisi hem bor hem de karbon kaynağı olarak kullanılmıştır. Bir peristaltik pompa yardımı ile sıvı buharlaştırıcıya beslenmiş ve bu şekilde malzeme plazma reaktörüne gaz fazında beslenmiştir. Bu şekilde yapılan deneyde bor karbür parçacıkları ortalama 31 nm boyutuna başarı ile elde edilmiştir. Bu üretimde gene ürünün önemli bir kısmının bor oksit olduğu gözlemlenmiş ve bor oksit metanol ile yıkanmak sureti ile yapıdan uzaklaştırlmıştır. Sentezin dönüşüm verimini arttırmak amacıyla TMB-M'ye, diizopropilamin (DIPA) ve azot gazı katkı malzemesi olarak eklenmiştir. Bu ilavelerin yapılması ile ortalama 51 nm büyüklüğünde nanoparçaçıklardan oluşan %70 B_4C lık ürünün elde edilmesi mümkün olmuştur.

Anahtar Kelimeler: Bor karbür, Isıl plazma, Trimetil borat, Sıvı prekürsör, Diizopropilamin

To my beloved family

ACKNOWLEDGEMENTS

I would like to express gratitude to my supervisor Prof. Dr. Tayfur Öztürk for the guidance, enlightening comments and inspiring discussions during this thesis work. I have learned to put solution-oriented thinking at first and there is not only one way to get through any issue. I am indebted him to notice a philosophy; analyzing in deep, thinking out of the box, trying the best and getting the results.

The initial part of this work, namely synthesis of B_4C using B_2O_3 - Methane and via trimethyl borate was supported by ROKETSAN A.Ş., a part where Cavit Eyövge was equally involved as researcher in this work. Both are gratefully acknowledged.

I would like to acknowledge the assistance provided by Serkan Yılmaz for his support during TEM studies. Eda Aysal and Fatih Sıkan for their help on XRD measurements. It was a great opportunity to share the ESM laboratory with its members; I would like to extend my thanks to Doğancan Sarı, Ezgi Onur, Pelin Livan, Fatih Pişkin.

My deepest appreciation belongs to my mother Nermin Altınok, my father Nedret Altınok and my sister Seray Altınok for their support and encouragement during my thesis studies. I would like to express the greatest appreciation to my beloved wife, Ezgi Tarhan Altınok, who did her utmost to assist me both physically by preparing the graphics, and most importantly for her patience, constant moral support and encouragement. I could not complete this work without their support.

TABLE OF CONTENTS

LIST OF TABLES

LIST OF FIGURES

CHAPTER 1

INTRODUCTION

Boron carbide has shown great interest among researchers owing to its superior properties including ultra-high hardness, very low density, high chemical stability. These properties are, at the same time, disadvantageous for the synthesis both top-down and bottom-up production techniques.

The recognition of boron carbide material dates back to 1850s and the chemical formula was found in the early twentieth century. Since it has high melting point and high hardness, the production techniques have been focused on not only reactions taking place at acceptable industrial temperatures but also obtaining in powder form to be sintered to fabricate net-shaped product. Boron carbide has been commercially produced by a carbothermic reduction route in which boric acid is reduced by carbon in a furnace, mostly electric arc furnace. The industry has been adopted this method due to the fact that the raw materials are cheap and the production technique is simple. However, the synthesized boron carbide is a chunky form which necessitate crushing and grinding operations to pulverize. The alternative reduction technique of boron anhydride is achieved by magnesium and its compounds in the presence carbon. The use of magnesium makes the reduction exothermic, which provides the reaction carried out in self-propagating manner. This route produces amorphous powder suitable for the sintering process, however, the high price of magnesium inhibits the widely use of magnesiothermic reduction of boron carbide. Boron carbide is also synthesized from pure boron and carbon by reacting the pelletized their constituent elements mixture above $1500^{O}C$. This technique has been used for specialized applications since the synthesis of elemental boron is very expensive. Using vapor phase reactants is a way of boron carbide synthesis as well. The reaction

of boron halides with hydrocarbons results in ultrafine powders and whiskers of boron carbide in certain conditions. But, it is more relevant for the thin film coatings on a substrate by CVD techniques. The synthesis of polymer precursors, on the other hand, offers a low temperature reaction technique for fine size of boron carbide production by organic compounds capable of forming sol-gel by precursors for boron carbide. This route requires high production times due to many steps followed, in addition, it is a batch process with low yield product. The liquid phase precursors have been also considered with many corresponding reactions at low temperatures. The reactions are generally in a complex manner to be purified with many operation or some are remained in a lab scale, which uses elemental boron for the reactions.

Considering the shaping and forming process of ultra-hard materials, sintering of fine particles is the most appropriate route to obtain net-shaped boron carbide products. Sintering process of boron carbide occurs at high temperatures due to low diffusion characteristics with coarser starting powder size. Since the sintering process is driven by surface characteristic of powders, the solid resultant powder is achieved by very fine powders with narrow particle size distribution. For this purpose, there have been many methods and attempts to synthesize boron carbide in particle sizes lower than ultrafine scale, none of them has fulfilled the industry requirements.

In this study, synthesis of boron carbide nanoparticles by radio frequency inductively coupled thermal plasma is investigated as an alternative method with the aim of synthesizing powders having a sinterable composition (>90 wt. % B_4C) with a mean particle size less than 100 nm. In this route, precursors are introduced into thermal plasma where the temperature exceeds 10.000 K, to be fully evaporated and subsequently condense into nanoparticles by the application of quenching gas. This route is a continuous one-step production technique appropriate for the synthesis of materials having high melting point. In this work, a variety of precursors are used some were solid as B_2O_3 which was fed into the plasma together with methane as carbon source. Some were liquid as TMB-methanol with some additives which was fed into plasma either as a liquid or as a gas.

CHAPTER 2

LITERATURE REVIEW

2.1 Boron Carbide

Boron carbide was accidentally discovered as a byproduct of reaction involving metal borides in 1858, however, its formulae, B_4C, was assigned in 1934 (Ridgway 1934). Boron carbide is the hardest material ever known after diamond and boron nitride at room temperature (Domnich *et al.* 2011). It has the Knoop hardness of approximately 30 GPa (K A Schwetz and Grellner 1981). There have been many reports that prove hardness of boron carbide higher than that of diamond above 1200°C (Thévenot 1990). Boron carbide is a lightweight material with a density of 2.52 g/cm^3 with at least 300 MPa strength as measured by 4-point bending test (Thevenot 1991). It is an inert material resistant to many chemicals. Besides, it has high neutron absorption ability (Suri *et al.* 2010).

For aerospace industry the components need to be as light as possible with superior strength with acceptable toughness. Boron carbide is fulfilling these requirements as it possesses high hardness, high fracture toughness with low density. The combination of high hardness with high fracture toughness makes boron carbides is a suitable candidate as ballistic materials.

2.1.1 Structure of boron carbide

The properties of any material are the consequences of the bonding characteristics of the constituent atoms. The bonding characteristic of boron carbide is fundamentally covalent by the combination of covalent bond energy of 9.24 eV and ionic bonding energy of 1.41 eV (Pierson 1996). It is rhombohedral with a unit cell that consists of 12-atom icosahedra located at the corners and three linear atom chain placed at the longest diagonal of the unit cell. Each end atom of the chain is covalently bonded

with an atom of three different icosahedra. In order to obtain the structural information of boron carbide, many models and characterization techniques have been used, however, the exact site occupancy of the constituent atoms has not been clearly distinguished (Domnich 2011).

Boron carbide is a solid solution formed by entering carbon atoms into rhombohedral α-boron structure (Widom and Huhn 2012). While carbon is able to substitute solely two sites among the all icosahedral atomic positions due to the bonding constraints, at the same time, it can occupy interstitial and substitutional sites in the linear chains (Thévenot 1990). This leads to a wide composition from 8.8 mole % C ($B_{10.4}C$) to 20 mole %C (B_4C), as shown in Figure 2.1. As carbon content in the structure increases, the lattice parameter of boron carbide decreases, which leads to enhancing its mechanical properties (Cho 2006). Boron carbide having the highest hardness, B_4C, is in equilibrium with free carbon in higher carbon contents. Therefore, the synthesis of B_4C is challenging without free carbon which deteriorates the properties of the product.

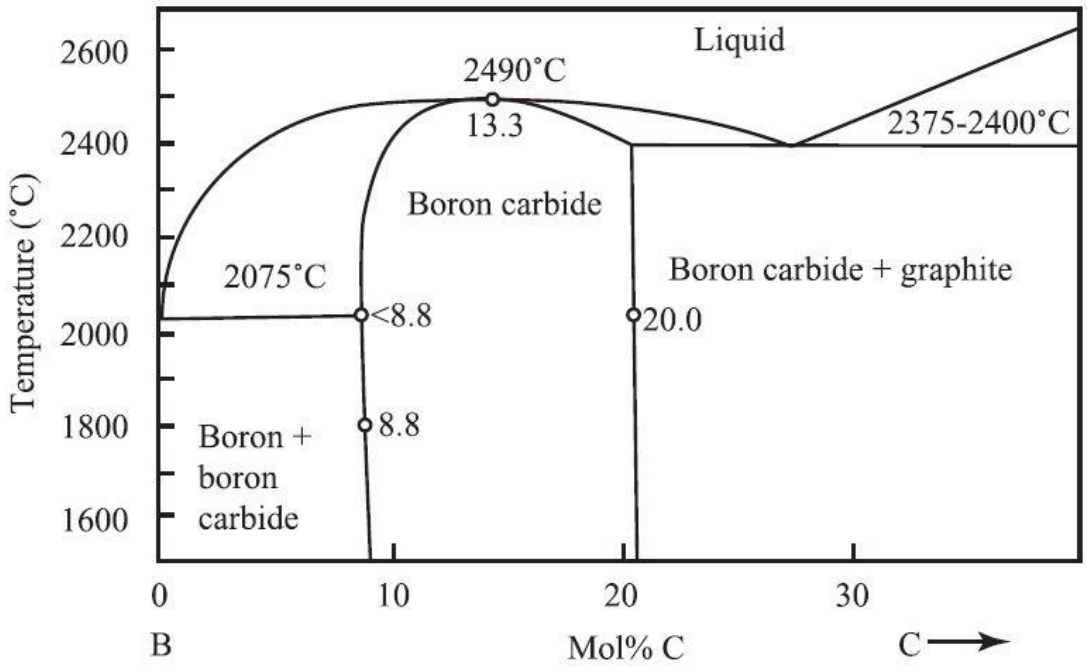

Figure 2.1 Phase diagram of boron carbide (Silver 2007)

2.1.2 Synthesis of boron carbide

2.1.2.1 Synthesis of boron carbide by carbothermic reduction

Carbothermic reduction is the most known and widely used synthesis technique that uses carbon as a reducing agent for the main reactant material under appropriate thermodynamic conditions. The main principle of this synthesis route is to reduce boric acid or boron trioxide by carbon (Spohn 1993). The overall reaction is represented as follows

$$4H_3BO_3 + 7C = B_4C + 6CO + 6H_2O \qquad \text{Eq. (2.1)}$$

The above reaction actually takes place in three steps (Spohn 1993):

$$4H_3BO_3 = 2B_2O_3 + 6H_2O$$

$$2B_2O_3 + 6CO = 4B + 6CO_2$$

$$4B + C = B_4C$$

Boric acid firstly takes out its water and become B_2O_3 during heating. At the temperature above 1400°C the reaction of boric acid with carbon monoxide is feasible to form elemental boron with byproduct of carbon dioxide (Subramanian and Suri 2004). So as to stay at acceptable reaction rate the temperature of the furnace is kept above 2000°C. The last step is the formation of boron carbide from elemental boron and carbon. The overall is highly endothermic reaction and necessitates 16800 kJ/mole (Goller *et al.* 1996).

Mainly two types of furnaces were used for reduction of boron carbide in industrial scale. These are Acheson and electric arc furnace. The use of Acheson furnace dates back to 1930's (Ridgway, R. R., and Bailey, B. L. 1936) patented the process for synthesizing boron carbide at above 90% purity. In the process, the energy is given to the system by a graphite rod around which the reactants are introduced. After the charge is heated to the point where carbon monoxide is formed, it starts to escape from the system, which contributes to heating of the charge as well. When boron

oxide is formed and melted, a glassy film is wetted onto the surface of the charge, which inhibits leaving carbon monoxide from the reaction zone. This leads to creating large CO bubbles which are burst as the pressure increases. Each burst results in throwing a small fraction of the charge out of the furnace. However, during the process boron also leaves the system as boron oxide vapors that reduce the efficiency of the synthesis. The boron carbide accumulated around the rod is collected and subject to unit operations including crushing, grinding and leaching. In the process with adhesion furnace, the synthesis is a batch process in which only small proportion of the reactants is able to be converted with considerable amount of boron oxide loss for each run.

Soon after the patent was taken for Acheson furnace, the electric arc furnace usage for the synthesis of boron carbide was patented by Schroll and Vogt (1939). The reduction process in an electric arc furnace is principally the same with that in Acheson furnace. The mixture of boron oxide and petroleum coke is firstly loaded to the arc furnace to be melted. By the application of voltage to the electrodes, the charge is heated and melted quickly. Around the electrodes, higher temperatures are obtained, leading to high loss of boron as in Acheson furnace. After cooling, the heavy block is subjected to crushing operation. The obtained powder is mixed with considerable amount of boric acid and then the process is repeated for the second time. The industrial adoption of the carbothermic reduction process has been explained by Scott (1964).

The quality of resultant boron carbide is determined by the kinetics of carbothermic reduction process which is directly dependent on type of carbon, heating rate and final core temperature of the charge and besides yield is a major concern (Alizadeh *et al.* 2004) concluded that the optimum ratio of boric acid to active carbon is 3.3 while this is 3.5 for the petroleum coke to obtain boron carbide without free carbon. Addition of sodium chloride at small amounts (1-5%) was found to enhance the yield of the process (Goller 1996).

Dacic *et al.* (2006) investigated the formation of boron carbide from boron suboxides depending on the feeding the precursors and temperature by Gibbs Energy

Minimization. The study revealed that the mole fraction of carbon and temperature directly affects the product phases. Furthermore, the study indicates the partial pressure of CO decreases, the formation of boron carbide is more feasible by enhancing the generation of B_2O_2 and BO.

Weimer and Sotiris (1976) examined the heating rates of the charge made up of 10% excess boron oxide and carbon with respect to stoichiometry of boron carbide. The charges were examined in three different heating rates. In the slow heating regime (<100K/s), boron carbide forms by the precursors via a nucleation-growth mechanism which results in large crystallites. At intermediate rates (10^3 to 10^5 K/s), the reaction occurs at the temperature between 1803K to 2123K where the boron suboxides present as gas phase with liquid boron oxide (Dacic 2006). Therefore, carbon reacts with both gaseous and liquid phases resulting in wide range of size distribution (90 to 420µm). As the temperature approaches the boiling point of boron oxide, the crystallite size becomes smaller due to high fraction of suboxides that are reacted with carbon. rapid heating rate (>10^5), results in smallest crystallite size (-45 µm).

There have been many studies that aim to obtain boron carbide in submicron size by carbothermic reduction process. Rafi-ud-din *et al.* (2014) studied on the ethylene glycol effect on synthesis of boron carbide from borate citrate by carbothermal reduction. The samples that would subject to different temperature conditions were prepared by boric acid, citric acid and different amount of ethylene glycol which had been expected to alter the thermodynamic conditions of the reduction by activating esterification reaction. The use of 0.4% mole of ethylene glycol at 1400°C for 4h reaction time of the solution resulted in promoting B_4C formation by reducing free carbon to 4 wt % C, however, the lowest obtained particle size remains 0.55 micron.

There are also studies that synthesized boron carbide materials in nanometer size. Herth *et al.* (2006) achieved to obtain mixture of both amorphous and crystalline particles with 70-260 nm in size from a precursor of boron oxide and amorphous carbon in a vacuum at 1573 – 1773 K in carbothermic methods. Ma and Bando, (2002) successfully synthesized pure boron carbide nanowires by a mixture of

elemental boron, boron oxide and carbon black. The precursor was subjected to high rate heating to 1650 where it was held for 2 h under argon atmosphere. The vapors of boron oxide and boron suboxides reacts with carbon monoxide, which lead to boron carbide nanowires. They have 50 nm in diameter and several hundreds of micrometer in lengths. Li-Hong *et al.* (2008) obtained nanowires with the diameter of 80-100 nm and length of 5-10 μm under argon atmosphere at 1100°C. Xu and Bando, (2004) formed nanoplates of boron carbide at 1950°C from boron oxide powder in a graphite crucible which was capped with boron nitride disc on top of graphitic mesh. The nanostructures accumulated on the disc with a belt-like shape with a thickness of 20-100 nm.

Carbothermic reduction has been adopted as widely used commercial technique despite the necessity of laborious mechanical unit operations of produced boron carbide ingots since the necessary equipment for the synthesis is simpler and the raw materials or precursors are acceptably cheap. The process can be offset for production boron carbide as powder form as well as nanocrystalline but these are in lab scale.

The yield of the products is very limited by the commercial method due to the evaporation of boron oxide vapors. Furthermore, they are not pure enough for use in advanced applications without performing a series of purification processes. Although it can be used for nanoscale boron carbide synthesis, the products are not in narrow size which make its processing challenging for full densification sintering that strongly influence the mechanical properties of boron carbide. The purity problem, high temperature requirement, low efficiency of process limit the use of carbothermic reduction as a synthesis method for B_4C even for the most appropriate technique for the industry.

2.1.2.2 Synthesis of boron carbide by Magnesiothermic reduction

Boron carbide can be synthesized by the reduction of boron oxide with carbon in the presence of magnesium or magnesium alloys. The overall reaction is as follows

$$2B_2O_3 + 6Mg + C = B_4C + 6MgO \qquad \text{Eq.(2.2)}$$

The above reaction takes place in two steps (Asgarian *et al.* 2014):

$$2B_2O_3 + 6Mg = 4B + 6MgO$$

$$4B + C = B_4C$$

Boron oxide firstly reacts with magnesium to form elemental boron and magnesium oxide since magnesium is more reactive than boron. Then, elemental boron and free carbon form boron carbide. The synthesis can also be done by B_2O_3 and $Na_2B_4O_7$ in the presence of carbon and magnesium at 1650-1700°C, which is explained in a patent by Gray (1958). Boron carbide synthesis via this route is highly exothermic (ΔH=−1812 kJ/mole) in nature (Suri 2010) and the adiabatic temperature of the process is 3141°C (Farzaneh *et al.* 2015). Hence, the process is regarded as self-propagating high-temperature synthesis (SHS) in which the reaction takes place intrinsically by only introducing the activation energy called as ignition.

Although the reaction is generally attained in tubular furnace at 1000-1700°C, the other processes such as mechanical alloying, combustion of carbon can also be used for ignition. When the reaction takes place above 1000°C at which the vapor pressure of magnesium is high, a cover gas such as argon, hydrogen is used and the system pressure is maintained high as well. After the synthesis, the products are washed in order to eliminate magnesium oxide, magnesium boride and unreacted magnesium from boron carbide (Suri 2010).

Muta *et al.* (1967) explained the metallic catalyst effect on the magnesiothermic reduction technique under different gas atmospheres. Boric acid, magnesium powder and carbon was mixed with a certain proportions and catalyst such as sodium sulfate was also added into it. The resultant mixture was placed into a carbon vessel and

heated under either argon, nitrogen or hydrogen atmosphere in a furnace. When the temperature is raised to 650°C-1000°C, the reaction starts and it continues intrinsically to proceed until one of the reactants run out. Khanra and Godkhindi (2005) considered the mixture boric acid, magnesium and carbon and found the ignition temperature as 670°C by thermal analysis method.

Asgarian (2014) studied the effect of different porous carbon for the synthesis of boron carbide by magnesiothermic reduction route. Starting materials; boron oxide, magnesium and carbon were mixed manually and fired at 600-650°C for 6h at heating rate of 5°C/min. The products were subsequently washed with hot water and then leached with HCl for 24 hours in order to eliminate the unreacted B_2O_3 and MgO. The synthesized B_4C with some residues depending on carbon had a particle size 24 nm.

One way of controlling the temperature of a SHS reaction is to vary the composition of the reactants. Kovalev *et al.* (2015) investigated the influence of combustion temperature with this principle. They used the additive of magnesium perchlorate ($Mg(ClO_4)_2$) to raise the reaction temperature by supplying heat to the system. In contrast, MgO was used inert additive and to reduce the reaction temperature. Five different compositions of Mg, C, B_2O_3, were prepared each composition with 200 grams. Then, they were ignited with tungsten coil under 3 atm of argon flow in graphite boat. The results indicate that the amounts synthesized and structural properties of boron carbides did vary depending on the synthesis conditions but there was no correlation between the directions of temperature rise.

Alkan *et al.* (2012) worked on the effect of initial compositions by self-propagating high-temperature synthesis followed by acid leaching. They used carbon black (surface area 27 m^2/g), magnesium powder and boron oxide powder (particle size less than 150 μm and 53 μm, respectively). The mixtures were charged into a magnesium oxide crucible by varying reactants ratio of B_2O_3:C:Mg as (1.0-2.0):(0.5-1.1):(2.5-3.5). Then, the crucible was closed after tungsten wire was placed on the mixture and the reaction was initiated by applying current under argon flow. After synthesis, the product was subject to leaching process in order to eliminate

contaminates from boron carbide. The highest amount of boron carbide (14.8 g boron carbide from 100 g reactants) was obtained from B_2O_3:C:Mg =1.0:0.8.3.0 ratio with the specific surface area of 15.56 m^2/g,

Magnesiothermic reduction of boron carbide has been also used in industry since the synthesis route only requires activation energy to be proceed, the production equipment is simpler, and the raw materials are inexpensive except magnesium. However, the formation of magnesium borides and the loss of boron carbide during elimination process of byproducts and catalyst cause the process in low yield. The synthesized boron carbides are not uniform in both size and morphology that deteriorate the quality of product. Most importantly, the high cost of magnesium gradually decreases the use of the production technique, even, it will soon the process obsolete (Suri 2010).

2.1.2.3 Synthesis of boron carbide from its elements

Boron carbide can also be synthesized from its constituents, elemental boron and elemental carbon. The standard formation of boron carbide is thermodynamically feasible at room temperature with the enthalpy of -39 kJ/mole, yet it is not sufficient to continue in a self-sustaining fashion (Weimer 1997). The formed boron carbide layer reduces the diffusion and prevents the completion of the reaction. Thus, the temperature needs to be high enough to facilitate the diffusion process to complete the synthesis with an acceptable rate. First boron and carbon are mixed to form uniform starting powder. Then, the powder is pressed into a pellet and kept under a vacuum or inert gas at a temperature above 1500°C. After synthesis, the product is subject to crushing and grinding operations to obtain boron carbide powder. The purity of product depends on the purity of reactants. Therefore high purity elemental boron is used to achieve high purity boron carbide (Nair *et al.* 1992).

Ramos *et al.* (2006) conducted a study about high-energy ball milling of powder mixtures. Two different compositional starting materials were prepared as B-10C and B-18C in terms of atomic weights. The powders were milled in a planetary Fritsch ball mill under argon atmosphere and 200 rpm with a ball-to-powder weight ratio of

10:1. Then milled powders were subject to heat treatment at 1200°C for 4h. The submicron boron carbide powder was successfully produced with several residue phases. Heian *et al.* (2004) achieved 95% pure boron carbide from amorphous boron and carbon by the combination of mechanical alloying followed by spark plasma sintering.

Kenjiro (1996) has tried to produce boron carbide from amorphous boron and graphite powder using trimethyl enetrinitramine as detonator by shock wave technique. The reactants were put into a steel container covered by plastic tube and the detonator is placed between the steel container and plastic tube. After the detonator was exploded by electric current, the reaction was started and ended in micro to milliseconds. Therefore, very high heating and cooling rates are achieved along with the high pressure formed by explosion. The samples were recovered from the container and characterized. The boron carbide was synthesized with some amount of carbon residue in 70-300 nm in size.

Although the synthesis of a compound from its fundamental constituents is generally thought to be the easy way, there are a few difficulties arisen for the diffusion limited process as in the boron carbide. Enhancing diffusion by increasing temperature, mechanical collision etc. is not enough to synthesize high-purity boron carbide with small particle size from its elements. Above all, the use of elemental boron for regular boron carbide synthesis is out of the question with a cost of 8.58 €/g (Sigma-Aldrich 2018).

2.1.2.4 Synthesis of boron carbide by Vapor Phase Reaction

There have been numerous studies regarding the synthesis of boron carbide by the gaseous raw materials containing boron and carbon. Basically, the gaseous sources for boron and carbon are provided to react each other by the help of enhancer or auxiliary gas such as H_2. Since at least one of the reactants is in gas phase, this way of synthesis technique is well suitable for the formation of boron carbide coatings on the substrate. Besides, it is possible to form powders and whiskers in submicron sizes. Boron halides, boranes and boron oxides are some of the useful boron sources,

however, BCl_3 is the extensively used owing to the abundance and low cost (Suri 2010). On the other hand, hydrocarbons and carbon tetra chloride CCl_4 are some of the appropriate carbon sources. The process is carried out in a reaction chamber, which is maintained at a desired temperature, pressure and atmosphere, that favors the reaction. In the event of using boron halides as boron source, hydrogen atmosphere is attained to react with halogen to form hydrogen chloride, bromide, iodide as a byproduct in gas phase that leaves the system. The composition and structure of the product depend on the types and flow of reactants as well as system parameters such as temperature, pressure etc.

The patent owned by Bourdeau (1967) describes the synthesis of boron carbide from boron halides and hydrocarbons . This was obtained under sub-atmospheric pressure between 0.1 mm to 200 mm of mercury by flow rate that vary 0.1 to 10 liter per minute in the temperature range of 1500°C to 2500°C. As for the boron carbide whiskers, Clifton (1970) presents the process in which hydrocarbon gas and solid boron oxide are heated to the temperature range of 700°C to 1600°C at atmospheric pressure in a graphite or other low reactivity container. At suggested temperature ranges, boron oxide exerts considerable vapor pressure that reacts with hydrocarbon by gas to gas interactions to form whiskers on the graphite, mullite and alumina substrates in the heating zone. The whiskers are produced in 0.05 to 0.25 micron with the 25000:1 L/D ratio. Ditter *et al.* (1977), on the other hand, patented the production of amorphous boron carbide from acetylene with diborane. The optimum ratio is suggested as 4 parts of acetylene and 1 part of diborane that makes the amorphous boron carbide with particle size less than 1 micron in diameter with surface area of 100 m^2/gr.

The most known and used technique for vapor phase reaction is chemical vapor deposition (CVD) technique. A substrate is placed in temperature and pressure controlled chamber into which gases are supplied. Depending on the surface conditions of the substrate; thin film, nanotubes and whiskers can be formed by the reaction of gases and the substrate. This process mainly depends on kinetics of the surface as well as the diffusion of gases. Therefore, one should consider the process

parameters in order to obtain the targeted stoichiometric ratio and properties of the products. For the boron carbide deposition, graphite single crystal silicon, carbon fiber and boron have been used as substrate materials in the temperature range of 450°C to 1450°C in vacuum (Suri 2010). Substrate temperature is an important parameter for the process and final product quality. The adhesion onto the substrate is better at low temperatures, however, the deposition rate is faster at high temperatures due to the increase in the kinetics of the reaction. Therefore, the optimization is necessary for a good adhesion of thin film on substrate with sufficient deposition rate.

Zeng *et al.* (2009) deposited amorphous boron carbide coatings on SiC substrate by CVD from the mixture of methane, boron chloride with hydrogen gas under 10 kPa argon atmosphere at temperature in the range of 900°C and 1050°C. Jazirehpour and Alizadeh (2009) obtained boron carbide nanotubes on graphite substrate at 1400°C by CVD with the mixture of boron oxide, activated carbon and sodium chloride as precursors. Shu-Fang *et al.* (2009) successfully grew boron carbide nanorods by CVD techniques using o-carborane ($C_2H_{12}B_{10}$) as precursor and ferrocene ($C_{10}H_{10}Fe$) as catalyst to favor the nanorod formation on substrate. Schouler *et al.* (1997) synthesized BC_x ($x \geq 3$) phase that shows whisker-like morphology on quartz substrate from the precursor of BCl_3 and B_6H_6 in the presence of H_2 and nickel at 1000°C. Karaman *et al.* (2006) investigated the kinetics of boron carbide formation on tungsten substrate from BCl_3-CH_4-H_2 gas mixture in CVD process. They proposed that boron makes two different products, B_4C and $BHCl_2$ between 1000°C and 1400°C and concluded that the reaction rate of boron carbide formation is lower than that of dichloroborane formation during the process.

2.1.2.5 Synthesis of boron carbide from polymer precursors

One of the challenges for the formation of boron carbide is the necessity of high temperature due to kinetic reasons as mentioned in previous sections. The polymer precursor route offers relatively low temperature boron carbide synthesis. The selection of the starting polymers determines the formation of boron carbide as well as the synthesis temperatures. Mondal and Banthia (2005) stated this route has the

advantage low temperature and easily forming of the product into a desired shape. The process has several steps. Starting materials for boron and polymer carbon sources are mixed in a gelation agent to form a solution. The mixture is heated to the temperature at which solution stabilization occurs. After obtaining gelation, the temperature is further increased where the boron carbide formation is thermodynamically feasible (Najafi *et al.* 2012).

A patent by Harris and Parsons (1975) describes a process to obtain fine boron carbide powders from boric acid and glycerol. The precursors are first dissolved in ethylene glycol to form sol-gel. Then, it is dried at 180°C and heated to 700°C in hydrogen atmosphere. After the product is subjected to grinding and then maintained at 1700°C for 7 hours, the fine boron carbide powders are synthesized. Mondal (2005) synthesized crystalline boron carbide at 400-800°C from a pre-synthesized polymer obtained by the reaction of boric acid and polyvinyl alcohol. But there were some residue of boron oxide in the product A research conducted by Sinha *et al.* (2002) indicates the boron carbide formation with 11.1% free carbon from the boric acid and citric acid as starting materials after a stable gel is formed from aqueous solution of the precursors and subsequently allowed to hold 1450°C under vacuum. Cihangir *et al.* (2009) worked on a method in which sulphuric acid dehydration of sugar to synthesize a polymeric precursor material that yielded crystalline boron carbide and B_4C/SiC composites at the temperatures between 1400°C and 1600°C.

2.1.2.6 Synthesis of boron carbide by liquid phase reaction

There are numerous researches aiming to synthesize boron carbide by liquid precursors. This method also known as solvothermal process or coreduction method, promotes boron carbide formation at much lower temperatures when compared to conventional ones (Suri 2010). Shi *et al.* (2003) worked on the formation of very fine boron carbide powders from boron tribromide and carbon tetrachloride as liquid precursors in the presence of sodium as reducing agent in autoclave at 450°C. Boron carbide crystals were obtained composed of uniformly distributed 80 nm average spherical particles together with 200 nm diameter rod-like particles. Gu *et al.* (2005) synthesized in an autoclave at 600°C boron carbide crystals that have particle sizes in

15-40 nm diameters by solvothermal reaction of CCl_4 with amorphous boron in the presence of lithium as reducing agent. Singh *et al.* (2014) have synthesized boron carbide nanoparticles by solvothermal synthesis. Starting materials were H_3BO_3, activated magnesium and acetone in predefined amounts in autoclave. The products were subjected to an acid treatment to remove unreacted Mg and subsequently washed by water and ethanol. The boron carbide particles had an average particle size 15 nm. The yield, however, was very low to apply this method in industrial application.

2.1.3 Sintering of boron carbide

The heat treatment process to obtain coherent and dense body by bonding powders chemically is known as sintering, which is preferred for processing of ceramics due to the challenges of high melting temperatures, refractoriness and brittleness.

In order to achieve the high mechanical properties of boron carbide densification is a crucial factor. The mechanisms in which the atomic diffusion results in a net flux of atoms from disordered to ordered area will decrease the vacancies in the grains and cause shrinkage. This occurs by adhering of individual particles to the neighbors chemically, which results in the densification and in the improvement of the properties.

The other mechanisms which favors an increase of the average particle size without a net decrease in the vacancies are the main cause of coarsening. The particles coarsen by growing of the large particles at the expense of the smaller ones. In fact, the atoms are rearranged to form negative curvature that leads to both the pores and grains get larger with time.

The sintering of boron carbide has been extensively studied. These studies indicate that densification of boron carbide is difficult due to strong covalent bonding and low plasticity. The strong covalent bonding gives a superior hardness to boron carbide however, it also causes the low self-diffusion of atoms which restricts the sintering process. Prior to sintering process, green density is also important to make higher contact and good arrangements between particles. The low plasticity of boron

carbide makes the green density at higher percentages challenging as well. As a result, high temperature is necessary to enhance the diffusion and so for the densification of boron carbide.

The major limiting condition is the formation of a thin boron oxide layer on boron carbide particles even with very low oxygen levels (Dole *et al.* 1989). Boron carbide and the surrounding oxide layer gives reaction to form a gaseous B_2O_2 and CO (Sigl 1998). The process leads to a mass transport in gas phase of boron, carbon and oxygen and hence permits the rearrangement of boron carbide which favors coarsening process. The other possibility is the vaporization of already formed boron oxide above 1850^{O}C and non-stoichiometric boron carbide (above 2150^{O}C). The vapor transport results in enhanced coarsening as well as leaving carbon behind at the grain boundaries (Suri 2010).

Dole (1989) showed that pure boron carbide was highly coarsened at 2000^{O}C and the considerable pore and grain growths were observed at temperatures below 1750^{O}C where the formation and mass transportation of boron oxide occurs. They explained the process by considering the evolution of starting structure in which there are uniformly interconnected particles and pores. Normally, the necking is formed between two particles and the atoms diffused towards the pore sides during heating of the sample for sintering. In pure boron carbide, the formation of boron oxide prior to necking and its mass transport even one atomic distances results in creation of larger particles having negative curvature. Due to the increased mass transport rate in higher temperatures, the particles are able to diffuse higher than average particle size towards negative curvature leading to the formation of both large polycrystalline grains and large porosities. The pores become stable as the ratio of pores to grain sizes is attained with dihedral angle of 60-120^{O}C depending on heating rate which controls the consolidation mechanism. Dole and Prochazka (1985) found that the compacts subjected to fast firing process, i.e. heated to 2500^{O}C, achieved higher density with lower coarsening than the compacts heated to 30^{O}C/min to the same temperature. The important finding was that the coarsening dominancy below 1900^{O}C is due to the boron oxide layer rather than boron carbide itself.

The pressureless sintering is a simple, economic process that can be used for complex shapes. The process occurs in two steps. Powders are firstly compressed by uniaxial die to obtain green pellets with sufficient handling strengths as well as higher densities as possible. Then, the green body are subjected to firing process at high temperature under controlled atmosphere. However, low plasticity and high strength of boron carbide resists the deformation, fracture and fragmentation during compaction, which inhibits to attain high green densities. In addition to this, the formation and diffusion of boron oxide favors the coarsening process, which is the dominant factor to increase the pore size. The sintering of boron carbide is consequently difficult to achieve near theoretical densities at temperatures below 2300^{O}C.

There has been a number of studies to suppress the boron oxide layer formation on boron carbide by some additives. Carbon was a common additive in the form of phenolic resin, carbon black and graphite. For the solid carbon additives, the powders have to be used in very fine size with exhaustively mixing to separate uniformly through the structure. Liquid carbon additives such as phenolic resin have given better results due to uniformly covered the surface of the grains and also acting as binder during green compaction (Yin and Wang 2003).

$$2B_2O_3(s) + 7C(s) = B_4C(s) + 6CO(g) \qquad \text{Eq.(2.3)}$$

Boron oxide layer is subjected to carbothermic reduction without the presence of humidity, Eq.(2.3). The reaction is favorable above 1300^{O}C according to Gibbs Energy calculation (Evans 2014). The research conducted by Lee and Speyer (2010) showed that the sintering of the sample with the addition of carbon initiated at 1350^{O}C and the changes in the dimension of the particle were uniform until 2070^{O}C. Thus, the inhibition of densification which peaks just after the boiling point of B_2O_3 to 2000^{O}C was prevented.

Sintering of boron carbide has been generally accomplished by hot pressing to obtain high density product. In this process, the powder compact is heated by typically graphite heating elements and compressed by a ram. Depending on the temperature

of the compact from 1800^{O}C to 2200^{O}C, the following mechanisms occur in hot pressing; particle rearrangements by decreasing the open porosities, plastic flow leading to closing of open porosities and the volume diffusion to elimination of closed pores. There are a few researches that shows the reaching of high densities without taking any measure against boron oxide layer with this method. Jianxin (2005) showed that 95.5% theoretical density was obtained by boron carbide powders smaller than 3 μm in size at 2150^{O}C under inert atmosphere with 36 MPa. Yin and Wang (2004) reported the theoretical density of 91.6% and %99.7 were obtained under 2150^{O}C for 10 min with the starting powders of 3.85 and 0.35 μm, respectively. The almost full densification of boron carbide under hot-pressing has been succeeded with the micrometer range particle sizes, however, hot-pressing is limited to simple shapes and suitable for the applications where the grain growth is not an issue as in the case of nuclear industry.

Hot isostatic pressing (HIP) is the combination of elevated temperature and the application of high pressure onto all surfaces of the sample to obtain near theoretical densities. The parts are placed into a vessel which is pressurized and heating simultaneously. The application of pressure is typically between 100-300 MPa, ten times higher than the hot pressing process. This accomplishes the sintering to take place at much lower temperatures rather than traditional sintering (Larker 1983). The system of HIP is mainly composed of a graphite die is assembled between the press rams around which the furnace is placed. The equipment has to be designed for both high temperature and high pressure which limits its size and the number of compacts at a time. For increasing the rate of the fabrication multi cavities are used to get many products in each press.

Larsson *et al.* (2000) revealed boron carbide with the addition of boron under 160 MPa pressure at 1850^{O}C for 1 hour led to decreasing the pores and graphite inclusions as well as particle erosion resistance. Schwetz *et al.* (1997) achieved the full densification of boron carbide with very fine grained of 4 wt.% carbon black doped by pressureless sintering at 2175^{O}C and subsequently subjected to post-HIP under 200 MPa argon atmosphere. This method has been used to fabricate personal armor to obtain near theoretical densely body.

HIP which is the most convenient method of sintering for boron carbide require long processing time and high temperature to obtain near full densified parts. Since the shaping process of boron carbide challenging, near net shape production is desirable. A process has been patented by Yoo *et al.* (1999) patented a process with the apparatus for rapid consolidation of ceramic bodies near net shape, known as spark plasma sintering. In this route, the powders are placed in a graphite die with punch assembly and the direct current passed through the sample simultaneously with the application of high pressure. the optical pyrometer can be used to indirectly measure the temperature of the graphite die which contacts with the sample.

Applying high voltage causes fast heating rate. This leads to localized heating and plastic deformation at contacts between particles, which results in high densification at lower temperatures in less than a few minutes. Since the dwell time is very short, the material maintains its finer microstructure without grain growth. As the size of the starting powders becomes less, the resultant microstructure is fine grained. Sairam *et al.* (2014) consolidated of 2.4 µm boron carbide powders under 50 MPa pressure at 1800^{O}C for 15 min. The compact had 94.4% theoretical density and 37.2 GPa hardness. They indicated that the fracture toughness of the 91% theoretical density sample showed 5.8 MPa.m$^{1/2}$, higher than that of near theoretical density powder, 2.8 MPa.m$^{1/2}$.

Ghosh *et al.* (2007) densified the submicrometer sized boron carbide to 96 and 99.2% of the theoretical density under 88 MPa at 1750^{O}C in 2 and 5 minutes, respectively. The compacts had a nearly equiaxed grains with 1.6µm and sizes with hardness and fracture toughness values of 25-41 MPa to 27-45 GPa and 3.22 to 3.61 MPa.m$^{1/2}$ respectively.

The full densification of boron carbide in simple shapes has been successfully achieved by HIP under high temperature in long times which deteriorates its ultimate mechanical properties due to enhancing the grain growth mechanism. For the complex shape products, the situation is even worse since the densification to near theoretical values has not been achieved at high temperatures for industry scale. Spark plasma sintering can be the most promising technique, in which the process is

done in relatively low temperatures in short time. The mechanical properties especially hardness of boron carbide depends on starting powder size as well as its uniform distribution. Prior to sintering process, as the starting particle size decreases, the pores between the particles are easier to be filled. Thus, the densification closer to theoretical values is expected to be obtained.

Sintering is driven by the force created by surface characteristic of a material and carried out by diffusion kinetics based on process parameters. The driving force of the process is thermodynamically dependent on surface energy of particles and curvature, given in Eq. (2.4) (Fang *et al.* 2017).

$$\sigma = \gamma * \kappa = \gamma * \left(\frac{1}{R_1} + \frac{1}{R_2}\right) \qquad \text{Eq.(2.4)}$$

Where γ is surface energy, κ is curvature, and R_1 and R_2 are the principle radii of a particle curvature. Depending on the equation, driving force is calculated as two order of magnitudes higher for 10 nm with respect to 1000 nm particles. The surface energy also increases as the particle size decreases (Campbell *et al.* 2002). Thus, the favorability of sintering is significantly enhanced by size reduction.

The particle size makes an impact on lowering the sintering temperature in nanometer size since the material behaves differently under the influence of grain boundary area which becomes comparable to grain a. The atoms placed at surface and high angle grain boundaries are high chemical energies due to missing bonds, which leads to undergo a reaction more favorably (Verhoeven 1975). Thus, the melting temperature of the materials decreases and so the sintering temperature which can be expressed as scaling law in Eq. (2.5).

$$n\ln\left(\frac{d_1}{d_2}\right) = \frac{Q}{R}\left(\frac{1}{T_2} - \frac{1}{T_1}\right) \qquad \text{Eq.(2.5)}$$

Where d_1 and d_2 are particle sizes, T_1 and T_2 are corresponding sintering temperatures, Q is the activation energy for sintering, and n is a constant determined by active sintering mechanism (Fang and Wang 2008). The equation depicts that

sintering temperature reduces as long as the particle size of starting powder decreases.

Mobility is the other phenomena that provides a process taking place. (Pan 2004) indicated the relation of non-linear diffusion flux as a function of the driving force,

$$J = \frac{D}{kT\Omega} * F \qquad \text{Eq.(2.6)}$$

Where D is a diffusion constant, Ω is atomic volume, k is the Boltzman constant, T is absolute temperature, and F is the driving force. For using small initial particle size at the same temperature, the diffusion flux is also higher for the process due to high driving force. (Pan 2004) revealed the neck size-to-radius ratio of 5nm particle remarkably increases than that for the 1 μm particle with sintering time by considering non-linear diffusion law. However, there are several diffusion mechanisms that plays roles for sintering of nanoparticles. (Shi *et al.* 2005) showed large particles grows in extent to the small one during the initial sintering of $BaTiO_3$ particles, which is a coarsening of particles resulted from surface diffusion.

The fact that the starting materials are used in nanometer size provides high driving force that leads to decrease the sintering temperature. In order to obtain ultimate strength of boron carbide by maximizing the grain size strengthening, the grain size of the sintered product should be in nanometer size as well. This is only achieved by suppressing the grain growth during sintering. There are two stages that contributes to grain growth as for the micron sized particles (Wang *et al.* 2011).

Slow grain growth occurs when relative density below 90% and followed by exponential grain growth above 90% of theoretical density. The majority of grain enlargement takes place at the last stage of sintering where curvature is the sole driving force. This stage significantly depends on the sintering temperature that leads to favor grain boundary migration. (Chen and Wang 2000) recommended two-step sintering that may be used to minimize the grain growth migration. The compact was firstly heated to high temperature called T_1 then subsequently cooled to T_2 and held for a period of time before grain enlargements start. The study resulted in preventing

grain growth while continuing the densification. The grain growth is also observed slowly during whole sintering process. After the initial neck formation between particles and the neck becomes stable, large particles grows by consuming the smaller ones owing to the curvature effect which results in coarsening (Kumar *et al.* 2010). So as to prevent the enlargement of particle size during sintering, the curvature effect must be minimized, which means that the use of narrow particle distribution plays an important role.

The synthesis of nanoparticles in narrow particle distribution is necessary to both reduce the sintering temperature and obtain near-shaped product with ultimate mechanical properties by nanograin size effect.

2.2 Thermal Plasma Synthesis of Nanoparticles

2.2.1 Introduction

Plasma is a macroscopically neutral state of matter in which there is a strong columbic interaction between free electrons, positive and negative ions formed by a fully or partially ionized gas. Practically, all plasmas are partially ionized and the ionization degree, the proportion of ions to total atoms, is closely related to the temperature of the electron within the plasma. In order to ionize the gases, the energy is required to eject an electron at least outermost shell of the atom. External heating, combustion, nuclear fusion, application of electric and magnetic fields can be used for this purpose. Besides of well-known examples in nature such as the sun, stars, lightning etc., there are immense man-made products fundamentally based on plasma technology. The fluorescent lightbulbs, plasma display televisions, computers, arc welding are typical examples of artificial plasma. In plasma processing of materials, the required energy to generate and sustain the plasma is supplied by direct current (DC), alternating current (AC) or magnetic field.

Plasmas are divided into two categories; high-temperature (hot) and low-temperature (cold) when considering the temperature of species. Hot plasmas are found typically in nuclear fusion devices at which the temperatures are at least on the order of ten million Kelvin, which is comparable to that of stellar interiors. Such temperatures are

attained by only that all atoms are ionized. Cold plasma, on the other hand, have a maximum temperature of hundred thousand Kelvin or less since a large proportion of the species in the plasma maintains its neutral state which corresponds to low ionization degree. This type of plasma is achieved by ionizing the neutral gas using DC or AC electric current passing through the gas or radio-frequency (RF) or microwave electromagnetic field. Almost all of material processing including nanomaterials by plasma technology carried out with cold plasmas since the generation and control of the plasma as well as the processes are much better than hot plasmas (Ostrikov and Murphy 2007).

Cold plasmas are further subdivided into thermal equilibrium (thermal plasmas) and out of thermal equilibrium (non-thermal plasmas) by the temperature relation between light electrons and heavy species (ions and neutrals). In thermal plasmas, the temperature of electrons (T_e) is almost the same with that of heavy particles (T_h) due to the frequent enough collisions leading to the same average kinetic energy of all species. The necessity of high amount of collisions is achieved at least 10 kPa pressure high temperatures with 10^{21}-10^{26} m^{-3} electron density (Henne 1999). The typical temperature of thermal plasma is $T_e \approx T_h \approx$ 1-2 eV (≈10000 -20000 K), which is high enough to transform the phase change of materials even evaporation of solid materials depending on residence time at the plasma. The ionization degree of thermal plasma is so high at the center that it is regarded as fully ionized in many cases and lowers as approaching to edges (Ostrikov 2007).

In non-thermal plasmas, the temperatures of heavy particles are much lower than those of electrons, which results in deviations from thermal equilibrium. Application of energy to initiate plasma accelerate electrons higher than heavy particles, and thus have higher energies. The low pressures below 10 kPa are enough to obtain this type of plasmas (Lang *et al.* 2015), in which $T_h \approx$ 0.025 eV while $T_e \approx$ 1-2 eV at room temperatures with the ionization degree is generally lower in the range of 10^{-5}-10^{-2}. The use of non-thermal plasma is well suitable for solid-state applications and

processing of low melting point materials since the heavy atoms are cold, leading to limited enthalpy for the processes (Ostrikov 2007).

The energy and temperature requirement of an application determines which type of cold plasma is used. Thermal plasmas are suitable for the high temperature applications such as spraying, welding, synthesis of nanomaterials, disposal of toxic wastes. The non-thermal plasma is used in the processes which does not require high energy and temperature such as surface treatments such as sputtering, etching etc. (Bapat *et al.* 2007).

Thermal plasma processing is one of the most appropriate technique to synthesize ultra-fine particles since the temperature of the plum varies between 3000 to 25000 K depending on the use of torch type (Henne 1999). There are commonly three types of thermal plasma torches used at atmospheric pressure, which are DC transferred arc, DC non-transferred arc and RF inductively coupled plasma (RF-ICP), Figure 2.2 (Seo and Hong 2012).

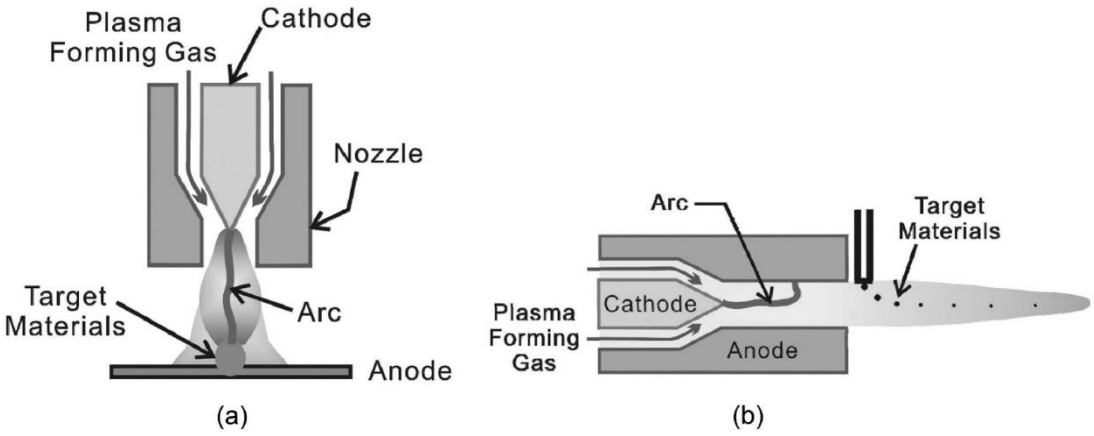

Figure 2.2 Schematic diagrams of thermal plasma torches used for nanopowder synthesis (a) DC Transferred arc, (b) DC non-transferred arc torches (Seo 2012)

DC thermal plasma torches have been widely used as heating source due to their simplicity, versatility and cost effectiveness. An arc is fundamentally generated between the electrodes by the application of voltage, which create a hot ionized gas plume. During the processes the cathode electrode is steadily consumed, and thus the resultant powders or coatings are contaminated by this erosion. Depending on the

relation of arc generation with target materials, DC arc torches are considered in two types, transferred and non-transferred.

In arc transferred DC torches, the arc is formed between the target bulk material as an anode and a cathode placed in the torch, as shown in Figure 2.2(a). Since the target materials involves the plasma formation, the transferred arc results in consuming the electrode materials which needs to be replaced after each batch of process. This type of plasma torch is generally used for heating and processing of bulk materials which do not readily vaporize. The common examples are welding, plasma-cutting, refining and surface treatment (Venkatramani 2002). Also, it is possible to use for the synthesis of 60 nm in size of nanopowders by evaporating target material and then subsequently condensing by transferred arc discharges (Stein *et al.* 1991). However, it is worth to mention that the properties of the target materials are important for the rate of the nanopowder (Ohno and Uda 1984; Uda. *et al.* 1983).

In non-transferred torches, the arc is generated and maintained when plasma gases are fed to complete the circuit between the nozzle as an anode and the cathode, indicated in Figure 2.2(b). The ionized plasma gases emerge from the torch as a hot and high velocity jet. The temperature of plasma jet is typically between 8000-14000 K with torch power 20-80 kW at the nozzle exit where the powder target materials are continuously injected at a flow rate of 3-6 kg/h (Fauchais *et al.* 2014). The precursors interacting with plasma jet directed onto a substrate as in the plasma spray coatings which is widely used application of the non-transferred torches. A research conducted by Mauer *et al.* (2011) indicates that the evaporation of YSZ precursor fed at the exit of the plasma spraying torch operated even 60 kW cannot be fully achieved since the mean temperature of the trajectories were $2400^{O}C$ while the melting temperature of YSZ is $2710^{O}C$. However, there are effective torch designs considering different injection zones which allows the precursors to absorb higher energies (Hales *et al.* 2016).

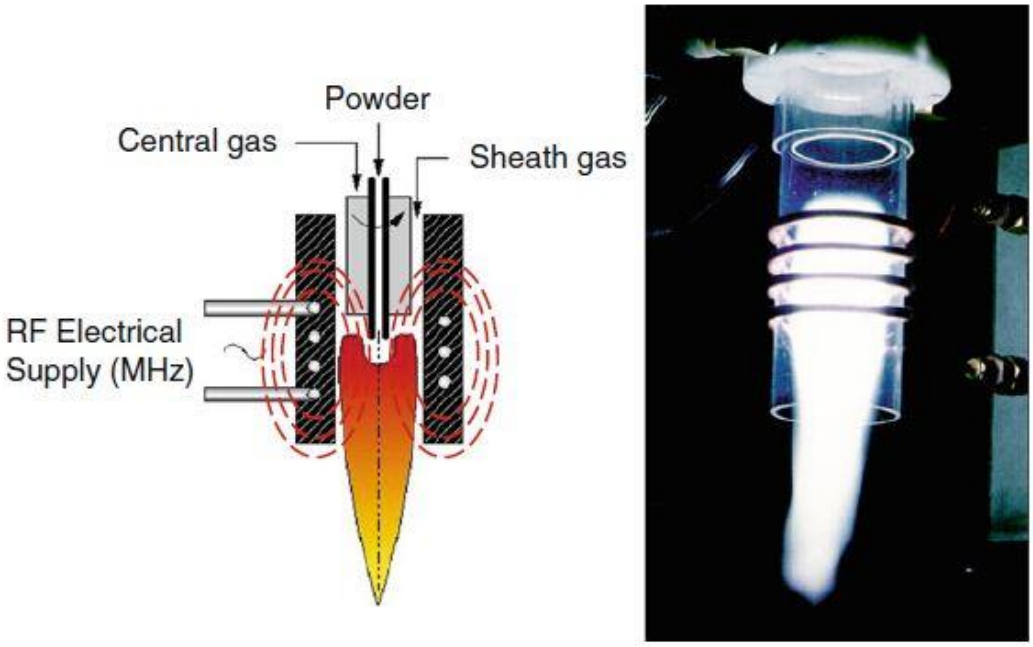

Figure 2.3 (a) Schematic drawing of a RF-ICP torch (red lines represent magnetic fields) (b) a photograph of quartz wall RF-ICP torch (Boulos 2017)

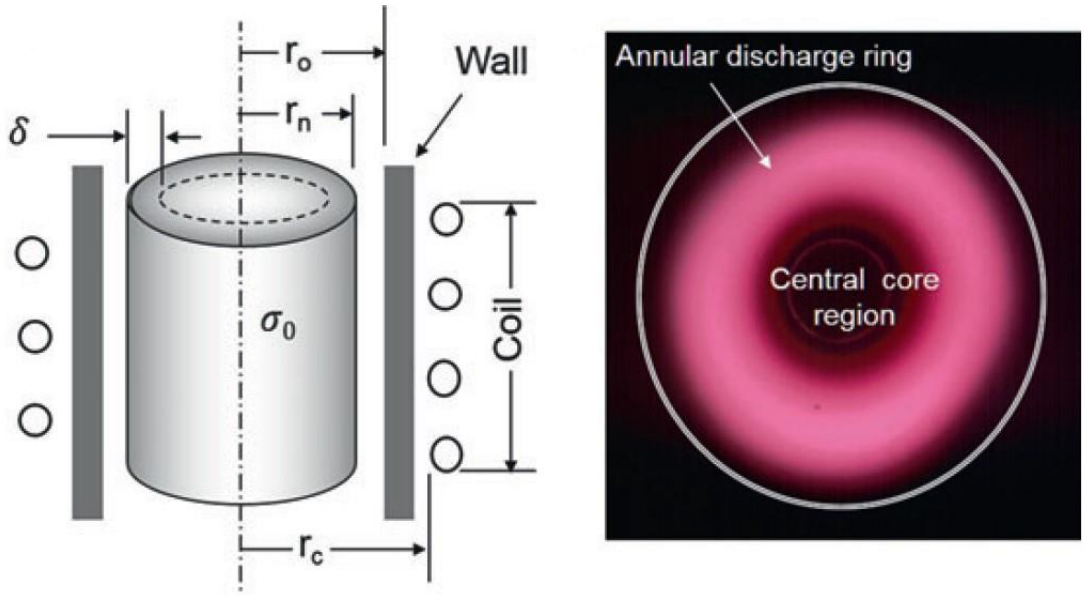

Figure 2.4 (a) Schematic of (b) Photograph of the plasma region image (Boulos 2017)

In RF-ICP torches, plasma is not generated using electrodes, which causes contamination in the resultant powder. Rather it is generated by the interaction between plasma gases and applied electromagnetic field through induction coils (Figure 2.3). The alternating current produces high frequency oscillating magnetic field around the coil where plasma gases pass through. When the frequency of magnetic field is high enough to oscillate the atoms, the electrons are emitted and flow perpendicular to the magnetic field. The generated electric current by ionized gases flows in the opposite direction of the current in the coil. Thus, the magnetic field at the center of the torch is suppressed, which results in the confinement of plasma at an annular discharge ring between the center and the inner wall of the cavity as seen in Figure 2.4(b) (Boulos *et al.* 2017).

The thickness of the region is known as skin depth (Figure 2.4(a), which can be determined by Eq. 2.7 based on the parameters μ_0 is the magnetic permeability of the medium equal to $4\pi \times 10^{-7}$ (V s/A m), σ_0 is 1000 A/V for a pure with the temperature of 8000 K at atmospheric temperature, the skin depth is 9 mm with 3 MHz of oscillatory frequency (Jiayin *et al.* 2010).

$$\delta_t = \left(\frac{1}{\pi * \mu_0 * \sigma_0 * f}\right)^{\frac{1}{2}} \qquad Eq.(2.7)$$

The frequencies of power supply required to attain effective energy dissipation from the region depends on the plasma compositions but it is typically around MHz range. For the induction heating of metals, kHz range is enough for the induction heating of the metals since their electrical conductivities are significantly higher than those of gases (Fauchais 2014). For an effective energy supply in the plasma region, the skin depth is estimated approximately 10 mm for MHz range.

In order to form a plasma by RF-ICP torch, there is a definite power, which is determined by the equilibrium condition between energy dissipation through ionized gas interactions and the energy losses from the discharge to surroundings by conduction, convection and radiation. The minimum required power to form stable plasma is substantially reduced with increasing the frequency and decreasing the

pressure. The use of plasma gases from monatomic to a molecular gas leads to higher necessity of applied power to sustain stable discharge (Poole *et al.* 1973).

The materials used to construct RF-ICP torches are those that have high melting point and transparent to RF radiation. Depending on the operating maximum temperature of plasma, these materials can be ceramic materials as well as quartz (Figure 2.3(b)). RF-ICP thermal plasma torches have been developed with several designs among which the double flux are widely used (Boulos 2017). In principle, the plasma gases are sent into the torch at different locations separated by an inner tube, as shown in Figure 2.3(a). The plasma forming gas, central gas, is introduced through the inner quartz tube while the sheath gas is fed into the torch through the annulus between inner and confinement tube. This design allows to use different gas compositions for each but most importantly, to protect the confinement tube against the excessive heat at the plasma region. At low pressures and applied power air cooling of the confinement tube with sheath gas is sufficient for maintaining the torch at non-damaging temperatures, however, the liquid cooling is necessary for the protection at higher power levels.

The plasma power is the exact value of the multiplication of measured current and voltage in DC torches, while, the applied power in RF torches is delivered into the discharges by a certain fraction that depends on the coupling efficiency. This is directly related to the ratio of the radius of discharge (r_n) to that of induction coil (r_c), Figure 2.4(a). The ratio is geometrically limited by the protection cooling of sheath gas and therefore, the plasma torches are generally operated below 50 kW power. As the plate power exceeds beyond 50 kW, the diameter of confinement tube is required to be larger, which enhances the coupling efficiency. Also, the lower levels of frequencies can be used, which increases skin depth, for the torches designed to be operable at higher power levels. Thus, they provide to distribute high temperature plasma region to a larger extent along with the torch, which offers higher enthalpy for the process.

Argon is generally used as both central gas and sheath gas. It is introduced through the inner tube of which the tip is positioned at the same level of the first coil. The

torch is maintained at low pressure and the plate power is applied to the coils and gradually increased. At the beginning, a capacitively coupled low density E-discharge formed by electrostatic field generated by the coils. Once the minimum sustaining power is achieved, there is a drastic increase in the plasma density which leads to the ignition of the stable inductively coupled discharge. Then, the torch pressure is being gradually increased, which needs to increase in the applied power in order to maintain the plasma. Since at higher torch pressures the density of plasma is further increases, resulting in high temperature distributions inside the torch, the addition of hydrogen is required into the sheath gas to improve the protection of the confinement tube.

Since RF-ICP torches are electrodeless and offer high energy density, high purity plasma environment in a large volume, they are used in many applications including plasma deposition of coatings, powder purification and spheroidization, melting and atomization of high-purity materials, synthesis of nanopowders etc.

For the synthesis of nanopowders, precursors are sent into the plasma region together with carrier gas by means of axially located probes such as injection, atomization probes. At the high temperature of plasma region, precursors are melted, evaporated and even dissociated into elements depending on how much enthalpy is absorbed. Once evaporated or dissociated precursors reach at the end of the plasma, they are faced with high temperature decrease, which leads to condensation as ultrafine particles.

2.2.2 Process Parameters in RF-ICP Thermal Plasma

Bernardi *et al.* (2003) evaluated the effect of coil and torch geometries on the temperature distribution of pure argon plasma at atmospheric pressure. They focused on conventional helicoidal, planar, double stage coil configurations and elliptical torch geometry by simulating the plasma operated at 5 kW with 3 MHz frequency except for double-stage and 5-turn helicoidal that were carried out with 25 kW. The conventional 2.5 coil turn torch design shows a considerable displacement from the center of the plasma to the confinement tube wall due to non-axisymmetry of the

coil. The double stage coil geometry leads to the axial extent of discharge volume and the RF power is distributed from the upper part. In planar configuration the temperature distribution is axially symmetrical, but it needs to higher radius of confinement tube. In elliptical torch design the non-axisymmetry dissipation of temperature is observed along minor axis. The 5-turn helicoidal is the same with conventional torch except the center of the probe has different distribution.

Park and Hong (1997) investigated the parameters of torch geometries by considering axial distance of coils, torch radii, number of coils under constant power and coil frequency.. In the study, as the distance between coils are increased for 3-turn helicoidal geometry, the high temperature is preserved for prolonged axial distances. For the radii of the torch, the discharge is confined close to the inner wall of confinement tube with lower skin depth as the torch radius is increased. But, the high temperature volume is enhanced throughout the reactor. The increase in the coil turn alters the streamlines in the torch, which directly influence the temperature distribution.

Castillo and Munz (2007) simulated the effect of plate power of RF-ICPs on temperature distribution along the reactor. In this study, it was found that as the plate power increases, the temperature at the torch becomes higher and the temperature reduction per unit length along the reactor decreases. Colombo *et al.* (2013) showed the evaporation rate of silicon precursors for silicon carbide synthesis at plasma region were enhanced by one-fifth by changing the plate power 10 kW to 15 kW. Yang *et al.* (2015) revealed the changing plate power 15 kW to 30 kW under atmospheric pressure quintupled the synthesized stainless steel nanopowder.

Mostaghimi and Boulos (1990) investigated the effect of induction frequency varying from 3 MHz to 40 MHz under atmospheric pressure and 1 kW plate power in both simulation and experimental studies. An increase in the frequency leads to enhancing the oscillation of electrons resulting in higher electric field density and power. So as to keep the power constant in the torch, the electrical conductivity will decrease. The same power with lower electrical conductivity causes to decrease the general temperature in plasma region. The lower temperatures deteriorate the

collision frequency between electron, atom and ions and ultimately the discharge is no longer to maintain thermal plasma. Their experiments verify that the temperature difference between electron and atom/ion was reduced from 1000K to 4000K in 3 MHz and 40 MHz, respectively. Colombo *et al.* (2010) simulated the three-dimensional PL-35 torch with reactor chamber for 3 and 13.56 MHz coil frequency under fixed 15 kW power dissipation. Because of helicoidal torch geometry, the temperature gradients were asymmetrically formed and the maximum temperatures were obtained at off-axis position due to the annihilation of magnetic fields by induced currents. For 13.56 MHz frequency the plasma is confined to a smaller skin depth as given by Eq.(2.7). The high temperature is maintained at longer distance along radial axis and temperature distribution in the downstream region of the torch is lower for 3 MHz. Park (1997) showed that 0.5 MHz create uniformly distributed temperature regions at the core while off-axis high temperature discharge is observed for 1 and 3 MHz frequencies.

Pristavita *et al.* (2011) worked on the synthesis of carbon black under 20.7, 55.2 and 101.3 kPa reactor pressures. After the plasma was generated by pure argon, diluted methane was added to central gas to be a carbon source. As seen in Figure 2.5, they showed that the change in pressures was not effective on temperature distribution, but it influenced the gas flow rate considerably. Similar study was conducted by Kim *et al.* (2010) to synthesize fullerene with 1 g/min feeding rate of carbon black under 20 kPa and 66 kPa reactor pressure by both pure argon and argon helium plasma. They also concluded the temperature distribution remained the same for two torch pressures but the gas velocity was higher throughout the reactor, which reduced the residence time of the particles at the plasma region. On the other hand, the temperature distribution was substantially influenced by altering the plasma forming gas composition. Figure 2.6 indicated the temperature distribution and evaporation of carbon particles depending on torch pressure and gas mixture. Pure argon plasma provides temperatures at the downstream of the reactor with colder torch exit than Ar-He plasma. However, the simulation indicated the particles require shorter times to become fully evaporated in Ar-He plasma, which has higher thermal conductivity that improves enthalpy absorption by particles. It is noted that the evaporation of

particles was fully achieved under 66 kPa, but the higher torch pressure would result in partially evaporation especially for pure argon plasma due to enhanced flow velocity, leading to low residence time of particles.

Punjabi-Vinoth *et al.* (2012) investigated argon, nitrogen, oxygen and air as plasma forming gas at atmospheric pressure with oscillatory frequency of 3 MHz by induction thermal plasma. The core plasma temperatures attained was 10600, 9100, 9000 and 6600 K at 15 kW plate power, respectively. Depending on the thermal conductivity of the gases, the generated plasma volume is the largest for argon whereas it is the smallest for oxygen. The study also considered the flow rate effect central and sheath gases with a total of 25 slpm plasma flow under 1 atm with 15 kW plasma power. An increase in central gas from 1 to 5 slpm flow rate, a decrease in sheath gas from 19 to 17 slpm enhances the plasma volume radially towards the confinement tube wall for all gas types. For the axial consideration, the temperature distribution is almost remained constant, yet, this is not true for oxygen and air plasma. Szépvölgyi *et al.* (2006) studied the helium effect in sheath gas on fullerene synthesis. The conversion efficiency of fullerene synthesis was enhanced when the content of helium in the sheath gas was increased since helium has 4-6 times higher thermal conductivity than that of argon which increases the enthalpy and temperature at the plasma region while the volume of the plasma is significantly reduced due to low electronic conductivity.

Dai Zhen *et al.* (2017) showed that the powder feeding rate of micron-sized Al_2O_3 powders influenced the spherodization process under pure argon plasma generated by 28 kW plate power. 50 g/min powder rate led to 100% efficiency in spherodization and the efficiency rate rapidly decreases as the feeding rate increases. Choi *et al.* (2014) synthesized CoB_2 nanoparticles with a particle size of 18-22 nm for the proper feeding rate. The increase in feeding rate resulted in larger diameter of the synthesized powders. Kobayashi *et al.* (2008) studied submicron copper powder production by different feeding rates under argon plasma with 40 kW plate power and 2 MHz coil frequency. It was found that the precursors were fully evaporated with 0.33 g/min feeding rate, however, the partial evaporation was observed for 1.7 and 3.5 g/min.

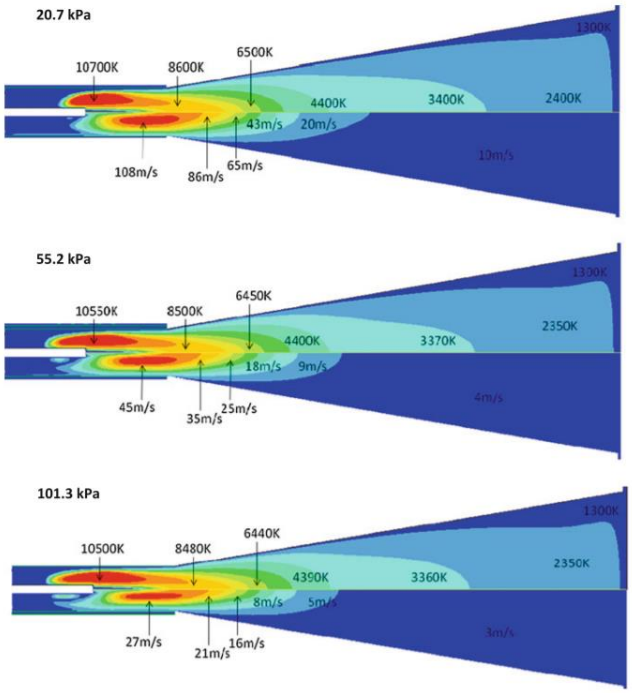

Figure 2.5 Distribution of temperature and velocity of flow throughout the reactor with respect to different pressures (Pristavita 2011)

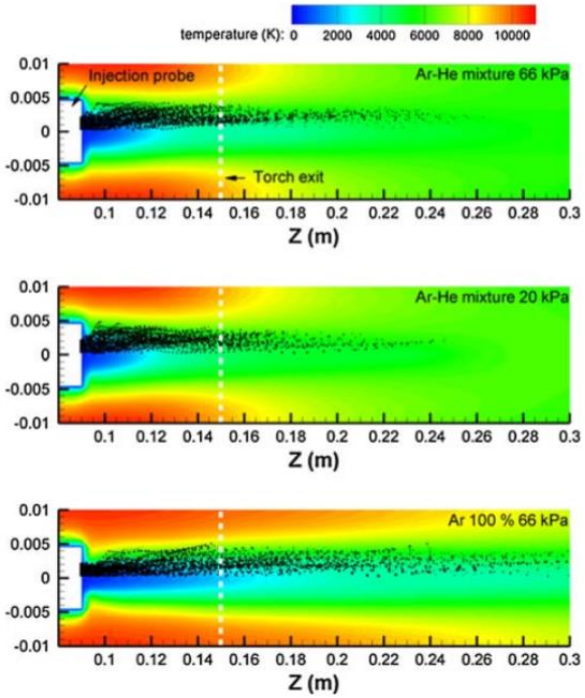

Figure 2.6 Distribution of temperature and evaporation of carbon particles for different pressure and plasma forming gases (Kim *et al.* 2010)

Ishigaki et al. (2005) synthesized TaC nanopowder from Ta(OC2H5)5 liquid precursor by atomization probe in pure argon plasma with 40 kW plate power under 2 MHz frequency. The decrease in the flow rate of carrier gas fed through atomization probe led to the formation of Ta2O5 which is the low temperature stable phase. This was occurred since the reaction product was able to enter the cooler sections of the reactor where TaC is no longer feasible. Rahmane et al. (1995) investigated the effect of carrier gas on the temperature distribution in the reactor by both numerical and experimental study. They compared the plasma condition with and without 8 slpm N2 carrier gas. The use of carrier gas reduced the temperature along the injector exit axis, leading to high temperature peak, normally formed at the center of the plasma region, is formed at an off axis. Also, the corresponding gas velocity increases with the carrier gas resulting in low residence time of precursors.

Goortani *et al.* (2006) studied the synthesis of SiO_2 nanoparticles in an pure argon RF induction plasma with 40 kW plate power under 90 kPa torch pressure. In the study, the effect of feeding rate and quenching gas injection was considered. The micronized quartz particles with a mean diameter of 2 μm were suspended in a solution and fed into plasma by means of peristaltic pump and atomizing gas. There were two sets of experiments carried out with and without quenching gas. The synthesized powders with 4.5 g/min and 11.1 g/min without using quench gas had particle size around 80 and 60 nm on average. For the experiment with application of 270 slpm N_2 quenching gas to 6.5 g/min feeding rate, the average particle size reduced to 25 nm. As shown in Figure 2.7, the temperature distribution was totally changed and SiO_2 nuclei was formed at the upper part of the reactor. The quenching gas also increased the size of fluid recirculation that led to change the powder morphology. Soucy *et al.* (2001) investigated several plasma and process parameters by enthalpy probe system during the in-flight nitridation of $MoSi_2$ in an induction plasma system. Nitrogen gas was introduced to the reactor from either sheath gas, quenching gas or both. In the absence of quenching gas, nitridation was limited to 1.65wt.% whereas 14.6 slpm argon quenching gas led to significant enhancement since the nitrogen gas concentration was improved by reducing gas velocity leading to increase in residence time. For the same quenching effect by replacing argon by

N_2, the flow rate was found as 11.5 slpm due to higher specific heat of nitrogen required lower quenching flow. The study also examined the sheath gas composition with Ar, N_2 and mixtures of Ar-NH_3. They revealed that the use of different type of gases with the same flow rate did not make any changes in the composition of resultant powder of $MoSi_2$, temperature distribution and gas velocity in the reactor. Thus, the quenching gas does not have any role for the participation in the reactions rather it affects the particle size by changing cooling rate, residence time the temperature distribution by the degree of flow rate.

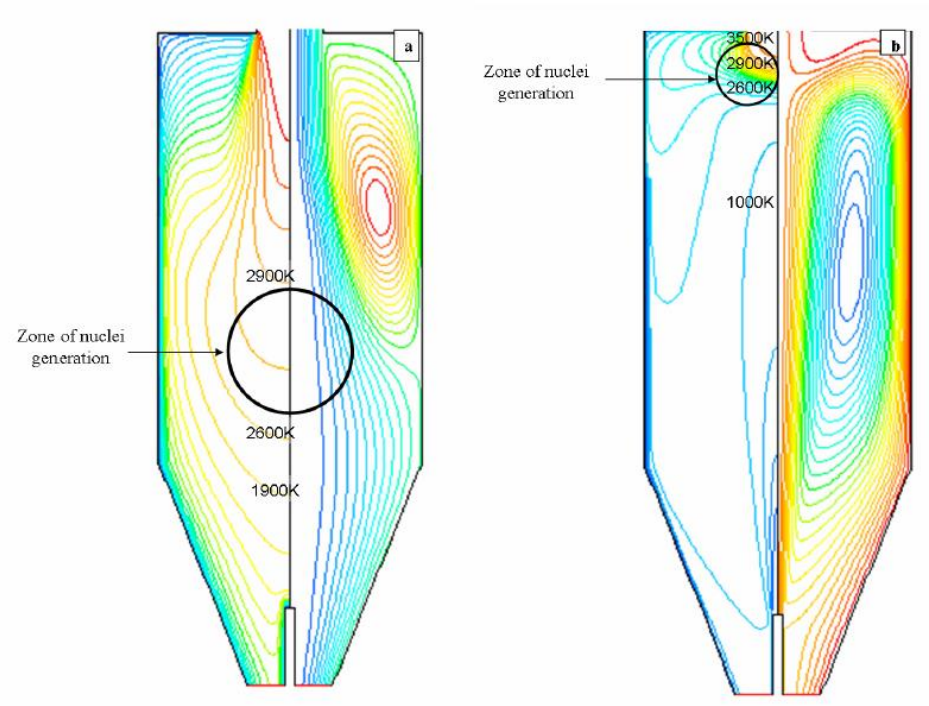

Figure 2.7 Contours of temperature (left), Streamlines colored by mass flow (right). (a) Without the application of quenching gas, (b) Quenching gas with 270 slpm flow rate (Goortani 2006)

Jiayin *et al.* (1997) studied the synthesis of ultrafine SiC powder from elemental silicon and CH_4 precursors under pure argon plasma at 66.6 kPa in RF-ICP thermal plasma with 3 MHz frequency . The increase of plate power from 41.3 kW to 52.2 kW resulted in the increase of SiC fraction while reducing Si. The sheath gas composition was investigated with the use of two gas compositions, Ar-N_2 (50 vol.% N_2) and Ar-H_2 (9 vol.%H_2). The replacement of nitrogen by hydrogen led to intensification of α-SiC peaks, higher free carbon and smaller SiC powders in the

resultant powder. This was probably due to increasing the plasma temperature and subsequently high cooling rates with the quenching gas. Also, there was no appreciable Si_3N_4 formation in the synthesized powders by the application of nitrogen as sheath gas. The reason was postulated that the quench rate was high enough to prevent the incorporation of nitrogen into the reaction. They also showed that the experiment carried out with a feeding rate of 4.40 g/min of silicon led to higher free silicon and carbon (low SiC conversion) than that with 2.38 g/min in the resultant powder since the available enthalpy or absorption rates became lower with higher feeding rate. The application of CH_4 as a carrier gas directly improved SiC synthesis since the dilution by argon carrier gas was eliminated. The last parameter investigated was the injection position of the precursor. Since SiC formation requires high energy, the probe position was pulled up by 32 mm to increase the residence in the high temperature. As expected, SiC formation was improved with high conversion of precursors with negligible free carbon content in the synthesized powder.

Synthesis of nanoparticles in an induction plasma can be adjusted by altering the plasma and process parameters. The plasma shape and temperature distribution are primarily based on coil and torch geometry. Frequency of coil influences the skin depth of the plasma where the temperature is dissipated throughout plasma torch and reactor. These parameters could be considered as invariables of plasma system which are not simply adjustable rather they should be determined before the construction of a system depending on the purpose of use. Plate power and torch pressure are the fundamental parameters, used for tuning plasma conditions for a process. Plate power affects the plasma volume and temperature by a degree of coupling efficiency determined by torch geometry. Higher plate power leads to higher ionization degree, and hence larger plasma volume, increased temperature and heat capacity. Torch pressure has an impact on the gas velocity which is directly related to the residence time of particle in plasma region. Increasing the torch pressure results in a significant reduction in gas velocity and so residence time which decreases the amount of heat absorption by particles per unit time. The type and composition of plasma gases are the other parameters owing to thermal and electrical conductivities. Argon is mainly

used as plasma forming gas owing to forming higher plasma volume than He, N_2, O_2 and air. The gases having higher conductivity such as H_2 and He can be added to argon gas to provide increase plasma temperature and distribution. The addition of He as carrier gas as well as plasma forming gas increases the plasma core temperature whereas it leads to shrink plasma volume when used as sheath gas. Quenching gas is a crucial factor for ultrafine particle synthesis since it does a remarkable impact on both temperature distribution and gas velocity. The increase in quenching flow results in narrower temperature distribution along the torch and more effective cooling by increasing cooling rate. The composition of quenching gas does not incorporate to a reaction with precursors at the plasma region, therefore, it does not matter which gas is used as quenching gas but flow rate to be used depends on heat capacity of the gas. The precursor feeding rate improves the amount of evaporated particles, however, the excessive feeding rate with respect to supplied plasma enthalpy leads to increase non-evaporated particles that prevents the desired reaction taking place.

2.2.3 The overview of nanopowder synthesis by induction thermal plasma

RF-ICP thermal plasma torches have been used to synthesize nanopowders of a variety of materials. With this route of synthesis, it is possible to carry out reactions ranging from a simple size reduction process by phase transformation to a sophisticated process including chemical reaction following with encapsulation process. Depending on design of a process it is possible to obtain following types of materials in nanometer size; metallic elements & alloys, oxides, nitrides, carbide as well as carbon-based nanostructures (Jiayin 2010).

Yang *et al.* (2016) studied the conversion of coarse silicon multicrystals into silicon nano-crystal by feeding the precursor with argon carrier gas into Ar-H_2 plasma generated by 30-50 kW plate power and 5 MHz frequency. The nanosilicon crystals were obtained as a particle size range of 20-85 nm with 327 g/h yield. Zhang *et al.* (2012) reported the synthesis of tungsten nanosized powders from dissociation of ammonium paratungstate following with hydrogen reduction of tungsten trioxide in argon plasma with 30 kW plate power and 4 MHz coil frequency. Almost pure

tungsten trioxide phase was attained with 100 nm average particle size in the absence of hydrogen. When the powders were fed by hydrogen carrier gas, the resultant powder was made up of equilibrium α-W phase with metastable β-W with 50 nm particle size for 19 g/min feeding rate. Bai *et al.* (2009) synthesized nickel nanopowders from nickel hydroxide powders by hydrogen carrier gas with the same plasma parameters. The synthesized powders were collected from filters as well as the chamber wall and characterized by XRD and FESEM. The spherical uniform particles with a size range of 60-100 nm were successfully obtained.

Oh and Ishigaki (2004) produced TiO_2 nanopowders from titanium nitride micron size precursor with a feed rate of 1.5 g/min in argon plasma with 40 kW plate power and 2 MHz coil frequency. Oxygen was added into either sheath gas or carrier gas. In-flight oxidation of titanium nitride was initiated by surface oxidation leading to core-shell formation and then oxygen diffused from the core-shell to reach TiN, which accelerated the evaporation of precursor by decreasing boiling point. At the end, TiO_2 was obtained with 50 nm average particle size. Dhamale *et al.* (2016) synthesized uniform Nd_2O_3 nanoparticles with 20 nm average size from its micron-sized in pure argon plasma atmosphere with 27 kW plate power. Castillo and Munz (2005) investigated the synthesis of CeO_2-based nanopowders for SOFC electrolytes. The precursor of nitrate salts dissolved in water were transferred by means of a peristaltic pump to an atomization probe that fed the precursor via argon carrier gas into the plasma region. 25-28 nm crystallite size of powders were obtained regardless of plasma operation parameters.

Hou *et al.* (2015) studied on Si_3N_4 nanosphere synthesis from large silicon nitride powders in argon plasma. The coarse silicon nitride particles were mixed with phenolic resin to make a composite promoting to obtain spherical morphology. The precursor was then introduced by NH_3 carrier gas into the torch operated at 10 kW plate power with 4 MHz frequency and the powder products were collected from filters as narrow size distribution of 30-50 nm spherical particles of α-Si_3N_4. Kim *et al.* (2014a) synthesized AlN nanopowder by micron sized aluminum powders and nitrogen used as sheath gas with 25 kW plate power under 4 and 15 psi torch pressure. The powders were taken from bottom, cyclone and nanopowder collectors.

The unreacted aluminum powders were observed in both bottom and cyclone collectors, yet, AlN nanoparticles with a range of 20-60 nm were collected from nanopowder collector.

Kim *et al.* (2014b) investigated the synthesis of boron nitride nanotubes (BNNTs) from both boron powder and hexagonal BN fed by nitrogen carrier gas into Ar-H_2 plasma region. Using boron precursor gave inefficient synthesis due to the presence of B-rich product. In the absence of hydrogen in plasma gas composition, there was no BNNTs formation. The hydrogen promoted the growth of the nanotube BN on the prenucleated small-sized boron droplets as postulated by TEM analysis. For the appropriate hydrogen introduction to plasma, an average diameter of 5 nm BNNT's was synthesized with the yield rate of 20 g/h (Kim *et al.* 2018).

Leparoux *et al.* (2005) studied the size reduction of WC in an induction thermal plasma. The precursor of impure WC with 1-3 µm particles were supplied at a feeding rate of 60 to 400 gh^{-1} into Ar-H_2 leading to carbon deficit nanopowder synthesis. Methane was then used as an additional carbon source to promote WC yield. The feeding of 4.8 slpm methane resulted in 20 nm WC with some substoichometric fraction. Ramachandran and Reddy (2013) produced SiC nanoparticles by SiO_2 powders with methane used as carrier gas under argon plasma with 21.6 kW plate power. The powder feeding rate of SiO_2 kept constant while the methane flow rate was changed. The maximum yield was obtained with 1:2 molar ratios. The decrease of methane molar ratio to below 1 or less with respect to SiO_2, SiC nanorods formation was observed due to the presence of silicon acting as a catalyst. Tong and Reddy (2005) examined TiC nanoparticle synthesis by pure titanium powder with methane by thermal plasma. They analyzed the possible reaction thermodynamically to determine the use of molar ratio of CH_4:Ti. According to thermodynamic analysis, the molar ratio was determined to be closer to 1:1. The one with a feed rate of 3.3 g/min Ti resulted in the average size of 25 nm nanoparticles with 98.4% pure TiC.

Aktekin (2013) studied Mg-Ni nanoparticles and their carbon encapsulation by RF-ICP thermal plasma. The elemental Ni and Mg were used as precursors and fed into

the plasma from top and bottom injector with a carrier gas, respectively. There were five different positions of bottom injector considered among which the injector position of 272 mm below the center of the coil led to the maximum yield for Mg_2Ni particles with 89 nm average particle size. The same study also considered the carbon encapsulation of Mg, Ni and pre-alloyed Mg_2Ni particles by methane as a carbon source. Solid powders and methane were introduced into the plasma alternatively at the top and bottom injectors for each type of powders. Nickel and magnesium were successfully encapsulated with 3-10 graphitic layer, however, for the pre-alloyed Mg_2Ni case, the elemental Ni and $MgNi_3C$ phase was formed with a single carbon encapsulated particles.

Tanaka *et al.* (1999) studied compositional modification of boron carbide by an induction plasma. The starting powder having a composition of $B_{5.25}C$ and an average particle size of 22.3 µm introduced via 5 slpm argon carrier gas into plasma generated by coupling of 30 slpm argon with 40 kW plate power and 2 MHz coil frequency. The quench gas was composed of 85 slpm Ar and 5 slpm H_2. The thermodynamic analysis done by Gibbs free energy minimization method indicated there were several feasible phases of B-C-H combinations. The feeding rates and torch pressure were varied to obtain the stoichiometry close to B_4C. As the plate power and torch pressure increased, the carbon rich boron carbide phase peaks were getting intensified. They explained the reason by comparing the thermodynamic result that the heat absorption by particles were enhanced due to improved heat capacity using higher plate power and increased residence time by higher pressure. The resultant boron carbide particle compositions were varied between 16.2-16.8 wt.% carbon, which had been lower than 17 wt.% C at the beginning.

Du *et al.* (2008) investigated RF plasma synthesis of boron carbide nanoparticles by commercial micron-sized B_4C in thermal plasma operated at 12, 16 and 21 kW. The decomposition of boron carbide increases with higher applied plate current, which resulted in the more formation of boron in the product powders. The free boron particles became boron trioxides when exposed to air. In order to eliminate boron oxide, the powders were washed by water and subsequently heat treated at $1700^{O}C$.

The purified powders with 21 kW plate power showed a size reduction to the nanometer particle range.

Thakkar and Reddy (2014) studied the processing of ultrafine boron carbide particle from B_2O_3 and methane by thermal plasma with 24 kW power. Boron oxide powders were fed by a mixture of argon and methane as carrier gas into the plasma generated by 3 scfm argon flow. The thermodynamic analysis of presumed carbothermic reduction reaction was done by Gibbs energy minimization method which suggested the perfect yield obtained with 2:7 molar ratio of B_2O_3:CH_4. The experiments also indicated that the highest boron carbide percentage in the powder was obtained for 2:7 ratio but remained at most 60%. This was explained by the presence of B_2O_3 and free carbon in the product powder. The higher feeding rate of 3.3 g/min B_2O_3 deteriorates the boron carbide conversion efficiency. This was caused by the decrease in residence time preventing complete vaporization.

Zhai *et al.* 2016) describes the preparation of ultrafine boron carbide using high-frequency induction plasma thermal plasma. They dwell on boron oxide and boric acid as boron source while methane and graphite as carbon source, respectively. In the given first example in the patent, the mixture of boric acid and boron oxide is proposed with the feeding mass ratio of 1.5-2.5 and 1 while the second example considers the precursors to be boric acid and graphite with the mass ratio 2.5-3.5:1. The synthesized powders under these conditions were analyzed in XRD indicating 99% purity of boron carbide particles and the median size of particles were stated as 100-600 nm.

A patent by Hung and Vanier (2010) states boron carbide can be produced from liquid starting materials rather than conventional solid phase synthesis using B_2O_3-carbon or gaseous precursors BCl_3-CH_4. It is stated that the specific surface area to be targeted is 5 m^2/g or higher and this value could be 100 or even 200 m^2/g. Also, t "De Laval" nozzle at the exit of the torch. It is used for cooling the product stream to some degree by introducing the quench gas to allow the formation of ultrafine boron carbide particle at the upstream of the nozzle. Also, the nozzle is used as a choke position that allows the operation of the reactor at higher temperatures, which results

in increasing the residence time. In an example, trimethoxy boroxine as boron source and acetone as carbon source were used in a D.C. plasma torch with specified torch parameters under 12 kW power for the ultrafine boron carbide synthesis. The specific surface area of the obtained powders was measured as 28 m^2/g, which corresponds to 85 nm by assuming all particles spherical. The other experiment was done with trimethyl borate as boron source and iso-octane as carbon source with the same plasma parameters except the power was increased to 24 kW. De Laval nozzle diameter was 7 mm in this study. The average particle size of the synthesized powders was 65 nm, which was lower than that of the previous experiment. In the same patent, the other carbon sources were also considered. Many of these experiments showed pure crystalline boron carbide with small amounts of other constituents e.g. boron oxide, silicon carbide or graphite depending the choice of the precursors.

A patent by Vanier and Hung (2008) addresses an issue of improving the purity of synthesized boron carbide. In this patent, micron-sized boron carbide particles are fed into the thermal plasma by the addition of chemicals containing nitrogen. These are urea, ureaformaldehyde, urazole, ammonium, N-Ndimethylformamide, methylformamide, formamide, ethylenediamin, methylamine and ammonia etc. The nitrogen containing materials can be fed into plasma as solid, liquid and gaseous phase. The role of these materials is to react with oxygen to form "NO_x" at the plasma region during the process. Thus, only free carbon available to react with boron to form boron carbide. They carried out two experiments with and without addition of urea. The first one was carried out with input materials containing carbon and boron. The result was 56% boron oxide and 44% boron carbide. On the other hand, the second experiment was done with addition of 17-gram urea to 100 gram of same input materials and it yields 99.1% boron carbide, 0.9% boron oxide. Also, the patent reveals that the reaction taking place at the plasma region can be controlled by addition of appropriate gas feeding. For instance, feeding of argon, helium or neon gas provides the plasma region to be "inert"; feeding of hydrogen, methane, ammonia and carbon monoxide makes the region "reducing". Similarly, oxygen, nitrogen or carbon dioxide for oxidizing. Among these gases, one of the benefits of

nitrogen selection is to form nitride layer on synthesized boron, making them oxygen resistant.

It is possible to use radio frequency inductively coupled thermal plasma for the synthesis and modification of nanoparticles of various type of materials. As seen in the literature, RF-ICP synthesis is a dynamic process that the control of synthesis becomes challenging as the complexity of required reaction and incorporation of species are increased. However, RF-ICP process offers a scale production with a minimal process time.

CHAPTER 3

EXPERIMENTAL PART

3.1 Materials

As a boron source two materials were used: B_2O_3 and $C_3H_9BO_3$ (TMB) for B_4C synthesis. Boron oxide was procured from Eti Maden İşletmeleri A.Ş, 98% pure, -45 mesh and from American Elements 98% pure, -325 mesh. The azeotrope solution (TMB-M), i.e. 70% trimethyl borate (TMB) and 30% methanol (M) was obtained from Vega Makina San. ve Tic. A.Ş.

As a carbon source, methane (CH_4) was used which had a purity of 99.5 vol.% procured from Linde. In some experiments, we made use of hexane (Merck), 98.5% pure. As a nitrogen source, we have either used diisopropylamine (Merck) 99% pure or in the form of nitrogen gas (Linde) 99.5 vol.% pure.

3.2 Thermal Plasma System

The equipment used for the synthesis of B_4C is an induction thermal plasma, Tekna Plasma Systems Inc. (Figure 3.1(a)). The system is composed of five parts, which are an R.F. power source, a plasma torch, a reactor, collection units and a scroll pump. The schematic of the nanopowder reactor is given in Figure 3.1(b).

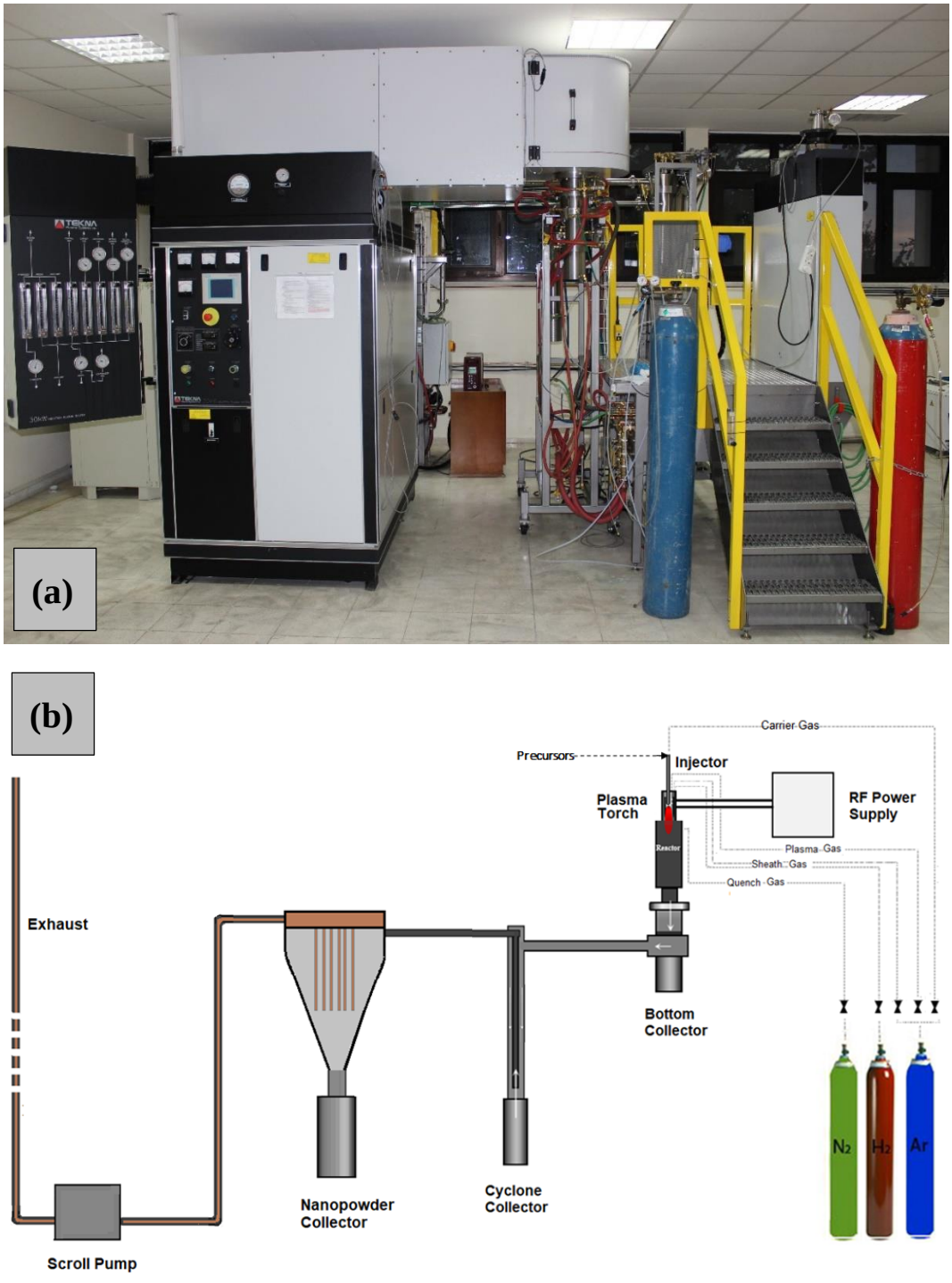

Figure 3.1 General View of the thermal plasma system; (a) Photograph of Tekna plasma System at the department of Metallurgical and Materials Engineering Department of METU (b) Schematic of components in R.F. thermal plasma

The R.F. power unit had a power of 30 kW with a nominal frequency of 2-5 MHz. This was connected to the plasma torch (Figure 3.1(a), (b)) where the plasma is formed via induction coupling with the plasma gases maintained to the torch, normally argon. As seen in the Figure 3.1(b), the reactor is located just below the torch.

The precursors either solid, liquid or gas are fed into the plasma via an injector placed into the torch. The precursors as they are injected into plasma are evaporated. They are then quenched by high flow rate gas (normally nitrogen) radially injected into the reactor just below the reaction zone. Aerosol obtained follow a route as seen in Figure 3.1(b) on which there are three powder collectors.

The last unit in the system is a scroll pump which maintains the whole system at pressure slightly less than the ambient. During the use of thermal plasma system, the torch is cooled by deionized water system. The reactor and powder collection units as well as the connecting components are double walled construction and were cooled via a 37 kW chiller.

3.2.1 Plasma Torch and Operating conditions

Schematic section of plasma torch is given in Figure 3.2. It is made up of induction coils, one quartz tube, ceramic confinement tube and double walled water path. The plasma forming gas, i.e. central gas, is sent into the inner quartz tube. When coupled the plasma is generated, at which temperature could be as high as 10000 K. Sheath gas is flown through the annular interspace between the outer ceramic tube and the inner quartz tube. The aim of using sheath gas is to protect the confinement/quartz tube as well as the torch body against the excessive heat. The body of the torch is also cooled with the high velocity de-ionized water used as a cooling medium. An injector is placed at the top center of the torch where precursor is fed with carrier gas into the plasma. The injector has a water jacket through which de-ionized water is circulated to protect the injector from the heat in the torch The operating parameters of plasma are tabulated in Table 3.1.

The plasma was ignited at 5 psia (approximately 350 mbar) pressure without the use of hydrogen in sheath gas for all experiments. After the plasma was ignited, the pressure was increased to 7 psia (480 mbar) where the hydrogen content was gradually increased in the sheath gas until its flow rate reached 6 slpm before the plate power was increased to 15 kW. Finally, the plasma power was set 25 kW and the pressure was increased to 14 psia (965 mbar) before the experiments were initiated.

Table 3.1 Thermal Plasma Parameters used in the experiments

Plasma gas types	**Gas type with flow rates**
Central gas	Argon 15 slpm
Sheath gas	Argon 60 slpm ; Hydrogen 6 slpm
Quenching gas	Either Nitrogen or Argon 150 slpm
Carrier gas	Argon 5 slpm

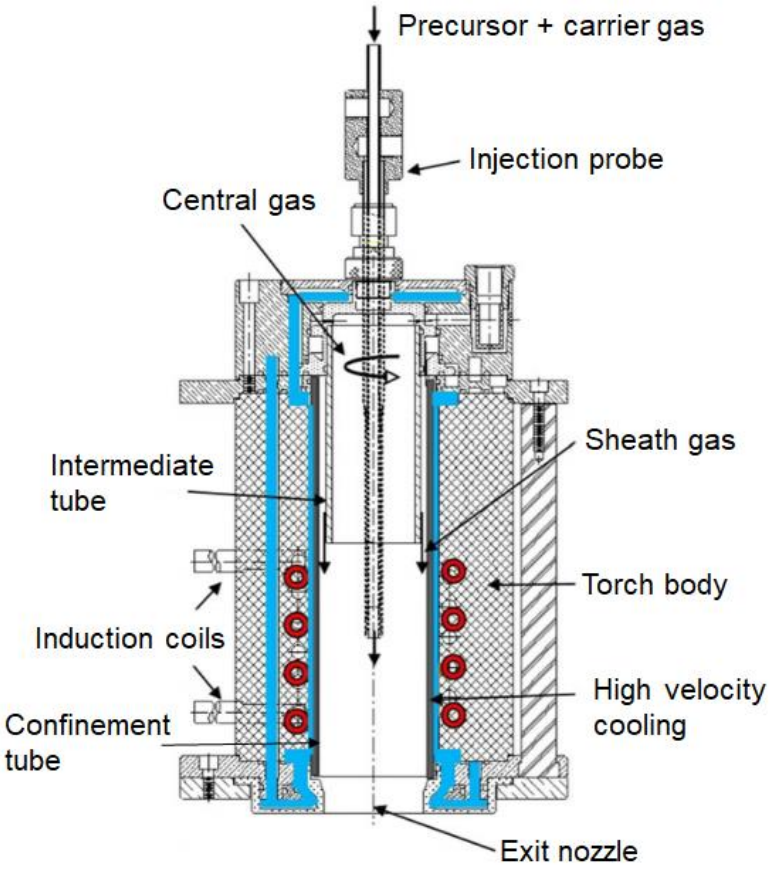

Figure 3.2 Schematic section view of plasma torch (Boulos 2017)

3.2.2 Feeding of precursor

Solid Precursor Feeding

Solid precursors were placed into vibratory powder feeder (Figure 3.3(a)). The output of feeder was transported by HDPE tube (6 mm inside diameter) and maintained into the plasma at the top of an injector by carrier gas. This was achieved with the use of carrier gas argon fed with a rate of 5slpm. Since the responses of the vibratory powder feeder changes with powder type and size the feeding rate was adjusted by trial and error for each experiments**.**

Liquid Precursor Feeding

The liquid precursors used in the experiments were fed through 6 mm HDPE tubing by means of a peristaltic pump (Figure 3.3(b)). This is simply a U-shaped flexible hose and a rotor in the center of the arc squeezed the hose twice per revolution to drive the liquid ahead. the flow rate of the precursor was controlled by changing the rotation speed of the peristaltic pump.

Liquid precursors were maintained into the plasma torch via an atomization probe in the experiments. The carrier gas is fed into the probe from an additional inlet at the center of the probe which opens to a thin radial path. The gas follows the path and encounter with precursors at the exit of probe, which results in atomization of precursors.

Gas Feeding

Where necessary, liquid precursors are fed into the plasma torch in the form of gas. For this purpose, an evaporator was connected between the peristaltic pump and the injector probe. The liquid precursors were sent by means of the peristaltic pump with the carrier gas into the evaporator. This is shown in Figure 3.3(c). The evaporator was simply copper container placed into a heating mantle set at $450^{O}C$. The speed of the peristaltic pump was adjusted at a flow rate such that the droplets of liquid precursor were evaporated as soon as they entered into the evaporator. Thus, a constant flow rate of gas feeding was achieved.

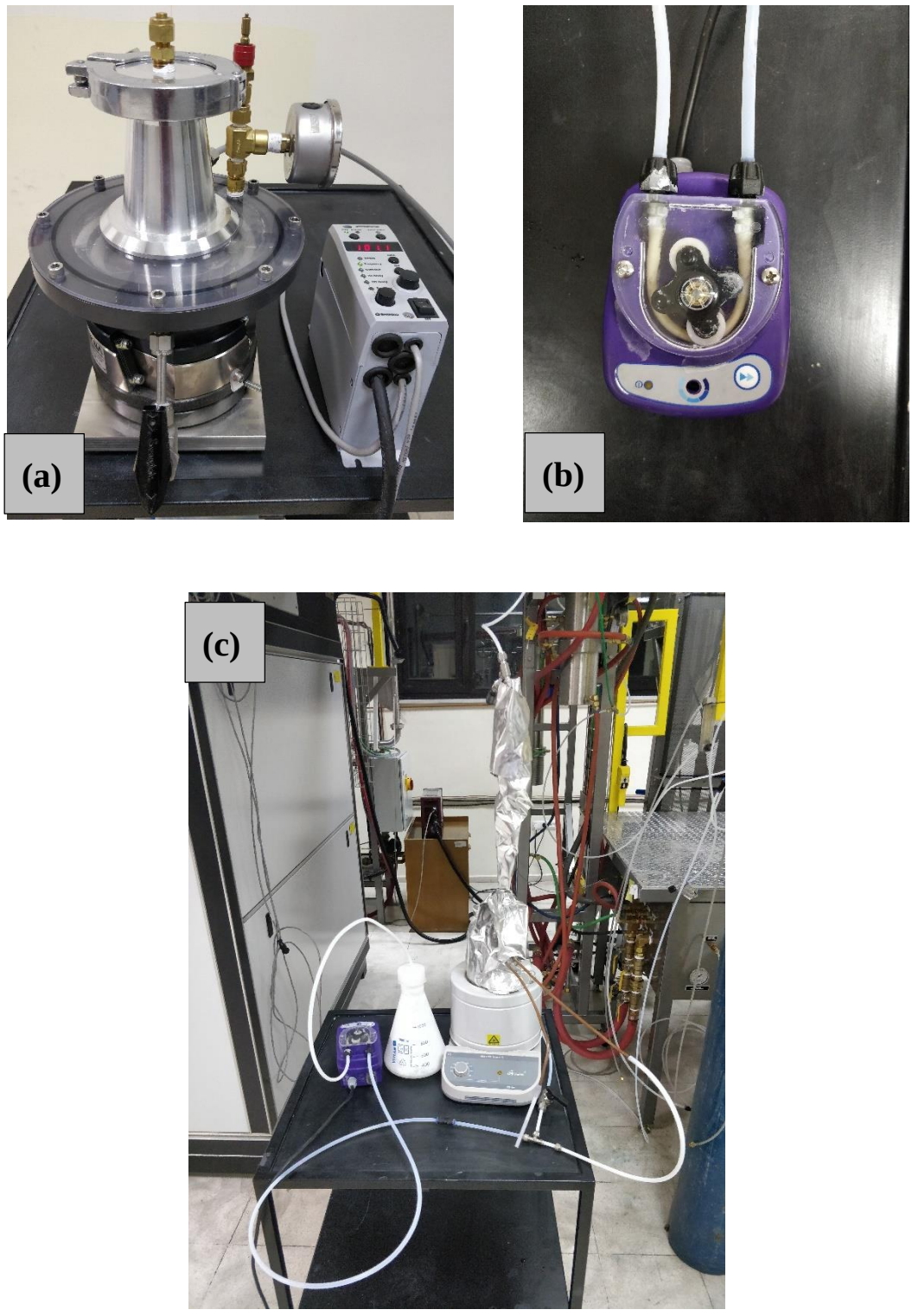

Figure 3.3 (a) The image of the vibrational powder feeder, (b) the peristaltic pump, and (c) the pump with evaporator

3.2.3 Collection of powders

There are three collector units attached to the system for gathering the powders. These are bottom, cyclone and nanopowder collectors, Figure 3.1(b). Aerosol generated in the nanopowder reactor makes a 90^{O} turn just below the reactor. Thus powders which cannot follow this turn or large particles that pass through the reaction zone unaffected are collected at the bottom collector (Figure 3.4(a)).

Aerosol flow then go through the cyclone collector. Here aerosol is maintained into the unit tangentially, and move downwards making 180^{O} turn into inner the central tube. The particles that are approximately 1-2 μm in size cannot follow the turn and are accumulated at the cyclone collector at the bottom (Figure 3.4(b)). Aerosol flow is then maintained to nanopowder collector

There were two nanopowder units used in the experiments**;** continuous nanopowder collection unit for large scale production and batch type nanopowder collection unit. **The continuous nanopowder collection** is a conical shape unit in which there are four quick-connect candle shaped porous stainless steel filters, Figure 3.4(c). The purpose of these filters is to separate particles from the flue gases. The aerosol which enters into the continuous collector tangentially are separated from the particles and maintained to the scroll pump which controls the pressure of the overall system. By the application of positive pressure of argon gas through the filters (blowback), the deposited powders on the filters are forced to fall into the collector at the bottom. This collector had a ball valve which was open normally but could be closed and removed from the unit, a new one could be connected for continuous production.

Batch nanopowder collector unit had a different construction. This unit had identical connections with the continuous nanopowder collector. Thus, they were interchangeable. As seen in Figure 3.4(d), it comprises two identical units which can be operated in sequence. Each unit is in the form of two cones mirror image of each other connected together on a plane where the filter (Whatman® Glass Fiber Filter Grade 6, 240 mm) is located by four C-clamps. The unit can be removed from its place via unlocking KF-50 clamps.

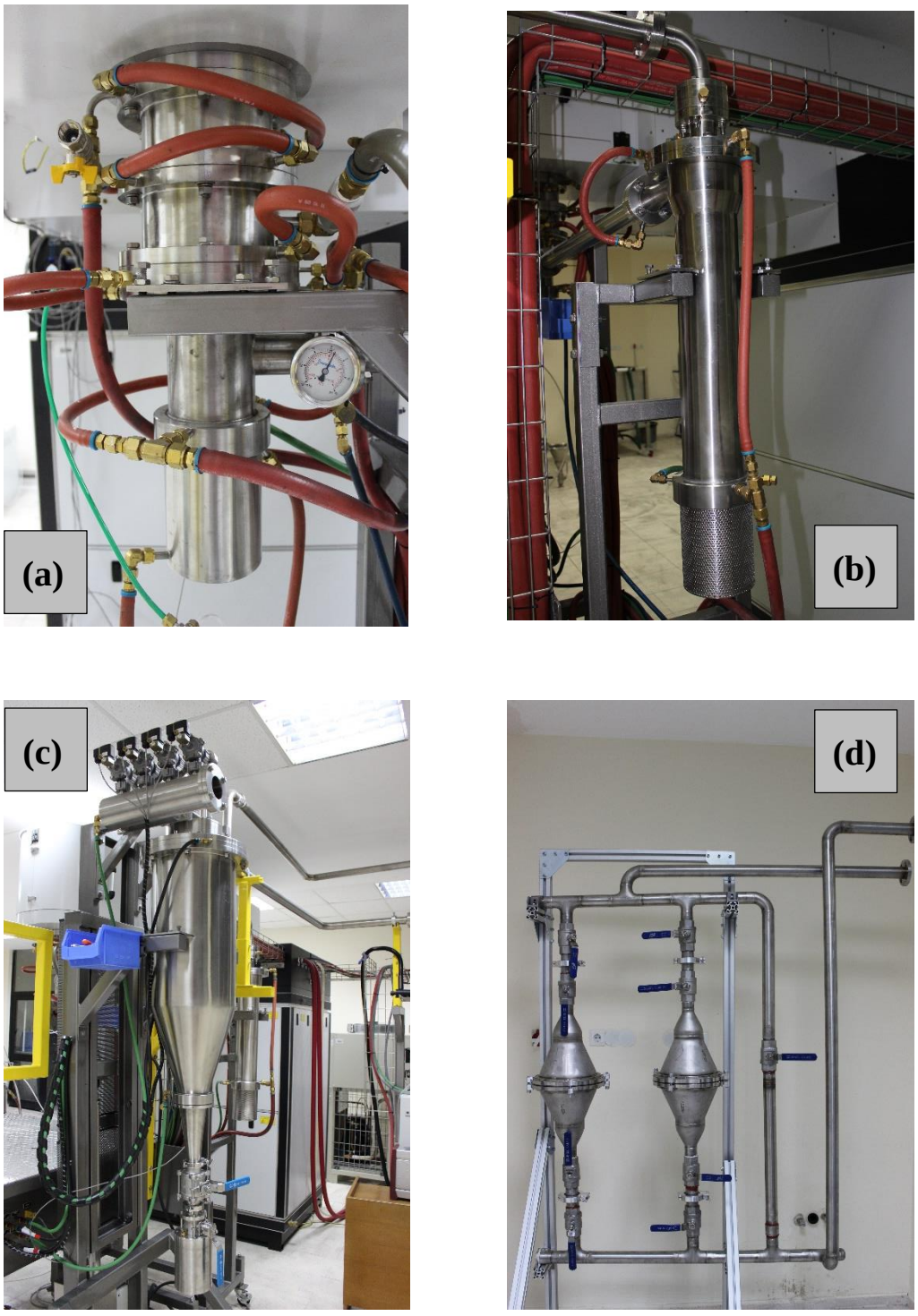

Figure 3.4 (a) Bottom collector unit with reactor, (b) Cyclone unit
(c) continuous nanopowder unit (d) batch nanopowder unit

3.2.4 Flue gas analyzer

Where needed the flue gas separated from the submicron particles at nanopowder collector was analyzed with regard to constituent gases. For this purpose, we made use of a gas analyzer, Figure 3.5. The probe of the gas analyzer was inserted to the exhaust gas tube prior to the scroll pump. Thus, the sample was taken from flue gases representing the byproducts of reactions. The gas was inserted back into the tube after analysis. The oxygen content of the sample gas was measured with a two electrodes electrochemical sensor. CO content was measured with a three electrode system. CO_2 and CH_4 were measured by means infrared analyzers. Thus the system is capable of analyzing O_2, CO, CO_2 and CH in the flue gas.

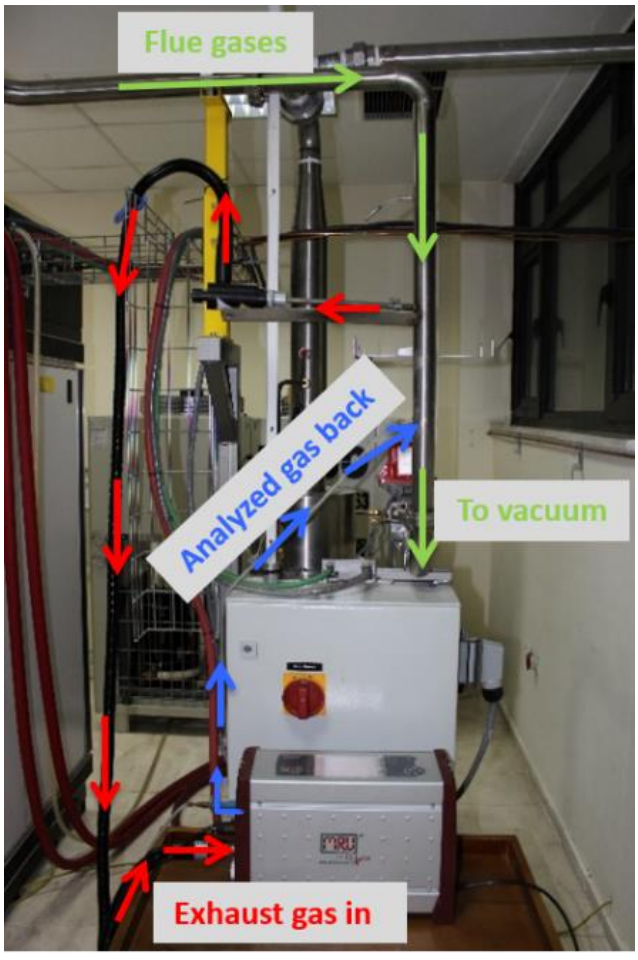

Figure 3.5 Gas analyzer connected to the thermal plasma flue pipe

3.3 Materials Characterization

Solid precursors and plasma-synthesized powders were characterized by X-ray diffraction (XRD) Rigaku DMAX 2200 using Cu-K_α radiation. Where necessary the diffraction patterns were refined by Rietveld method (Rietveld 1969) using the Maud Software (Lutterotti 2000) The morphologies of synthesized powders were examined by FEI Nova 430 scanning electron microscope equipped with a field emission gun. Samples for SEM examination were prepared using double-sided carbon tape in order to mount them onto aluminum holders. The SEM also had a facility for energy-dispersive X-ray spectroscopy (EDX) used to check the chemical make-up of the samples.

Field Emission Transmission Electron Microscopy by Jeol JEM2100F was used for both observing the morphology of synthesized particles. A sample obtained from synthesized powders was dispersed in ethanol and the suspension was subjected to ultrasonification for a period of 30 minutes to separate the particles from agglomerates. Then, a drop of suspension was taken onto TEM grid and dried. The grid was, finally, inserted in TEM to be analyzed.

Surface area of synthesized powders were determined with BET analysis using Quantachrome Corporation Autosorb-6. Where necessary the surface area is converted to their average particle size using;

$$d_{BET} = \frac{6}{S_{BET} * \rho} \qquad (Eq. 3.1)$$

Where d_{BET} is the average particle size, S_{BET} is the surface area from analysis and ρ is the density of the material (Zielinski and Kettle 2013)

CHAPTER 4

RESULTS AND DISCUSSION

4.1 Thermal Plasma Synthesis of B_4C from B_2O_3 and CH_4

Preliminary experiments of thermal plasma synthesis of boron carbide were carried out with coarse boron oxide powder (-45 mesh) as boron source and methane as carbon source. This route would yield boron carbide;

$$2B_2O_3 + 7C = B_4C + 6CO \qquad \text{Eq.(4.1)}$$

The ratio of B_2O_3 to CH_4 was systematically changed during the experiments. Plasma parameters used in the experiment were given in Table 3.1. In each experiment, the feeding rate of B_2O_3 was kept constant with a mass flow rate of 2.2 g/min and CH_4 flow rates were changed from 0.35, 1.4, 2.5 and 3.6 slpm. The precursors were mixed together via a T junction just before the injection probe.

The synthesized powders were accumulated mostly at bottom collector, indicating that the particle size was rather coarse on average. Still a small fraction of products was collected at the nanopowder collector. Figure 4.1(a) shows XRD pattern of the starting powder. It comprises two broad peaks over 2-theta range rather than sharp peaks implying that the starting powder was amorphous.

XRD patterns of the synthesized powders with 0.35 slpm CH_4 indicate distinct B_2O_3 peaks over the entire range, though a weak B_4C peak can also be discerned (Figure 4.1(b)). There was a relatively a dominant carbon peak in the experiment with 1.4 slpm CH_4 (Figure 4.1(c)), which intensifies further as the flow rate of CH_4 further increased (compare Figure 4.1(d), (e)). For all of the samples, Rietveld analysis was done to determine the weight percent of the phases in the synthesized (Appendix I(a) to I(d)), These are tabulated in Table 4.1, As seen in the table the fraction of B_4C is extremely small, and not more than 5 wt.%.

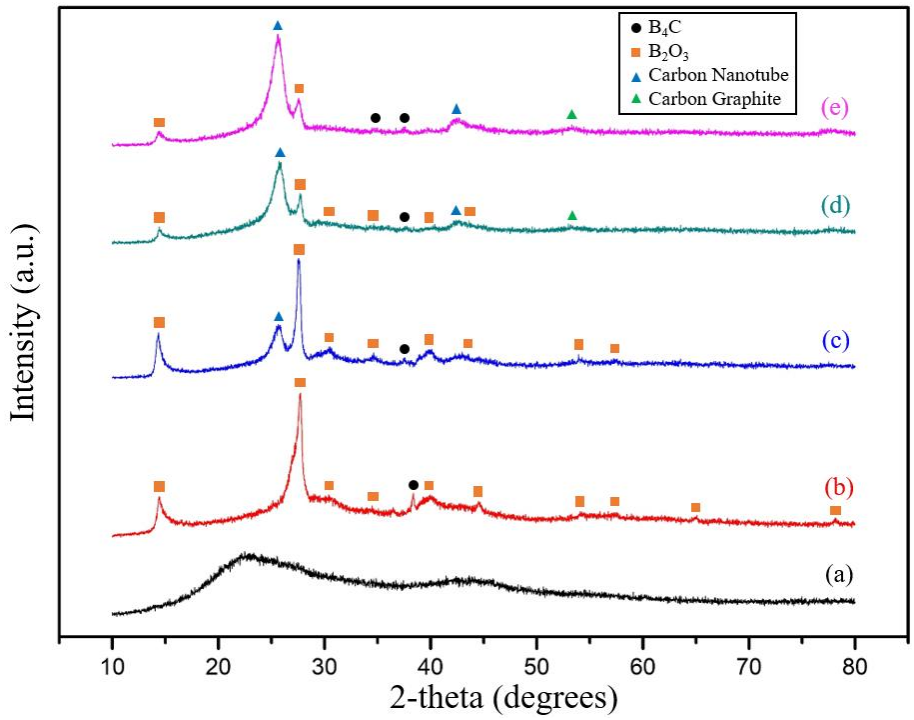

Figure 4.1 XRD patterns of the samples; (a) as-received B_2O_3 powder (b) 0.35 slpm CH_4 (c) 1.4 slpm CH_4, (d) 2.5 slpm CH_4, (e) 3.6 slpm CH_4

Table 4.1 Percentages of the phases present in the powder products synthesized with -325 mesh B_2O_3 according to Rietveld

Precursors		**Products**			
B_2O_3	**CH_4**	**B_2O_3**	**B_4C**	**Carbon**	**HBO_2**
2.2 g/min	**0.35 slpm**	84.83	1.49	0.69	12.99
	1.4 slpm	63.38	1.97	36.65	-
	2.5 slpm	35.98	3.54	60.48	-
	3.6 slpm	16.33	4.96	78.71	-

This experiment was not successful for two reasons. The first, greater fraction of powder was collected at the bottom collector implying that they did not vaporize and therefore did not take part in the reaction. The study conducted by (Marion *et al.* 2009) indicated that the precursor powder size up to 90 µm is fully vaporized with 50 kW plasma power. In our experiments, considering that we had a plasma power of 25 kW, -354 µm B_2O_3 powder size was too coarse, (see Table 4.1). The second, the

weight fraction of B_4C is quite small as greater fraction of the product is B_2O_3 re-formed during the plasma processing.

Since the experiments with coarse B_2O_3 powders was not successful, new experiments were conducted with a finer B_2O_3 powders. This was -325 mesh much finer than the previous precursor. A total of six experiments were conducted as given in Table 4.2. Due to uncertainties in vibrational powder feeder, the feeding rate values reported in Table 4.3 should be treated as approximate values. In each experiments, a sufficient amount of samples was synthesized and collected from nanopowder collector, yet, there were also considerable amount of powders accumulated in other collectors.

Two sets of experiments were carried out with B_2O_3 where the feeding rate was 1 g/min and 2 g/min. Values of CH_4 feeding rates, 1.11 slpm and 2.22 slpm shown in Table 4.2 are, according to Eq. 4.1, the exact stoichiometric rates with respect to 1 g/min and 2 g/min B_2O_3.

Table 4.2 Percentages of the phases present in the powder product synthesized with -325 mesh B_2O_3 according to Rietveld analysis

Precursors		**Products**			
B_2O_3	**CH_4**	**B_2O_3**	**B_4C**	**Carbon**	**Particle size**
1 g/min	**1.1 slpm**	89.78	5.74	4.48	66 nm
	1.5 slpm	79.63	6.93	13.44	87 nm
	2 slpm	63.38	9.21	27.41	83 nm
2 g/min	**1.5 slpm**	74.21	7.06	18.73	102 nm
	2 slpm	56.76	9.32	27.3	98 nm
	2.2 slpm	40.02	12.34	47.64	109 nm

XRD patterns of the first set of experiments, i.e. B_2O_3 1 g/min are shown in Figure 4.2 along with that of the fine as-received B_2O_3 precursor. As-received powder consists two broad peaks and an explicit sharp peaks B_2O_3, Figure 4.2(a). This indicates that the starting powder is partially amorphous and partially crystalline. XRD pattern of the one having a feed rate of 1.1 slpm CH_4 carries the traces of the starting B_2O_3 powder, Figure 4.2(b). As the flow rate of CH_4 increases, the intensities

of free carbon peaks are getting stronger, Figure 4.2(c), (d). The patterns of the experiments carried out with -325 mesh B_2O_3 were analyzed by Rietveld refinement and the weight percentage of phases are tabulated in Table 4.2. It is seen that the powder synthesized with 1 g/min B_2O_3 and 1.1 slpm CH_4 is under the substantial dominancy of B_2O_3 phase. The increase in the rate of CH_4 enhances B_4C leastwise, but carbon percentage in the synthesized powders apparantly enters to the structure a lot more.

XRD pattern of the second set of samples with the federate of 2 g/min are given in Figure 4.3. It is seen that the carbon intensities are persisting with higher CH_4 flow rate despite the doubled B_2O_3 amount per minute, however, there is a considerable enhancement in carbon intensities between 2 and 2.2 g/min. The phase percentages of the patterns of the second set of experiments these patterns are also given in Table 4.2. When the same CH_4 flow rates for both 1 and 2 g/min B_2O_3 are considered, the resultant powder obtained by higher boron feeding rate consists of higher carbon phase percentages despite the presence of higher boron amount in the system. This must be resulted from the use of higher total feeding rate into the plasma generated with the same conditions, which lowers the available enthalpy per the unit particle. Hence, the general temperature distribution is decreased in the plasma, leading to lower vaporization degree for solid precursor.

The fact that the presence of the significant accumulation of powders at the bottom and cyclone indicated the complete evaporation of precursors could not be achieved. The collected powders from nanopowder collector were the evaporated fraction of the precursors. The average crystallite sizes of synthesized nanopowders were calculated in the range of 66 to 114 nm range. This implies that the high fraction of vaporized B_2O_3 precursor was not undergone to the reaction, instead, it was formed as ultrafine and nanometer sized B_2O_3 due to only evaporated and recondensed during the plasma processing. Also, the broadening of the peaks of B_2O_3 is an indication of the powders getting finer in size when compared to the raw pattern. This is an indication of insufficient enthalpy present for the solid precursors to be involved into the reaction.

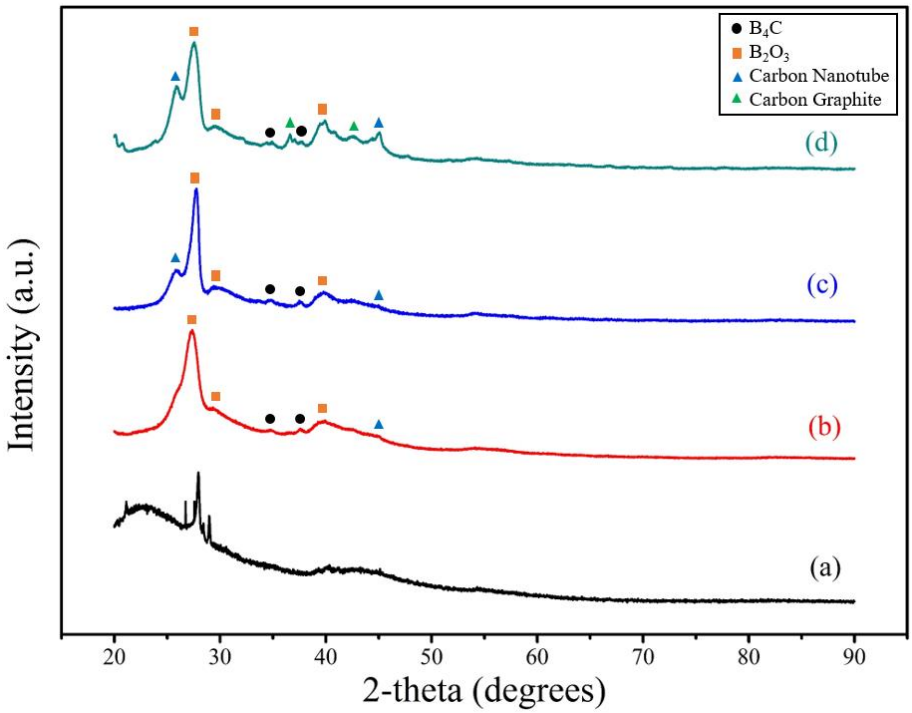

Figure 4.2 XRD Patterns of the first set samples (1 g/min B_2O_3)
(a) as-received B_2O_3 powder (b) 1.1 slpm CH_4 (c) 1.5 slpm CH_4 (d) 2 slpm CH_4

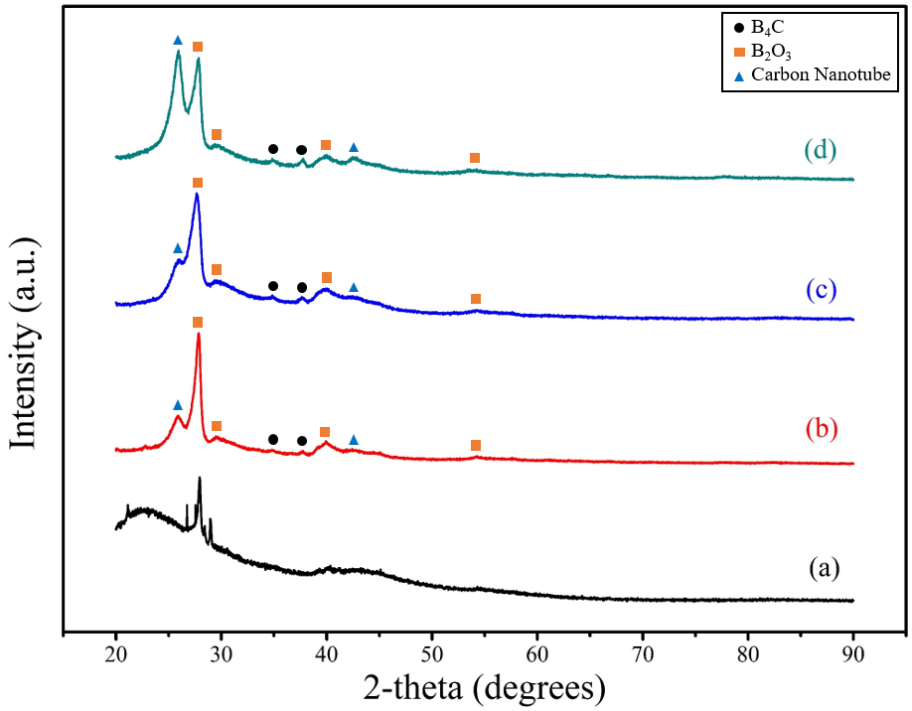

Figure 4.3 XRD Patterns of the second set samples (2 g/min B_2O_3)
(a) as-received B_2O_3 powder (b) 1.5 CH_4 slpm (c) 2 slpm CH_4 (d) 2.2 slpm CH_4

The experiments conducted with fine B_2O_3 are said to be successful in a way that all samples contain B_4C with regard to analyze the XRD patterns. Yet, all of the experiments shows substantial amount of B_2O_3 and free carbon. Since B_2O_3 dissolves in methanol, it is possible obtain a product much richer in B_4C content. For this purpose, two samples from each set (1 g/min B_2O_3 -1.5 slpm CH_4 and 2 g/min B_2O_3 - 2.2 slpm CH_4) was selected and they were washed with methanol.

Each sample was put into a breaker and methanol was poured onto the samples. The breaker was ultrasonicated for half an hour. After the sonication process, the liquid in the breaker was slowly poured onto the filter paper in order to eliminate the +0.45μm particles from the suspension. The suspension passed through the paper were collected and the liquid was evaporated leaving behind a solid powder

Figure 4.4 shows that XRD pattern powders before and after the methanol-washing process of 1 g/min B_2O_3 - 1.5 CH_4. The strongest B_2O_3 peak around 28^O was completely vanished along with its entire peaks. The elimination of B_2O_3 peak made B_4C more visible after methanol wash and the samples were made up of B_4C and carbon nanotubes. The weight fraction of B_4C after methanol was as high as 38 %.

The results with regard to 2 g/min B_2O_3 are given in Figure 4.5. Here the observations are the same. B_4C weight fraction after methanol was 23 %. This value is less than that obtained with 1 g/min B_2O_3 since the resultant powder obtained with 2 g/min contains higher in carbon content which cannot be eliminated by methanol-washing. The presence of free carbon was not desired and its elimination was not easy from the powder product as in the case of B_2O_3 rather it is generally separated by chemical reaction, which deteriorates both mechanical properties and morphology of the particles.

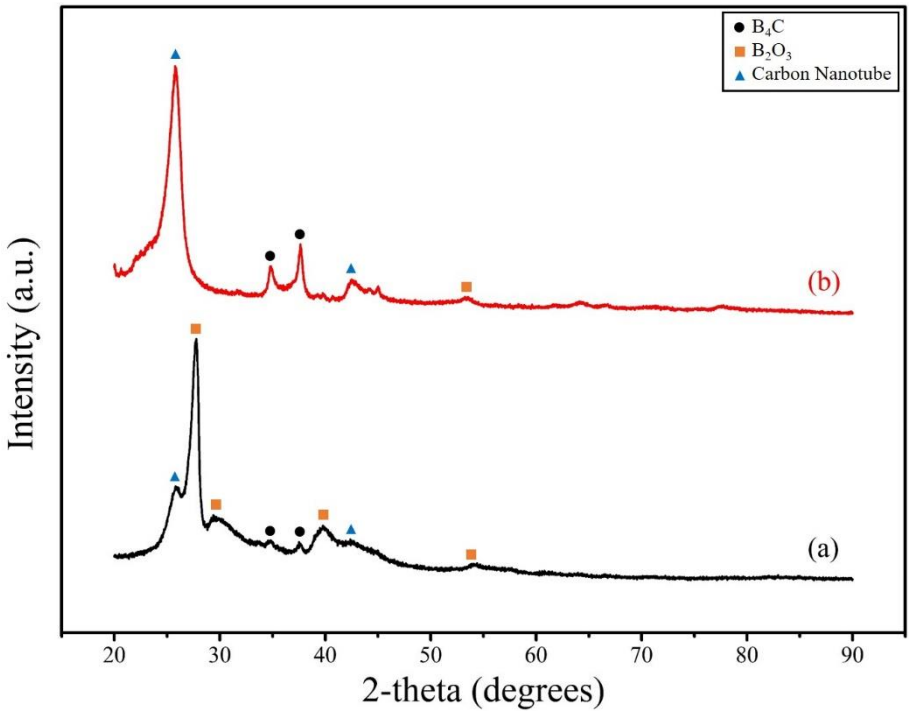

Figure 4.4 XRD Patterns of the synthesized sample 1 g/min B_2O_3 1.5 slpm CH_4 (a) as-synthesized (b) methanol-washed

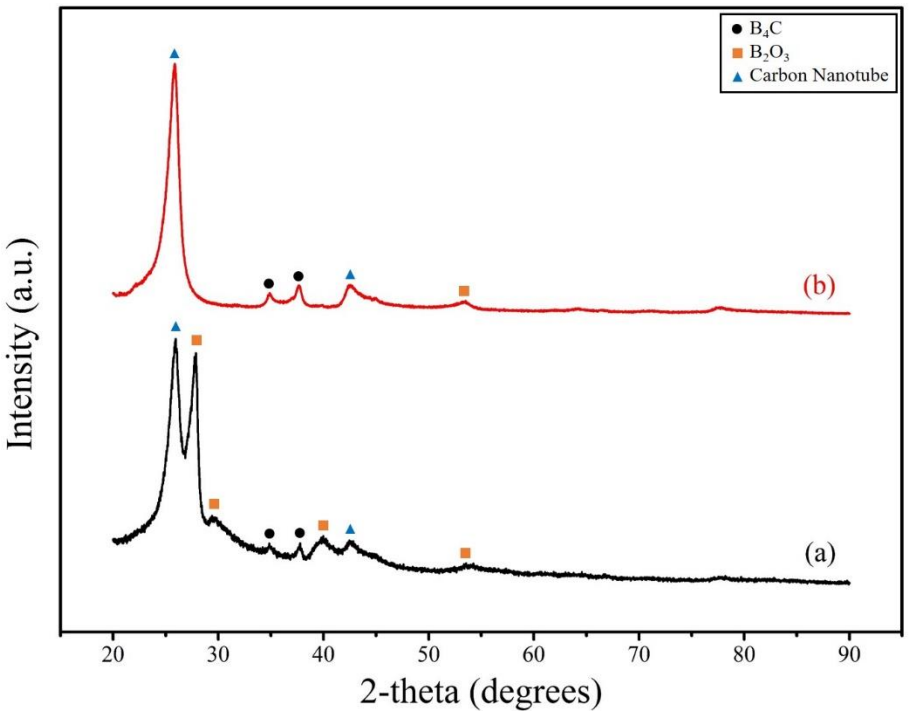

Figure 4.5 XRD Patterns of the synthesized sample 2 g/min B_2O_3 2.2 slpm CH_4 (a) as-synthesized (b) methanol-washed

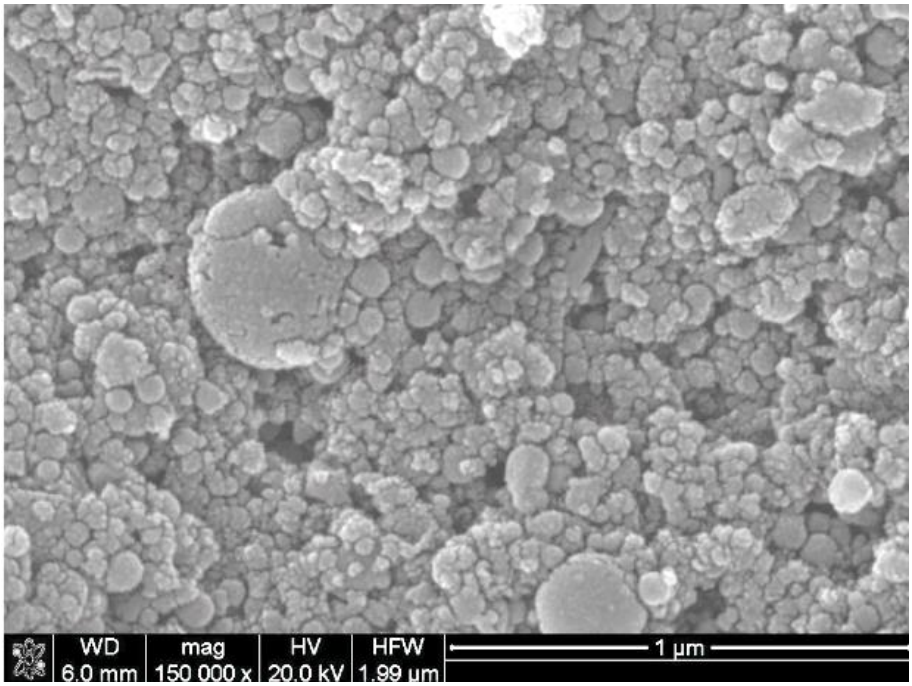

(a)

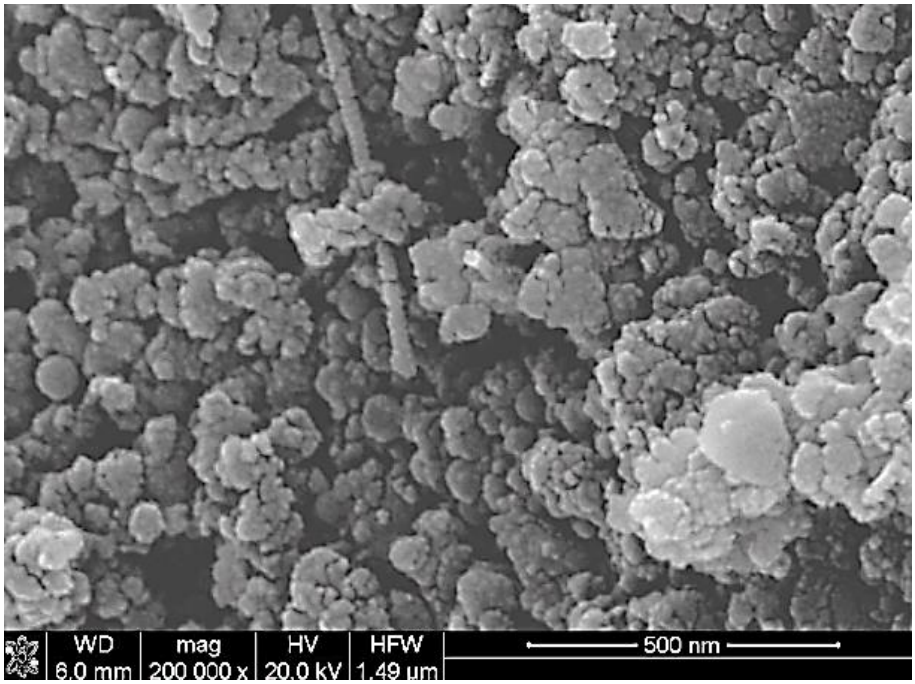

(b)

Figure 4.6 SEM images of the washed samples

(a) 1 g/min B_2O_3 1.5 slpm CH_4 (b) 2 g/min B_2O_3 2.2 slpm CH_4

According to SEM images, carbon was not observed as a distinct phase in Figure 4.6(a), yet XRD pattern indicates a vast amount of carbon present in the sample. The formation of carbon phase at a great quantity in the sample synthesized was due to the use of higher CH_4 rather than a necessary flow to obtain pure B_4C. However, Figure 4.6(b) belongs to the specimen obtained with exact stoichiometric ratio of B_2O_3 to CH_4 for 2 g/min of B_2O_3 feeding rate theoretically. It was seemed that B_4C particles were surrounded by carbon matrix and the black regions were compared with white particles in terms of weight percent by EDS data. Despite the inaccuracy of EDS for low-atomic elements due to the detector, the difference was quite high that verified the black regions were carbon rich in the structure. This also shows the increased amount of precursor per time at the plasma region due to the doubled B_2O_3 precursor. It is not expected to enhance vaporization degree in the sample synthesized with 2 g/min B_2O_3 and 2.2 slpm CH_4 while B_2O_3 could not be fully evaporated with low feeding rate of precursors.

The other reason why there existed substantial amount of B_2O_3 remained before the washing with methanol must be due to the improper feeding of B_2O_3 powders causing unstable feeding rates. During the synthesis it was seen from the translucent HDPE pipes that B_2O_3 was being flowed as accumulatively or none at all. B_2O_3 was present in excessive amount with respect to carbon at the plasma region when B_2O_3 entered as accumulated amount. Similarly, carbon was higher when there was no flow of B_2O_3 entering to the plasma. Thus, the samples were consisted of B_2O_3 and carbon phase much higher than B_4C.

The experiments carried out with B_2O_3 powders as boron source and CH_4 gas as carbon source revealed that there existed high amount of boron oxide in as-synthesized product and the increase of the flow rate of CH_4 led to the formation of free carbon rather than enhancing boron carbide synthesis. The vibrational feeder was not stable to feed B_2O_3 powders properly, resulting in non-uniform precursor at the plasma region. Even the proper feeding had been satisfied, the resultant powder would not have been rich in boron carbide, since the experiment showed there was incomplete evaporation of solid precursors and the vaporized powders could not be involved into the reaction. Therefore, the use of liquid precursor was considered.

4.2 Thermal Plasma Synthesis of B_4C from Trimethyl borate (TMB)

The solution of B_2O_3 and methanol was considered as the use of a single liquid precursor rather than two separate sources for the synthesis of B_4C. In order to achieve the compositional stoichiometry of B_4C in the precursor, the solubility of B_2O_3 in methanol was determined and compared with requirements of Eq.(4.1).

First 200 ml methanol was prepared and B_2O_3 powders were added into it until methanol could not dissolve B_2O_3 anymore. The conducted experiments revealed that 45 grams of B_2O_3 are readily soluble in methanol, which showed that the solubility of B_2O_3 was 225 grams per 1-liter methanol.

According to Eq.(4.1) it is necessary to have C:B ratio equal to 7:4 to obtain B_4C. Simple calculation shows that in order to satisfy the required stoichiometry it is necessary to have 492 g B_2O_3 in 1 liter of methanol. Since the solubility limit of B_2O_3 in methanol is nearly half of this value, an additional source of boron would be needed to obtain B_4C or if B_2O_3-M was fed with its maximum solubility there would be definitely free C together with B_4C

In this work rather than preparing B_2O_3-M solution as in above, the use was made of azeotrope trimethyl borate-methanol solution. This precursor (TMB-M) is a white-colorless liquid at RT with the boiling point of 54.41^{O}C (Samuel and Frank 1955) and the proportions of the constituents are the same in both liquid and vapor phase due to being the azeotrope at 30 vol.% methanol and 70 vol.% TMB. TMB-M could therefore be fed into plasma at either liquid or gas phase without any change in the proportions.

TMB-M was used as both boron and carbon source for the synthesis of B_4C. 500 ml solution was fed into the plasma in gas phase with the peristaltic pump via an evaporator. The feed rate at the peristaltic pump was initially 16.6 ml/min, but this was reduced to 13.43 ml/min TMB-M into the evaporator. The thermal plasma parameters were the same as before, see Table 3.1, except for the quenching gas which was pure argon with a flow rate for 175 slpm.

During the run, there was an accumulation of 200 ml of dark-colored liquid in the bottom collector. This liquid was flammable. The run was otherwise successful in that powders accumulated at the nanopowder collector gray in color with needle-like shape, the accumulation of liquid in the bottom collector was a sign of improper feeding of the precursor, but the fraction accumulated at nanopowder reactor was sufficient to evaluate this experiment

XRD pattern of the collected powder is given in Figure 4.7(a). It shows that the synthesized powder consists of B_2O_3 and B_4C, B_6O phases. According to the Rietveld analysis, the phase percentages are 70.40 wt.%, 28.52 wt.% and 1.07 wt.%, respectively.

Figure 4.7(b) refers to the same sample after methanol-wash. The pattern is pure B_4C without any indication of carbon phase. This was also verified by Rietveld analysis given in Figure 4.8. The pattern is well-matched with B_4C with fit parameters σ =1.2 and R_w =8.7.

BET analysis of the washed sample indicates a specific surface area 76.95 m^2/g. The corresponding average particle size assuming that all particles have spherical shape was 31 nm. The SEM image of synthesized powders after methanol-wash is given in Figure 4.9(a). The particle size distribution of the synthesized powder was obtained by analyzing the SEM image and the mean particle size was calculated as 95 ± 1.18 nm The particle size difference between BET and SEM analysis implies that the particles were in the form of agglomerates.

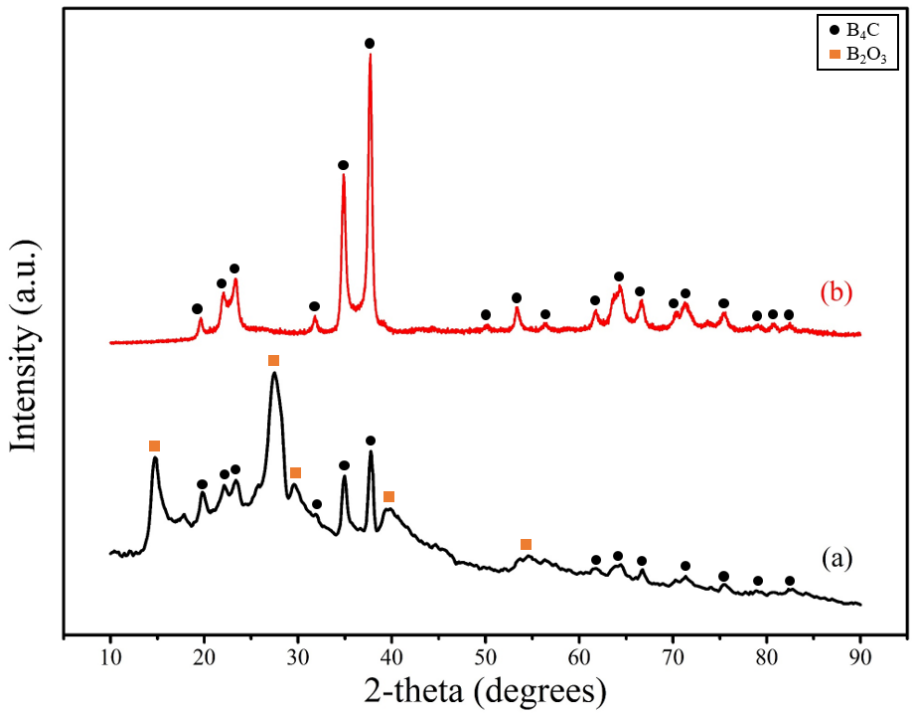

Figure 4.7 XRD pattern of the synthesis with TMB-M as single precursor
(a) as-synthesized (b) methanol-washed

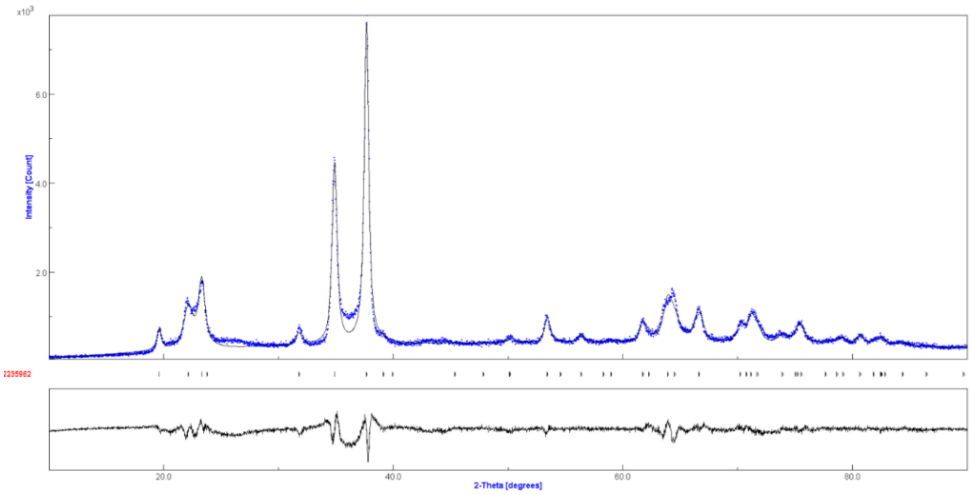

Figure 4.8 Rietveld analysis of methanol-washed sample (σ=1.2 and R_w=8.7)

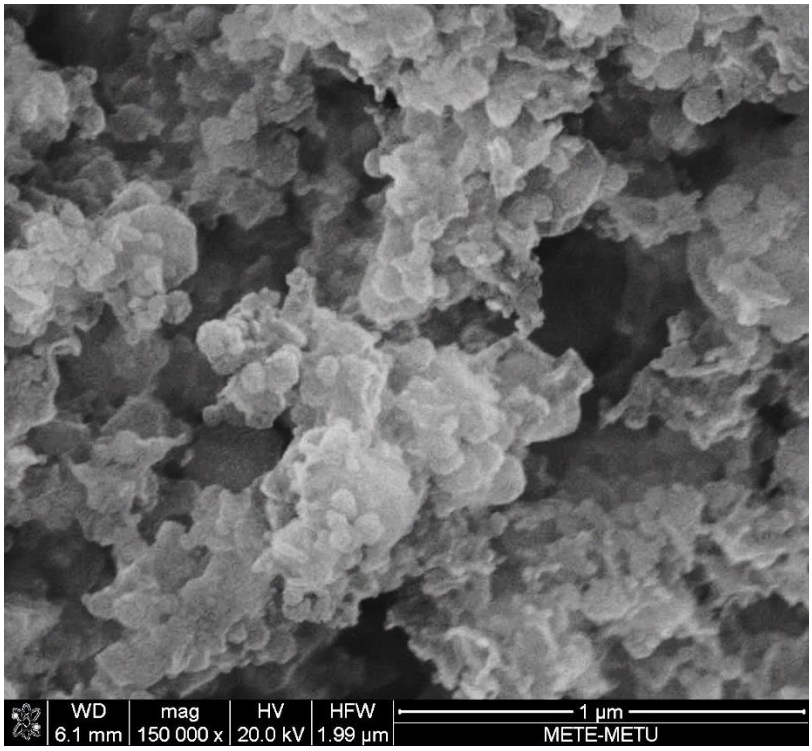

(a)

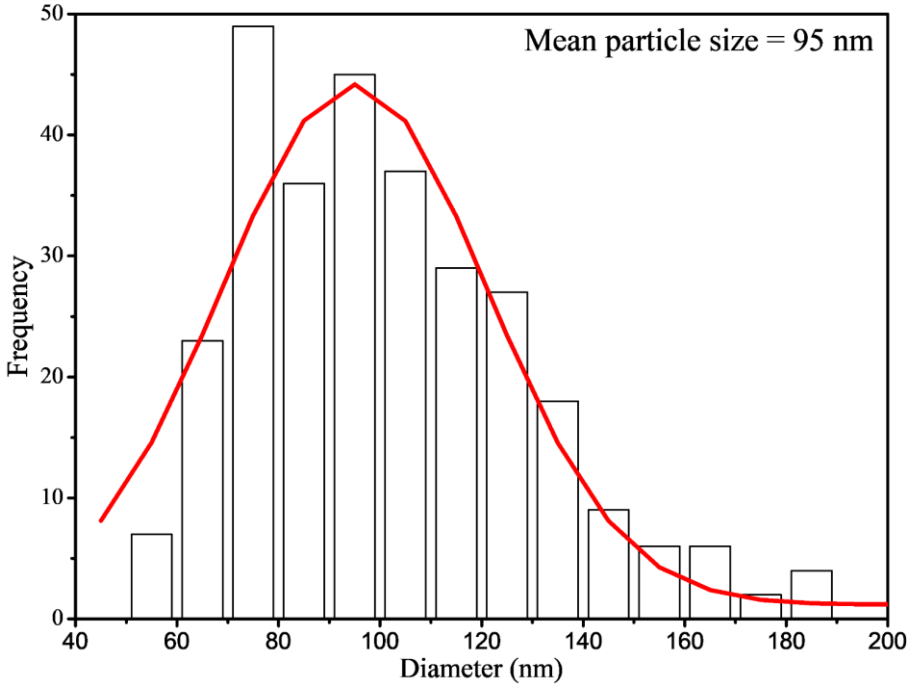

(b)

Figure 4.9 (a) SEM pattern ,(b) Particle size distribution of methanol wash powder synthesized by TMB-M as single precursor

4.3 Discussion

4.3.1 Thermodynamic Analysis

During thermal plasma processing there are a number of options depending on the environment in the reaction chamber. Carbothermic reaction is applicable for normal processing conditions but conditions prevailing in the thermal plasma are quite different. Fact-Web is a thermodynamic software which would allow detailed evaluation of equilibrium between reactants and the expected products using Equilib-Web module.

4.3.2 B_2O_3 – CH_4

Using Fact-Web the thermodynamic analysis was carried out on the reaction products as a function of temperature at a pressure of 1 atm for 1 mole of boron in B_2O_3 with stoichiometric CH_4.

The stability of reactants as well as the precursor can be followed in Figure 4.10. The presence of B_2O_3 first as solid and then liquid continues up to approximately 1500^OC. Similarly, CH_4 rapidly diminishes when the temperature reaches 1000^OC beyond which it dissociates into C and H. It should be noted that in the temperature window approx. between 1500 -2500^OC, the dominant phases are B_4C CO and H_2.

In classical carbothermic synthesis of B_4C, the above observations are equally valid. This is except for hydrogen since the ingredient used in carbothermic synthesis is C rather than CH_4.

Returning to the thermal plasma experiment with B_2O_3 with methane, it should be stressed that the precursors depending on their flight in the reaction zone are subject to various temperature history. In a properly done experiment with small particle size it is logical to assume that the precursors are subject to temperatures well in excess of 10,000 K. The graph clearly shows that the precursors are broken down to their elements as at 6000^OC there are (in the order of relative dominance) H, B, C and O. Only molecule which is present at this temperature CO which also show a sign of disintegration. Since temperature in the plasma is well in excess of 10000 K and it is

more appropriate to view that the precursors are all in elemental forms comprising elements H B, C and O.

In terms of product formation, it is more logical to look at the graph while cooling. Figure 4.10 shows that upon cooling boron has two options; it can either combine with C to form B_4C or it can combine with oxygen to form B_2O_3. It appears that in the current experiment both have taken place, but conditions are in favor of B_2O_3 formation as this was the dominant was in the product. Since CO ties up considerable fraction of C in the system, the relative dominance of B_2O_3 in the product would be the expected case.

4.3.3 TMB-M

Using FactSage, the thermodynamic analysis was carried out on the reaction products as a function of temperature at a pressure of 1 atm for 1 mole of TMB-M solution. Results are shown plotted in Figure 4.11. As seen in the figure, from TMB-M solid B_2O_3 starts to form around $400^{O}C$ and continues to be present in that form above $1000^{O}C$. It is liquid starting from $1500^{O}C$. The results clearly show that the stability region of B_4C extends from $1400^{O}C$ and $2500^{O}C$. It should be noted that beyond $3500^{O}C$ boron, carbon and oxygen are in elemental form. Since in thermal plasma the temperature reached could be well above 10000 K, it is logical to think that precursors are subject to a range of temperatures during their flights across the reaction zone.

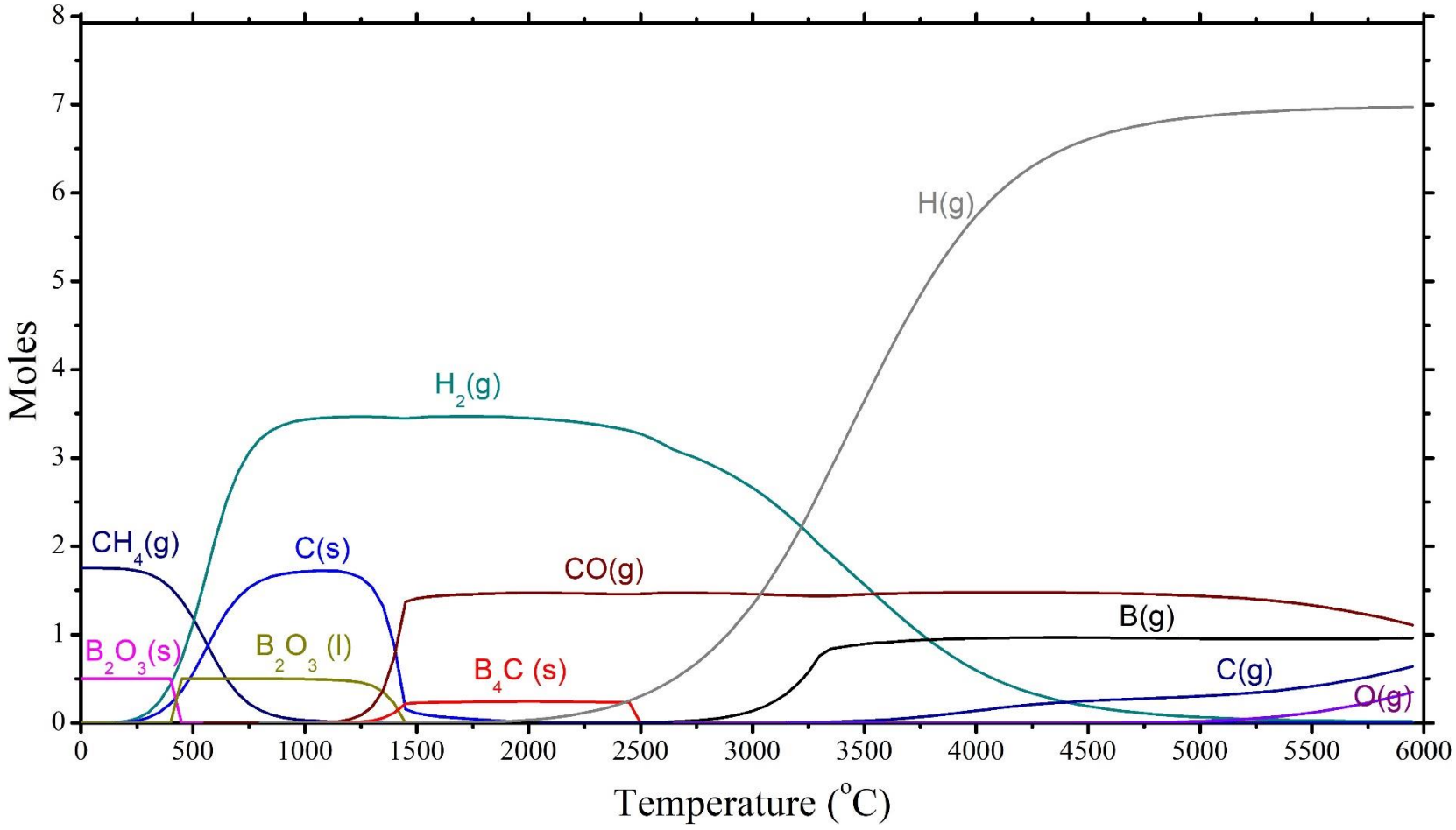

Figure 4.10 Equilibrium phases in 1 mole of boron containing B_2O_3 and stoichiometric CH_4 based on Eq.(4.1) a function of temperature under 1 atm pressure determined via Gibbs energy minimization (Bale and Bélisle 2016).

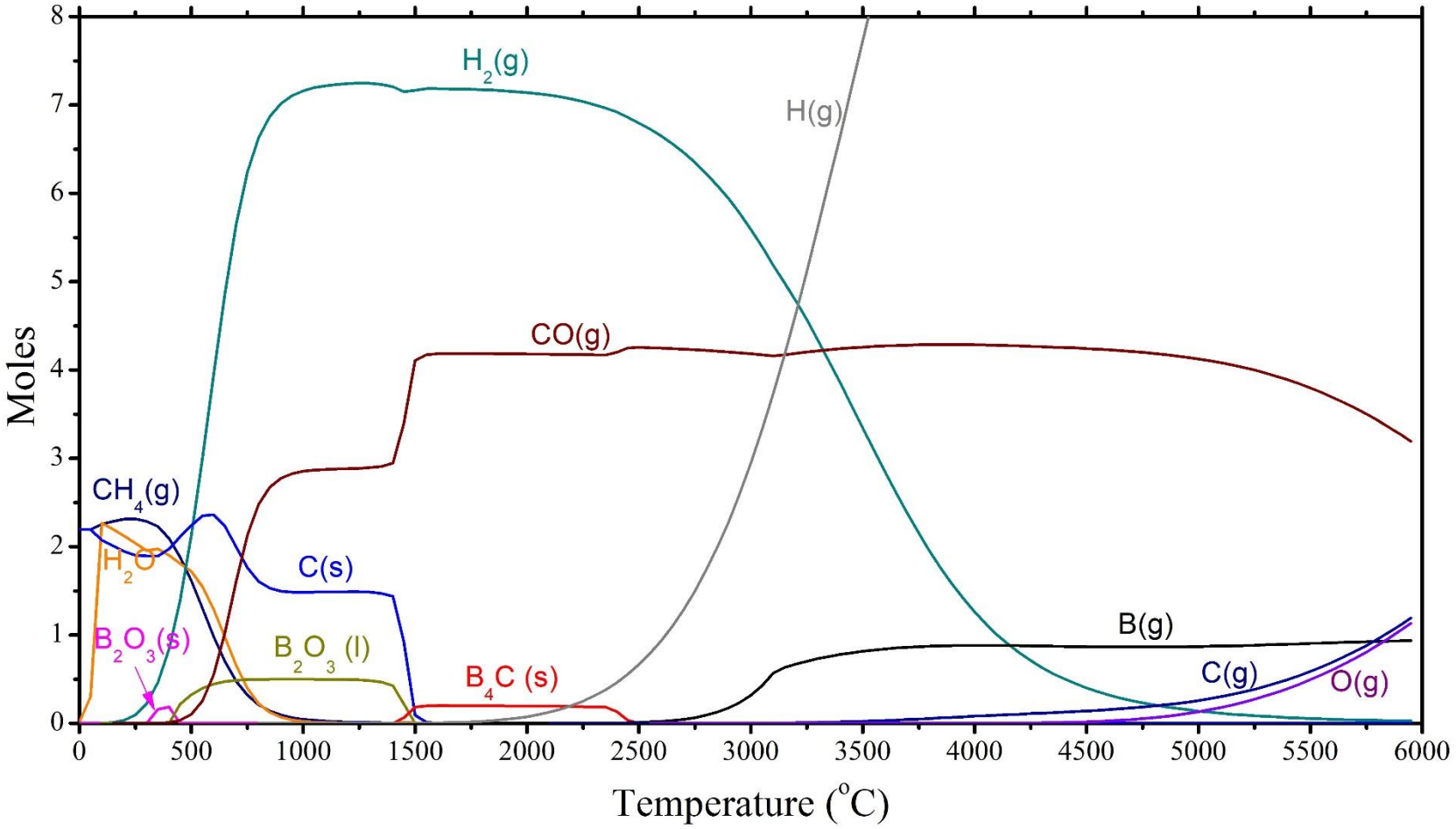

Figure 4.11 Equilibrium phases in 1 mole of boron containing in TMB-M precursor a function of temperature under 1 atm pressure determined via Gibbs energy minimization (Bale and Bélisle 2016).

In the synthesis with TMB-M there was no observation of carbon phase despite B_2O_3 formation. This probably occurred because the precursors were deficient in their carbon content. Considering the chemistry, 1 mole of TMB-M, would yield *0.25 moles* of boron carbide assuming a perfect yield, the amount of CO in the product would then be 2.75 mole. These values should be compared with the thermodynamic analysis given in Figure 4.12. According to this graph the amount of B_4C is 0.197. This implies that the difference, i.e. 0.053 mole of B_4C could not form because of thermodynamic reason. This value corresponds to the loss of one fifth of boron (0.21) from the initial TMB-M precursor. This experiment was quite successful in that the product consisted of B_4C (28 wt.%) and B_2O_3 (70wt.%) and after washing, the product was pure B_4C. Therefore, in order to improve the conversion efficiency, it would be necessary to increase C content of the precursor.

Table 4.3 The calculations assuming all boron in TMB-M is used to form B_4C in synthesis

	For 1 mole boron in TMB-M					
	Amount (grams)	**Amount (moles)**	**Moles of B_4C**	**Moles of C**	**Moles of C in B_4C**	**Moles of C in CO**
TMB (70%)	103.91	1	0.25	3	0.25	2.75
M (30%)	44.53	1.39	-	1.39	-	1.39
Total	148.4	-	0.25	4.03	0.25	4.14

.

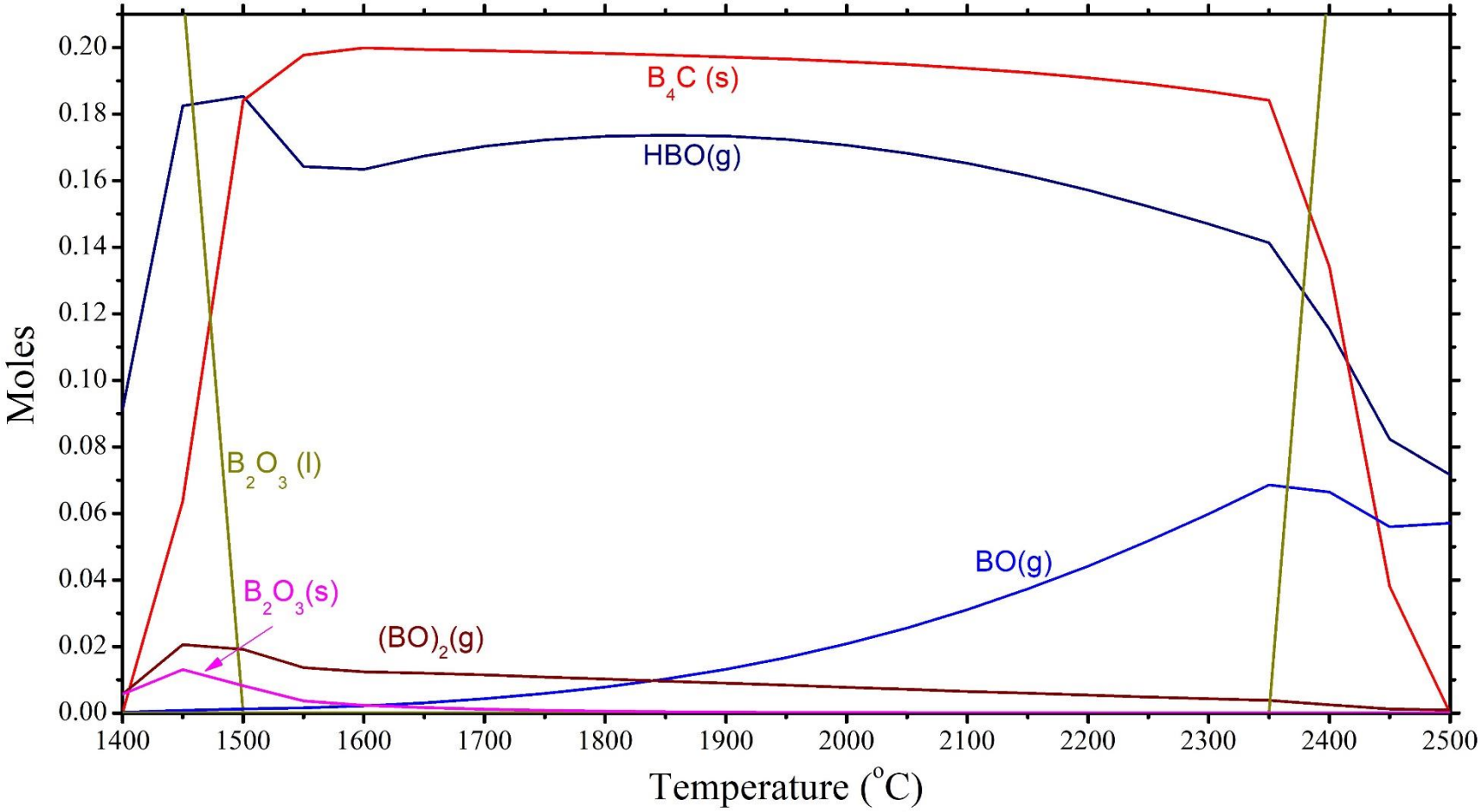

Figure 4.12 Equilibrium phases in 1 mole of TMB-M as a function of temperature under 1 atm pressure determined via Gibbs energy minimization. Note that The fraction of B4C is 0.197 mole. Also note the presence of other boron bearing compounds such as BO, HBO BO_2 etc.

4.3.4 TMB-M with hexane addition

The analysis above indicates that additional carbon would be needed so as to increase the conversion efficiency of B_4C in the synthesis. Hexane (C_6H_{14}) was used as an additional carbon source. It is soluble in methanol and has boiling point of 68^OC. Thus TMB-M with hexane is feedable into thermal plasma in gas phase.

The necessary amount of hexane addition was calculated based on Table 4.4. The basis was 1 mole of B_4C. It is assumed that in the synthesis of B_4C, carbon would be supplied by hexane and boron would come from TMB-M. The role of methanol in TMB-M was neglected since there would be no net C when it forms CO.

Table 4.4 The amounts of the sources for 1 mole of boron carbide in TMB-M with hexane

	TMB	**Methanol**	**TMB-M**	**Hexane**
Percentage in TMB-M	70	30	100	-
Molecular Weight (g/mole)	103.9	32.04	148.4	86.18
Density (g/ml)	0.932	0.792	0.885	0.655

Boron source	**B (mole)**	**Amount (g)**	**Carbon source**	**C (mole)**	**Amount (g)**
TMB-M	4	593.71	Hexane	1/6	14.36

The required volume fraction of hexane for the stoichiometric B_4C was calculated as 0.032. In this regard, 1-liter precursor was prepared by the addition of 32 ml hexane into 968 ml TMB-M and fed into the plasma as in the previous experiment, only difference was that the quenching gas was nitrogen (150 slpm) rather than argon

The XRD pattern of as-synthesized powders are given in Figure 4.13(a). B_2O_3 peaks are again visible on the pattern with B_4C but carbon phase was not as clear. After elimination of B_2O_3 with methanol wash, the carbon peaks are observed. The resulting product was 72 wt.% B_4C ad 28 wt.% C.

The hexane addition was increased to 60 ml (940 ml TMB-M) so as to prevent B_2O_3 formation and the experiment was repeated. It was found that there was still significant amount of B_2O_3 present. The intensities of carbon peaks were higher as

the addition was increased. In fact, the carbon addition adulterated the purity of the powders rather than suppressing B_2O_3 formation. In consequence, the attempts to improve the efficiency of boron carbide synthesis with the addition of hexane was not successful. As already pointed out B_2O_3 could be eliminated by methanol wash. But carbon cannot easily be removed from the product.

The existence of B_2O_3 and C in the product probably originates from the same reason, i.e. B combines with oxygen forming B_2O_3 leaving C uncombined in the product. Therefore, to increase the conversion efficiency, it would be necessary to tie up oxygen so that B would combine with C. It is well known that NO_x compounds are quite stable and therefore they could be used to tie up oxygen at elevated temperatures.

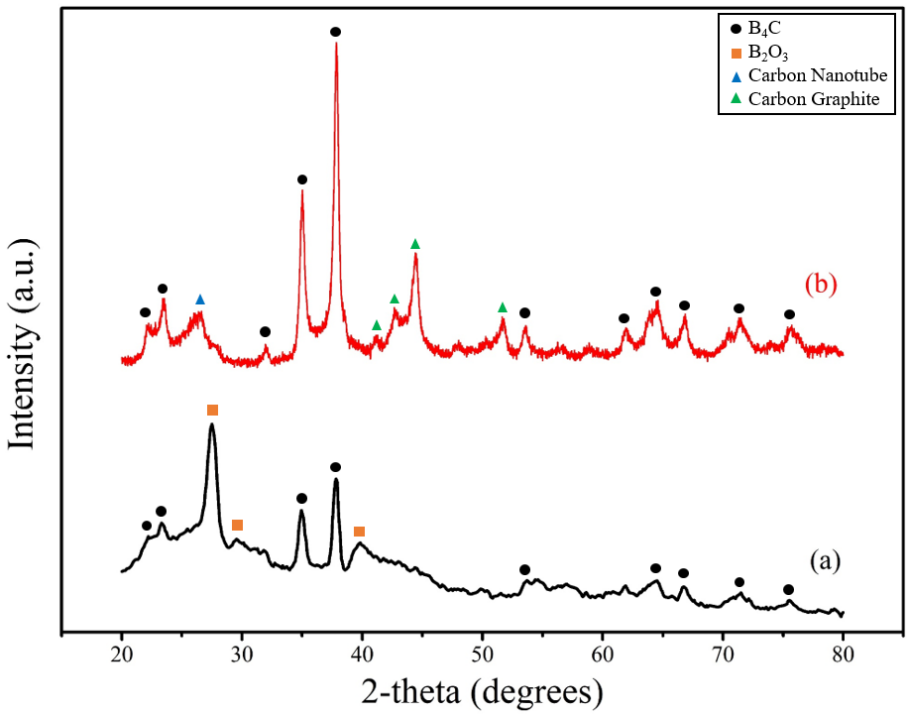

Figure 4.13 XRD pattern of the synthesis with TMB-M with 30 ml hexane addition (a) as-synthesized (b) methanol-washed

4.3.5 TMB-M with Diisopropylamine ($C_6H_{15}N$) (DIPA) additives

Diisopropylamine ($C_6H_{15}N$) was used as nitrogen source to tie up oxygen as well as the additional carbon source. The importance of this replacement was to observe the effect of nitrogen existence in the system. The necessary amount of addition to TMB-M solution was calculated. This yielded 0.034 ml DIPA from data reported in Table 4.5 in a manner similar to that used with hexane.

The two different precursors of 500 ml containing 17 and 25 ml DIPA and the rest TMB-M were prepared. This was fed in liquid form rather than the gas form which was the case in the previous experiments. The precursors were mixed together and fed into the plasma with atomization probe. The thermal plasma conditions were the same as given in Table 3.1. The resulting powders were collected from the batch nanopowder collector

Table 4.5 Data related to the TMB-M with DIPA experiment

		TMB	**Methanol**	**TMB-M**	**Hexane**
Percentage in TMB-M		70	30	100	-
Molecular Weight (g/mole)		103.9	32.04	148.4	101.19
Density (g/ml)		0.932	0.792	0.885	0.717
Boron source	**B (mole)**	**Amount (g)**	**Carbon source**	**C (mole)**	**Amount (g)**
TMB-M	4	593.71	DIPA	1/6	16.87

Using FactSage thermodynamic analysis was carried out on the reaction products as a function of temperature at a pressure of 1 atm. This calculation referred to 1 mole of TMB-M solution with 0.042 mole of DIPA (this corresponds to 17 ml DIPA in 500 ml solution). The results are given in Figure 4.14. The formations of solid and liquid B_2O_3 are quite similar as that reported for TMB-M. This is as would be expected since DIPA contains no boron and no oxygen.

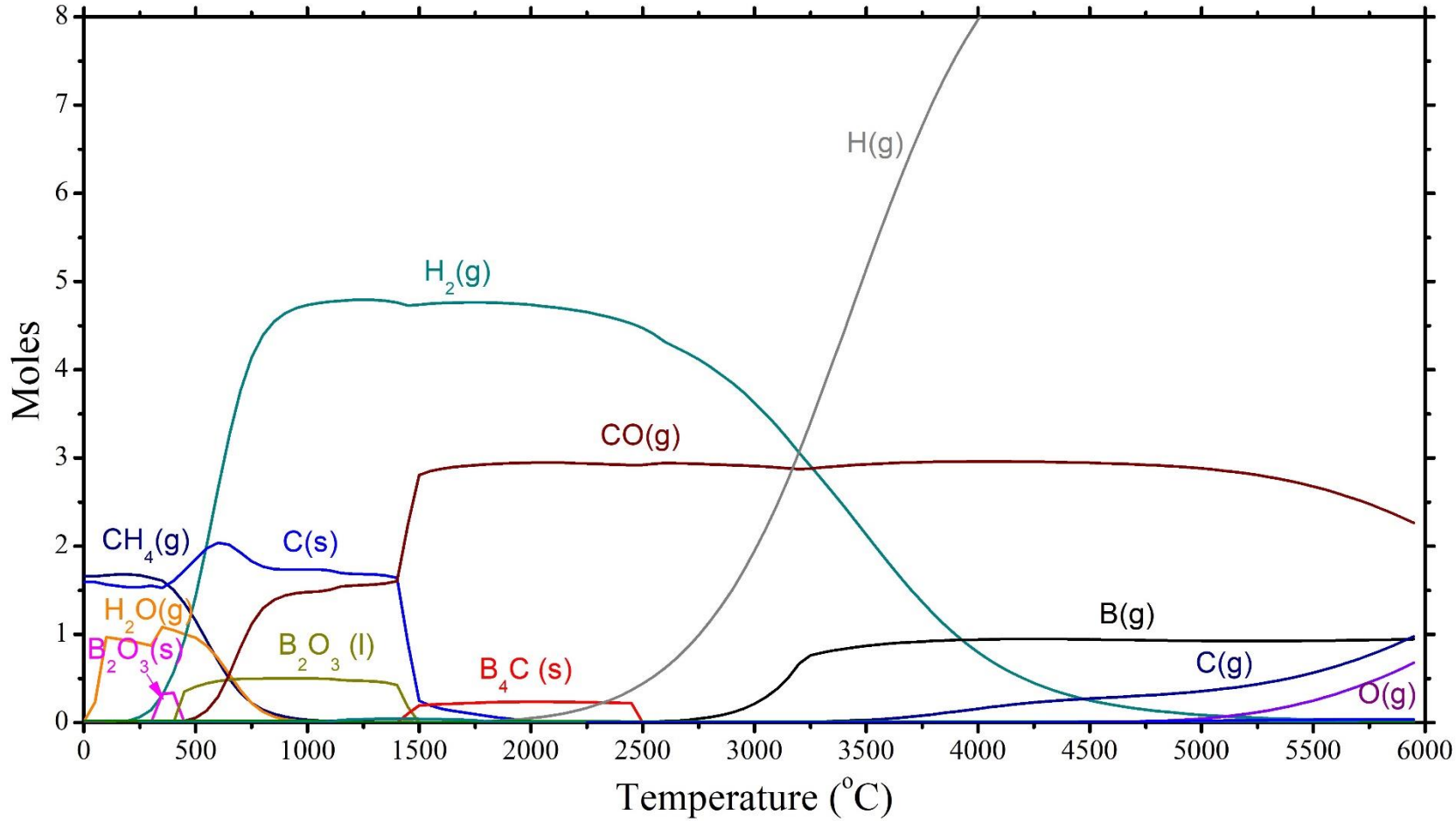

Figure 4.14 Equilibrium phases in 1 mole of boron containing in 500 ml TMB-M with 17 ml DIPA precursor as function of temperature under 1 atm pressure determined via Gibbs energy minimization (Bale and Bélisle 2016).

Above 3500^{O}C temperature boron, carbon and oxygen are in elemental form. There exists elemental nitrogen gas and nitrogen oxide (NO_x) above 4000^{O}C on the graph but their amount is very low. Our calculation was limited up to a temperature of 6000^{O}C. The trend of NO is such that the fraction NO probably increases at higher temperatures. Since in thermal plasma, the temperature reached could be well above 10000 K, the presence of NO would be expected to reduce the available oxygen for B_2O_3 formation. Hence, the boron and carbon would be constrained to form boron carbide only.

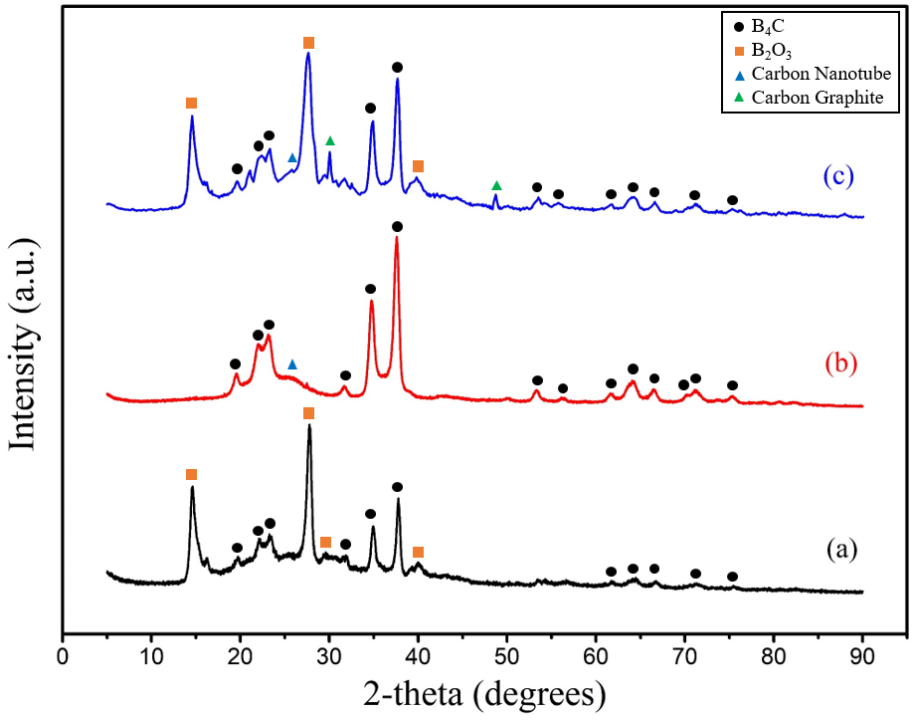

Figure 4.15 XRD pattern of the synthesis with TMB-M with DIPA addition
(a) 17 ml DIPA as-synthesized (b) 17 ml DIPA methanol-washed (c) 25 ml DIPA as-synthesized

Upon processing the solution of TMB-M mixed with DIPA (500 ml TMB-M with 17 ml DIPA in), the resulting powder was analyzed with X-ray diffraction. Figure 4.15(a) shows the pattern where B_2O_3 and boron carbide peaks are clearly seen in synthesized powder. B_2O_3 peaks have lower intensity than that in previous experiments, which is a sign of that nitrogen addition was helpful in improving the synthesis of boron carbide. The Rietveld analysis indicates that the powder is made up of 54.66 wt.% B_4C, 37.62 wt.% B_2O_3 and 7.72 wt.% carbon. XRD pattern after

methanol washing is given in Figure 4.15(b). B_2O_3 phase washed away, C peak now is quite visible. An additional experiment was carried out where the DIPA content was increased to 25 ml. The XRD pattern resulting from this mixture is shown in Figure 4.15(c)). This has led to significant increase the carbon content and also the content B_4C seemed to be higher than that of B_2O_3.

When compared to 32 ml hexane addition which supplied the same mole fraction of carbon to the precursor (Figure 4.13(b)), XRD pattern of TMB-M with 17 ml DIPA methanol-washed powder is very clean in terms of carbon content. The phase percentages were found as 87.32 wt.% B_4C and 12.68 wt.% carbon with an average crystallite size of 86 nm by Rietveld method. TEM image of the sample is given in Figure 4.16(a). The particles are spherical in shape due to homogenous nucleation of clusters at the reactor during plasma processing. The particle size distribution was obtained by measurements over 500 particles in SEM images. This has yielded the mean particle size of 61 ± 5.7 nm (Figure 4.16(b)).

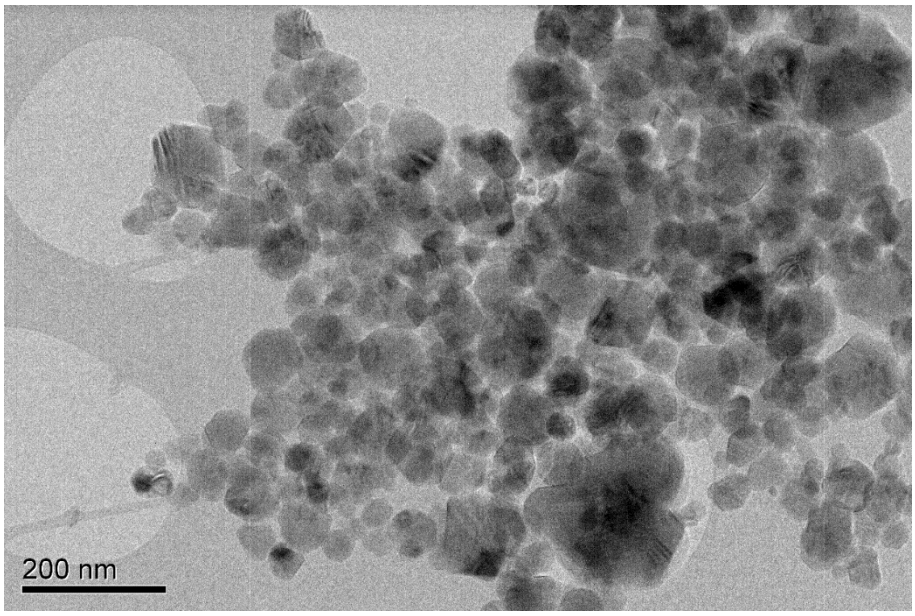

(a)

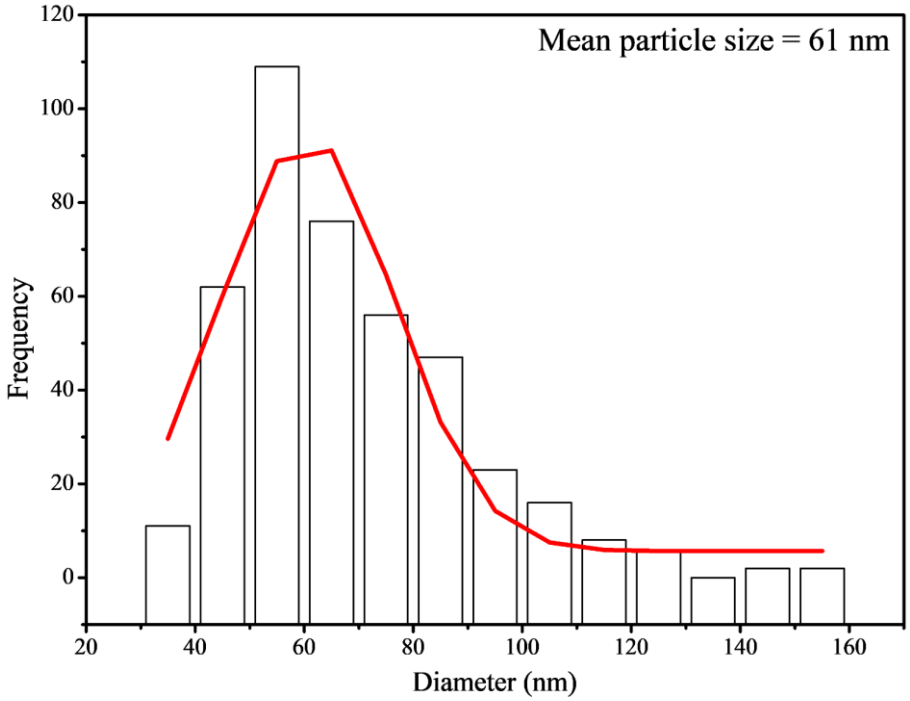

(b)

Figure 4.16 (a) TEM image (b) Particle size distribution of particles obtained by methanol-washing of TMB-M with 17 ml DIPA

4.3.6 TMB-M with Diisopropylamine ($C_6H_{15}N$) and Nitrogen additives

Noting the favorable effect of nitrogen in the previous experiment, an additional experiment was carried out using 483 ml TMB-M-17 ml DIPA fed with a rate of 12 ml/min together with nitrogen which was used as carrier gas with a rate 5 slpm.

Using FactSage the thermodynamic analysis was carried out on the reaction products as a function of temperature at a pressure of 1 atm for solution. As seen in the Figure 4.17, the increased amount of N_2 gas alters the diagram considerably. Solid B_2O_3 formation is favorable in a narrow range between 250^{O}C and 450^{O}C; beyond this the compound is liquid and continues up to 1000^{O}C. At this interval C is also stable. The introduction of large amount of nitrogen has stabilized BN(s) over a quite wide range of temperature between 1000^{O}C to 2250^{O}C. It is clearly observed that the current conditions forces boron carbide to shrink into a narrow range centered on 2350^{O}C.

While C, O, H and B occur in elemental form above 4000^{O}C, N_2 gas is still in molecular form and largely remain so up to 6000^{O}C, i.e. the maximum temperature studied in this work. The elemental N is formed starting from 3500^{O}C. The same is true for NO. But their fractions are quite small at this temperature but tend to increase with increasing temperature. Another phase which is present at 2500 - 6000^{O}C is CN(g).

Two experiments were carried out with nitrogen input. The experiments were rather special in that a flue gas analyzer was connected to the exhaust gas which allowed monitoring of CO. There were two experiments carried out with a precursor composed of with two different feeding rates. The liquid precursor 483 ml TMB-M with 17 DIPA was fed into the plasma with 12 ml/min.

Two nitrogen flow rates were employed, 0.012 and 5 slpm. 0.012 slpm flow rate was calculated by assuming that all boron in the TMB-M would be used for boron carbide synthesis and the remaining carbon in the precursor was to combine with oxygen to form CO. The excess oxygen was left to react with nitrogen.

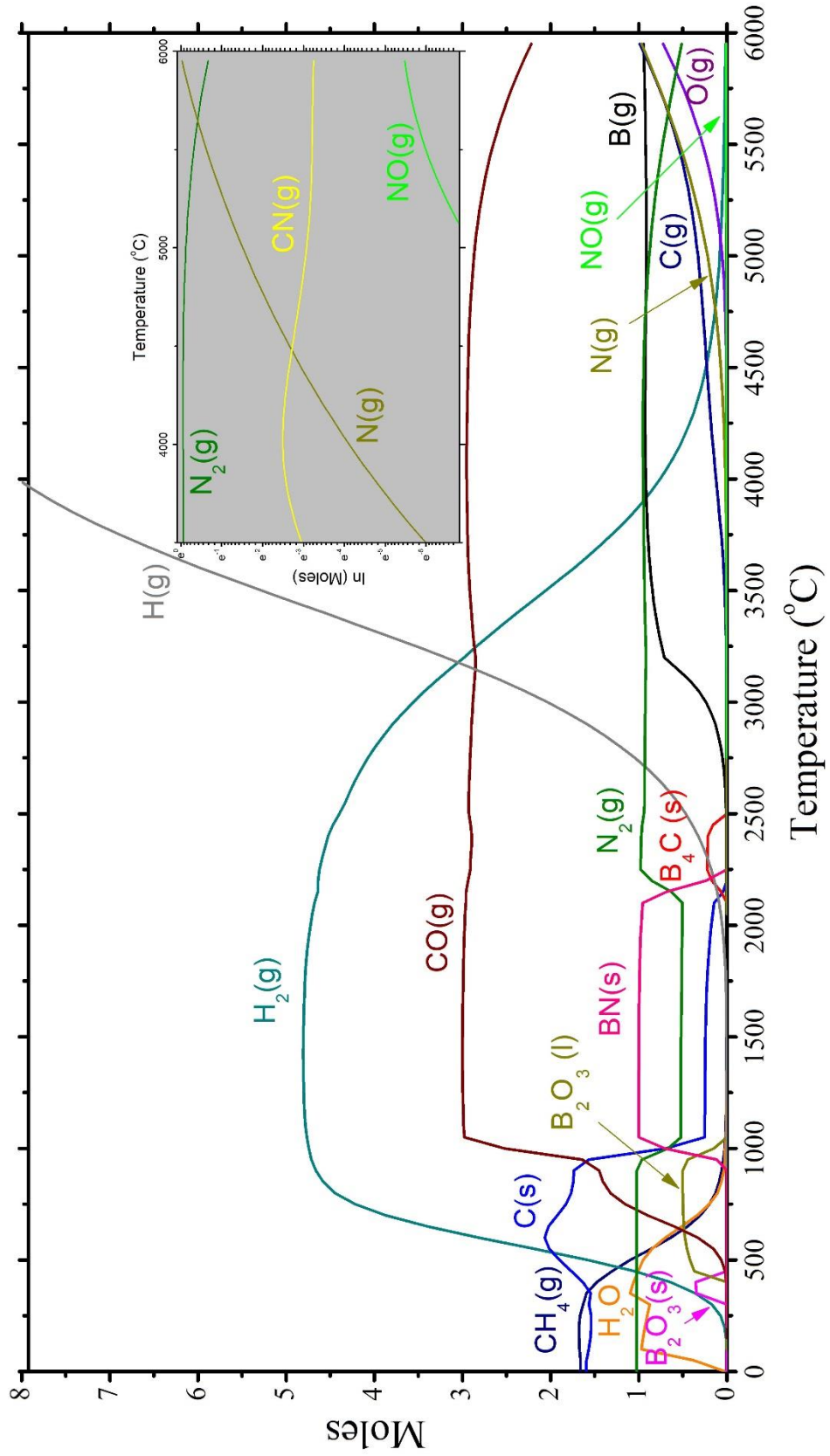

Figure 4.17 Thermodynamic graph of feasible products of normalization to 1 mole of boron containing in 500 ml TMB-M with 17 ml DIPA and 5 slpm N_2 precursor

CO content monitored by flue gas analyzer is reported in Figure 4.18. The initial part refers to the experiment where the flow rate of N_2 was 0.012 slpm. The CO content fluctuates. This was probably due to insufficient control of nitrogen flowmeter, i.e. flow rate could not be adjusted properly. Throughout this period of 45 minutes the synthesized product was collected in the first cone collector. As soon as the flow was switched to the second collector, the flow rate of nitrogen was increased gradually. There was a gradual decrease of CO content in the flue gas as can be seen in Figure 4.18. The flow rate of nitrogen was increased until there was no reduction of CO content in the flue gas. This value was 5 slpm N_2. Therefore, the second experiment was carried out with 5 slpm N_2. After 35 min, the experiments were finished.

XRD pattern of synthesized powder from the first cone collector, i.e. 0.012 slpm N_2 is given in Figure 4.19(a). This diffractogram is very similar to the that of powder obtained with TMB-M with DIPA without nitrogen addition, see Figure 4.15(a). Nitrogen could have formed NO_x by bonding with oxygen, but, its amount must have been so low that there was no distinguishable effect of it on XRD pattern.

XRD pattern from the second cone of collector is given in Figure 4.19(b). Here, the nitrogen flow rate of 5 slpm did make an impact on the synthesized powder. The decrease in the intensities of B_2O_3 peaks are clear.

This is clearly seen in Table 4.6 where the phase fraction of constituent in the resulting power were calculated both for 0.012 slpm N_2 and 5 slpm N_2. B_2O_3 which had a weight fraction of 0.35 with 0.012 slpm N_2 was decreased to 0.24 when the nitrogen flow rate was increased to 5 slpm. The values for B_4C were 0.57 and 0.70 in the respective order.

Table 4.6 Phase percentages present in the powder product obtained by nitrogen carrier gas for TMB-M with 17 ml DIPA

	B_4C	B_2O_3	Carbon
0.012 slpm N_2 – as-synthesized	57.40	35.28	7.33
5 slpm N_2 – as-synthesized	69.64	23.94	6.42
5 slpm N_2 – methanol-washed	91.33	-	8.67

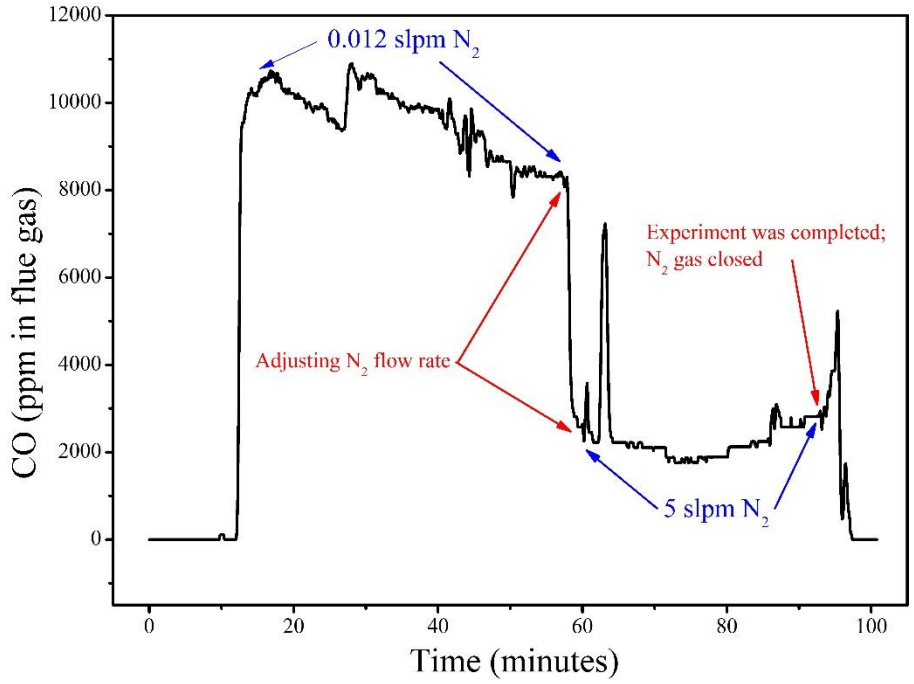

Figure 4.18 Syngas data of CO amount ppm in the flue gas during nitrogen used as carrier gas

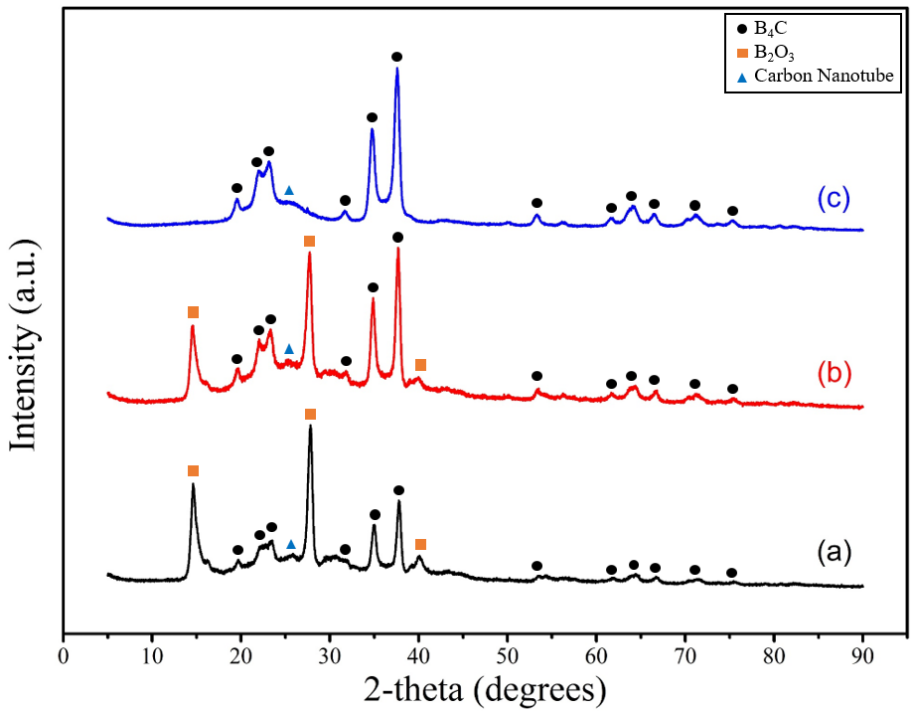

Figure 4.19 XRD patterns of the synthesis carried out by TMB-M with 17 ml DIPA fed by N_2 (a) as-synthesized by 0.012 slpm N_2 (b) as-synthesized by 5 slpm N_2 (c) methanol-washed by 5 slpm N_2

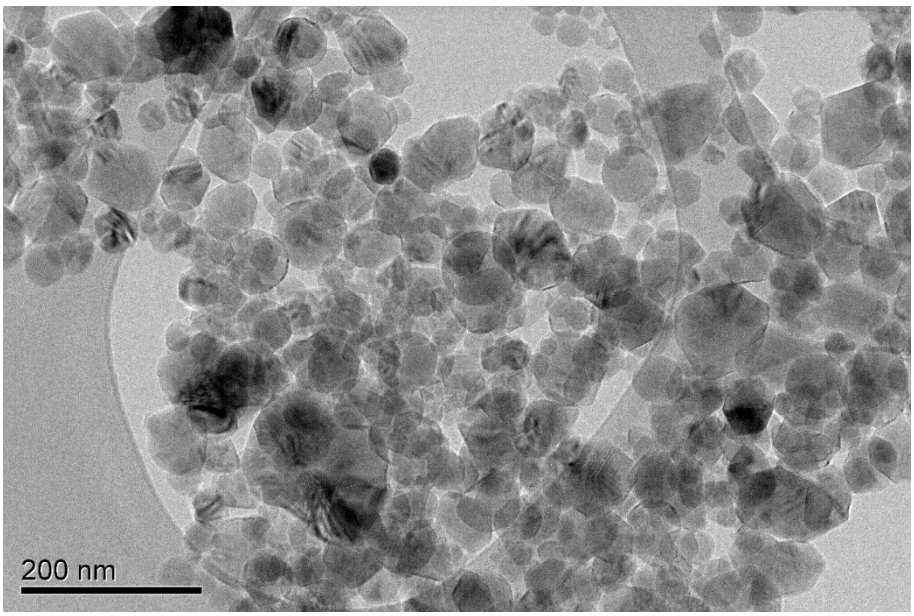

(a)

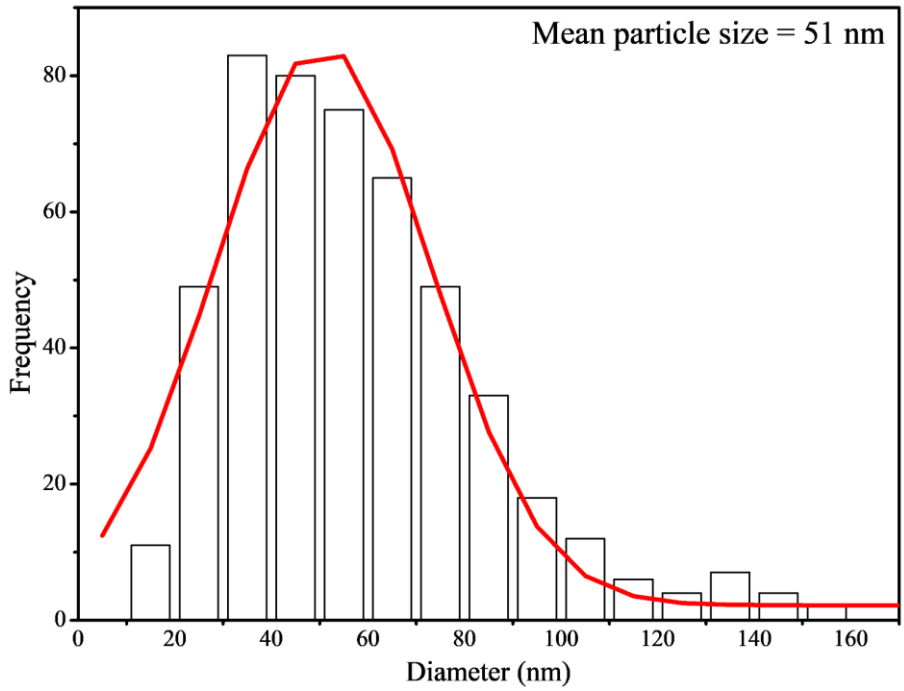

(b)

Figure 4.20 (a) TEM image (b) Particle size distribution of particles obtained by methanol-washing of TMB-M with 17 ml DIPA-5 slpm N_2

The increase in the weight fraction of B_4C and the decrease in B_2O_3 content have probably resulted from the tying up of oxygen with nitrogen in the form of NO_x gas. Thus, CO in the flue gas was suppressed by the application of nitrogen gas. Surprisingly, there were no condensed nitrogen phase in the XRD pattern. The excess nitrogen remained must have been departed from the system as N_2 gas.

The synthesized powders were subjected to methanol washing and this gave the phase percentage of 91.33 wt. % B_4C with 8.67 wt. % carbon in the resultant powder. The presence of 8.67 wt. % carbon as discussed by Shi *et al.* (2015) could actually beneficial and may act as a sintering agent suppressing the formation of boron suboxides

Figure 4.20(a) shows SEM micrograph of the sample produced from TMB-M–DIPA with 5 slpm N_2 after methanol wash. The powders have a mean particle size of 51 ± 2.2 nm which a rather narrow range.

The boron carbide synthesis in the washed product could be approximately 70 wt.% and It was possible to be improve this to 91.33 wt.% after methanol-washing. The use of atomizer probe was helpful in improving the conversion efficiency since with this method the precursor could be maintained into plasma in a more controlled manner. The nitrogen used as precursor was helpful by suppressing B_2O_3 formation whereby improving the efficiency of synthesis.

It should be noted that the recommended precursor as boron source was TMB-M. Considering a mole of TMB-M, i.e. 148.4 grams of TMB-M, the boron content in this compound is only 10.81 grams. This implies if all boron in the precursor was used up for boron carbide synthesis, the maximum amount of boron carbide would be 13.81 grams. This is only 9.3% of the total. Considering that the heat input in thermal plasma is rather high, the precursor should contain higher boron content. As the fraction of boron in the precursor increases, this would improve the efficiency of the process.

In thermal plasma processing, the desired products are obtained during the cooling of reactants from very high temperatures. This fact could allow design of experiments with improved the synthesis of boron carbide. When looked generally it may be stated that the system is uniform at very high temperatures with gaseous mixtures, and as the cooling proceeds the stability of phases change depending on the temperatures. The system is differentiated when a condense phase is formed. The formation of a first condense phase (in our cases B_4C) removes a certain fraction of material from gas cloud, altering the thermodynamic conditions. Therefore, perhaps it would be useful first to look at B_4C where it forms below that point the reading of the thermodynamic graphs becomes difficult. In the experiment with TMB-M- DIPA with 5 slpm N_2, we obtained almost pure B_4C despite the fact that at slightly lower temperature there was a very wide range of boron nitride phase. The formation of the boron carbide at slightly elevated temperature probably changes the system dynamics.

CHAPTER 5

CONCLUSION

Radio frequency inductively coupled plasma system was used to synthesize boron carbide nanoparticles so as to improve its sinter ability. Different precursors were considered and fed in solid and gas phase by means of injection probe and liquid phase via atomization probe.

For the solid precursors, two different B_2O_3 powders were used and the study showed the followings;

i. The experiments carried out with 45 mesh B_2O_3 powders with CH_4 was not successful as greater fraction of powders have passed through plasma without much evaporation and reaction.

ii. The use of 325 mesh B_2O_3 with CH_4 was more suitable as the fraction evaporated was quite high. This has yielded a product comprising B_2O_3 and B_4C. The fraction of B_4C was not more than 13 wt.%.

For the liquid precursor, azeotrope solution of Trimethyl borate-methanol (TMB-M) was used as a single source both boron for and carbon. This was fed into plasma in gas phase which showed that

iii. Pure boron carbide particles can be successfully synthesized with TMB-M which would yield B_2O_3 and B_4C, the former phase can be removed by methanol-wash. The average size of particles based on BET measurement was 31 nm.

iv. Hexane was added to TMB-M as an additional source of carbon but this has incorporated carbon as an additional phase in the synthesized product and therefore was not a useful additive.

For the liquid precursor, the addition of diisopropylamine (DIPA) instead of hexane into TMB-M was considered since nitrogen in the precursor would tie up oxygen by forming NO_x releasing B and C for B_4C formation;

v. The use of DIPA as additive was quite successful as it increased boron carbide conversion efficiency by suppressing B_2O_3 formation. Boron carbide had an average particle size of 61 ± 5.7 nm.

vi. The use of DIPA together with nitrogen gas added to TMB-M further improved the synthesis. The flow rates of TMB-M-17 ml DIPA with 12 ml/min and N_2 5 slpm with R.F. plasma operated at 25 kW power yielded 69.64 wt.% B_4C, 23.94 wt.% B_2O_3 and 6.42 wt.% carbon. After methanol wash, the fractions were 91.33 wt.% B_4C and 8.67 wt.%C.

It should be mentioned that 91 wt.% B_4C and 9 wt.%C is sinterable composition, carbon acting as a sintering aid. It might also be added that with DIPA and nitrogen, B_4C has a mean particle size of 51 ± 2.2 nm which should be rather easy to sinter at a temperature as low as $1200^{O}C$ with spark plasma sintering process.

REFERENCES

Aktekin, B. (2013). Induction Plasma Synthesis of Mg-Ni Nanoparticles. Middle East Technical University.

Alizadeh, A., Taheri-nassaj, E., and Ehsani, N. (2004). Synthesis of boron carbide powder by a carbothermic reduction method, *24*, 3227–3234.

Alkan, M., Sonmez, M. S., Derin, B., and Yücel, O. (2012). Effect of initial composition on boron carbide production by SHS process followed by acid leaching. *Solid State Sciences*, *14*(11–12), 1688–1691.

Asgarian, P., Nourbakhsh, A., Amin, P., Ebrahimi-kahrizsangi, R., and Mackenzie, K. J. D. (2014). The effect of different sources of porous carbon on the synthesis of nanostructured boron carbide by magnesiothermic reduction. *Ceramics International*, *40*(10), 16399–16408.

Bai, L., Fan, J., Hu, P., Yuan, F., Li, J., and Tang, Q. (2009). RF plasma synthesis of nickel nanopowders via hydrogen reduction of nickel hydroxide/carbonate. *Journal of Alloys and Compounds*, *481*(1–2), 563–567.

Bale, C. W., and Bélisle, E. (2016). Fact-Web suite of interactive programs, www.factsage.com.

Bapat, A., Gatti, M., Ding, Y.-P., Campbell, S. A., and Kortshagen, U. (2007). A plasma process for the synthesis of cubic-shaped silicon nanocrystals for nanoelectronic devices. *Journal of Physics D: Applied Physics*, *40*(8), 2247.

Bernardi, D., Colombo, V., Ghedini, E., and Mentrelli, A. (2003). Three-dimensional effects in the modelling of ICPTs. *The European Physical Journal D-Atomic, Molecular, Optical and Plasma Physics*, *25*(3), 271–277.

Boulos, M. I., Fauchais, P. L., and Pfender, E. (2017). *Handbook of Thermal Plasmas*.

Bourdeau, R. G. (1967). *US3334967 (A). Process of preparing boron carbide from boron halide and a hydrocarbon*. Union Carbide Corporation.

Campbell, C. T., Parker, S. C., and Starr, D. E. (2002). The effect of size-dependent nanoparticle energetics on catalyst sintering. *Science*, *298*(5594), 811–814.

Castillo, I. A., and Munz, R. J. (2005). Inductively coupled plasma synthesis of CeO 2-based powders from liquid solutions for SOFC electrolytes. *Plasma Chemistry and Plasma Processing*, *25*(2), 87–107.

Castillo, I. A., and Munz, R. J. (2007). New In-situ Sampling and Analysis of the Production of CeO 2 Powders from Liquid Precursors using a Novel Wet Collection System in a rf Inductively Coupled Thermal Plasma Reactor. Part 1: Reactor System and Sampling Probe. *Plasma Chemistry and Plasma Processing*, *27*(6), 737–759.

Chen, I.-W., and Wang, X.-H. (2000). Sintering dense nanocrystalline ceramics without final-stage grain growth. *Nature*, *404*, 168.

Cho, N. (2006). *Processing of boron carbide*. Georgia Institute of Technology.

Choi, S., Lapitan Jr, L. D. S., Cheng, Y., and Watanabe, T. (2014). Synthesis of cobalt boride nanoparticles using RF thermal plasma. *Advanced Powder Technology*, *25*(1), 365–371.

Cihangir, S., Ergun, C., Yılmaz, S., and Şahin, F. Ç. (2009). Synthesis of B4C/SiC composite from sugar based precursor. In *Defect and Diffusion Forum* (Vol. 283, pp. 268–272). Trans Tech Publ.

Clifton, R. (1970). *US3525589 (A). Production of Boron Carbide Whiskers*. Interior USA.

Colombo, V., Ghedini, E., Gherardi, M., and Sanibondi, P. (2013). Evaluation of precursor evaporation in Si nanoparticle synthesis by inductively coupled thermal plasmas. *Plasma Sources Science and Technology*, *22*(3), 35010.

Colombo, V., Ghedini, E., and Sanibondi, P. (2010). A three-dimensional investigation of the effects of excitation frequency and sheath gas mixing in an atmospheric-pressure inductively coupled plasma system. *Journal of Physics D: Applied Physics*, *43*(10), 105202.

Dacic, B. Z., Jokanović, V., Jokanović, B., and Dramićanin, M. D. (2006). Thermodynamics of gas phase carbothermic reduction of boron-anhydride. *Journal of Alloys and Compounds*, *413*(1), 198–205.

Dai Zhen, C. Y., Chaoyang, M., Fei, T., Jiantao, Z., Wenchao, W., Du Miaomiao, L. J., and Xuanyi, Y. (2017). Effect of Main Operating Parameters on Al2O3 Spheroidiza-tion by Radio Frequency Plasma System. *Rare Metal Materials and Engineering*, *46*(2).

Dhamale, Mathe, Bhoraskar, Sahasrabudhe, Dhole, and Ghorui. (2016). Synthesis and characterization of Nd 2 O 3 nanoparticles in a radiofrequency thermal plasma reactor. *Nanotechnology*, *27*(8), 85603.

Ditter, J. F., Gerhart, F. J., and Williams, R. E. (1977). *US4017587 (A). Boron carbide*. The United States of America as Represented by the Secretary of the Navy.

Dole, L. S., and Prochazka, S. (1985). Densification and Microstructure Development in Boron Carbide. *Proceedings of the 9th Annual Conference on Composites and Advanced Ceramic Materials: Ceramic Engineering and Science Proceedings*, 1151–1160.

Dole, L. S., Prochazka, S., and Doremus, H. R. (1989). Microstructural Coarsening During Sintering of Boron Carbide. *Journal of the American Ceramic Society*, *72*(6), 958–966.

Domnich, V., Reynaud, S., Haber, R. A., and Chhowalla, M. (2011). Boron carbide: Structure, properties, and stability under stress. *Journal of the American Ceramic Society*, *94*(11), 3605–3628.

Du, S. W., Tok, A. L. Y., and Boey, F. Y. C. (2008). RF plasma synthesis of boron carbide nanoparticles. In *Solid State Phenomena* (Vol. 136, pp. 23–38). Trans Tech Publ.

Evans, J. (2014). *Pressureless Sintering of Boron Carbide*. Imperial College of London.

Fang, Z. Z., and Wang, H. (2008). Densification and grain growth during sintering of nanosized particles. *International Materials Reviews*, *53*(6), 326–352.

Fang, Z. Z., Wang, H., and Kumar, V. (2017). Coarsening, densification, and grain growth during sintering of nano-sized powders—A perspective. *International Journal of Refractory Metals and Hard Materials*, *62*, 110–117.

Farzaneh, F., Golestanifard, F., Sheikhaleslami, M. S., and Nourbakhsh, A. A. (2015). New route for preparing nanosized boron carbide powder via magnesiothermic reduction using mesoporous carbon. *Ceramics International*, *41*(10, Part A), 13658–13662.

Fauchais, P. L., Heberlein, J. V. R., and Boulos, M. I. (2014). Thermal spray fundamentals: From powder to part. In *Thermal Spray Fundamentals: From Powder to Part* (pp. 39–40).

Ghosh, D., Subhash, G., Tirumalai, S., S., Radhakrishnan, R., and Xin-Lin, G. (2007). Dynamic Indentation Response of Fine-Grained Boron Carbide. *Journal of the American Ceramic Society*, *90*(6), 1850–1857.

Goller, G., Toy, C., Tekin, A., and Gupta, C. K. (1996). The production of boron carbide by carbothermic reduction. *High Temperature Materials and Processes*, *15*(1–2), 117–122.

Goortani, B. M., Mendoza, N., and Proulx, P. (2006). Synthesis of SiO2 nanoparticles in RF plasma reactors: Effect of feed rate and quench gas injection. *International Journal of Chemical Reactor Engineering*, *4*(1).

Gray, E. G. (1958). *US2834651 (A). Process for the production of boron carbide*.

Gu, Y., Chen, L., Qian, Y., Zhang, W., and Ma, J. (2005). Synthesis of nanocrystalline boron carbide via a solvothermal reduction of CCl4 in the presence of amorphous boron powder. *Journal of the American Ceramic Society*, *88*(1), 225–227.

Hales, S., A. Alexa, J., J. Jensen, B., and L. Thomsen, D. (2016). *Radio frequency plasma synthesis of boron nitride nanotubes (BNNTs) for structural applications: Part I*. Virginia.

Harris, G. L., and Parsons, D. S. (1975). *US3885022 (A). Method of producing boron carbide from water-alcohol solution of carbon source*. Gte Sylvania Incorporated.

Heian, E. M., Khalsa, S. K., Lee, J. W., Munir, Z. A., Yamamoto, T., and Ohyanagi, M. (2004). Synthesis of Dense, High-Defect-Concentration B4C through Mechanical Activation and Field-Assisted Combustion. *Journal of the American Ceramic Society*, *87*(5), 779–783.

Henne, R. (1999). Thermal plasmas for material processing. *Contributions to Plasma Physics*, *39*(5), 385–397.

Herth, S., Joost, W. J., Doremus, R. H., and Siegel, R. W. (2006). New approach to the synthesis of nanocrystalline boron carbide. *Journal of Nanoscience and Nanotechnology*, *6*(4), 954–959.

Hou, G., Cheng, B., Ding, F., Yao, M., Hu, P., and Yuan, F. (2015). Synthesis of Uniform α-Si3N4 Nanospheres by RF Induction Thermal Plasma and Their Application in High Thermal Conductive Nanocomposites. *ACS Applied Materials & Interfaces*, *7*(4), 2873–2881.

Hung, C.-H., and Vanier, N. R. (2010). *US2010003180 (A1). Production of Ultrafine Boron Carbide Particles Utilizing Liquid Feed Materials*. Ppg Industries Ohio, Inc.

Ishigaki, T., Oh, S.-M., Li, J.-G., and Park, D.-W. (2005). Controlling the synthesis of TaC nanopowders by injecting liquid precursor into RF induction plasma. *Science and Technology of Advanced Materials*, *6*(2), 111.

Jazirehpour, M., and Alizadeh, A. (2009). Synthesis of Boron Carbide Core−Shell Nanorods and a Qualitative Model To Explain Formation of Rough Shell Nanorods. *The Journal of Physical Chemistry C*, *113*(5), 1657–1661.

Jianxin, D. (2005). Erosion wear of boron carbide ceramic nozzles by abrasive air-jets. *Materials Science and Engineering: A*, *408*(1–2), 227–233.

Jiayin, G., Gitzhofer, F., and Boulos, M. (1997). *Effects of Process Parameters on Ultrafine SiC Synthesis Using Induction Plasmas*. *Plasma Chemistry and Plasma Processing* (Vol. 17).

Jiayin, G., Xiaobao, F., Dolbec, R., Siwen, X., Jurewicz, J., and Boulos, M. (2010). Development of Nanopowder Synthesis Using Induction Plasma. *Plasma Science and Technology*, *12*(2), 188–199.

Karaman, M., Sezgi, N. A., Doğu, T., and Özbelge, H. Ö. (2006). Kinetic investigation of chemical vapor deposition of B4C on tungsten substrate. *AIChE Journal*, *52*(12), 4161–4166.

Kenjiro, Y. (1996). Boron Carbide Particles Formed from an Amorphous Boron/Graphite Powder Mixture Using a Shock-Wave Technique. *Journal of the American Ceramic Society*, *79*(4), 1113–1116.

Khanra, A. K., and Godkhindi, M. M. (2005). Synthesis of boron carbide by self-propagating high temperature synthesis. *Journal of the Australasian Ceramic Society*, *41*(1), 30–35.

Kim, K.-I., Choi, S.-C., Kim, J.-H., Cho, W.-S., Hwang, K.-T., and Han, K.-S. (2014). Synthesis and characterization of high-purity aluminum nitride nanopowder by RF induction thermal plasma. *Ceramics International*, *40*(6), 8117–8123.

Kim, K. S., Couillard, M., Shin, H., Plunkett, M., Ruth, D., Kingston, C. T., and Simard, B. (2018). Role of Hydrogen in High-Yield Growth of Boron Nitride Nanotubes at Atmospheric Pressure by Induction Thermal Plasma. *ACS Nano*, *12*(1), 884–893.

Kim, K. S., Kingston, C. T., Hrdina, A., Jakubinek, M. B., Guan, J., Plunkett, M., and Simard, B. (2014). Hydrogen-Catalyzed, Pilot-Scale Production of Small-Diameter Boron Nitride Nanotubes and Their Macroscopic Assemblies. *ACS Nano*, *8*(6), 6211–6220.

Kim, K. S., Moradian, A., Mostaghimi, J., and Soucy, G. (2010). *Modeling of Induction Plasma Process for Fullerene Synthesis: Effect of Plasma Gas Composition and Operating Pressure*. *Plasma Chemistry and Plasma Processing* (Vol. 30).

Kobayashi, N., Kawakami, Y., Kamada, K., Li, J.-G., Ye, R., Watanabe, T., and Ishigaki, T. (2008). Spherical submicron-size copper powders coagulated from a vapor phase in RF induction thermal plasma. *Thin Solid Films*, *516*(13), 4402–4406.

Kovalev, I. D., Ponomarev, V. I., Konovalikhin, S. V, Kovalev, D. Y., and Vershinnikov, V. I. (2015). SHS of Boron Carbide : Influence of Combustion Temperature, *24*(1), 33–37.

Kumar, V., Fang, Z. Z., and Fife, P. C. (2010). Phase field simulations of grain growth during sintering of two unequal-sized particles. *Materials Science and Engineering: A*, *528*(1), 254–259.

Lang, J., Kling, R., Brachhold, H., Müller, R., and Pross, G. (2015). Plasma Reactions. In *Ullmann's Encylopedia of Industrial Chemistry* (pp. 1–22). Wiley-VCH.

Larker, H. T. (1983). Hot Isostatic Pressing of Ceramics. In F. L. Riley (Ed.), *Progress in Nitrogen Ceramics* (pp. 717–724). Dordrecht: Springer Netherlands.

Larsson, P., Axén, N., and Hogmark, S. (2000). Improvements of the microstructure and erosion resistance of boron carbide with additives. *Journal of Materials Science*, *35*(14), 3433–3440.

Lee, H., and Speyer, R. F. (2010). Pressureless Sintering of Boron Carbide, *73*(187676), 1468–1473.

Leparoux, M., Schreuders, C., Shin, J., and Siegmann, S. (2005). Induction Plasma Synthesis of Carbide Nano-Powders. *Advanced Engineering Materials*, *7*(5), 349–353.

Li-Hong, B., Chen, L., Yuan, T., Ji-Fa, T., Chao, H., Xing-Jun, W., … Hong-Jun, G. (2008). Synthesis and photoluminescence property of boron carbide nanowires. *Chinese Physics B*, *17*(12), 4585.

Lutterotti, L. (2000). Maud: a Rietveld analysis program designed for the internet and experiment integration. *Acta Crystallographica*.

Ma, R., and Bando, Y. (2002). High purity single crystalline boron carbide nanowires. *Chemical Physics Letters*, *364*(3), 314–317.

Marion, F., Munz, R. J., Dolbec, R., Xue, S., and Boulos, M. I. (2009). Effect of Plasma Power and Precursor Size Distribution on Alumina Nanoparticles Produced in an Inductively Coupled Plasma (ICP) Reactor. *Ispc_19*, (March 2015).

Mauer, G., Vaßen, R., and Stöver, D. (2011). Plasma and Particle Temperature Measurements in Thermal Spray: Approaches and Applications. *Journal of Thermal Spray Technology*, *20*(3), 391–406.

Mondal, S., and Banthia, A. K. (2005). Low-temperature synthetic route for boron carbide. *Journal of the European Ceramic Society*, *25*(2–3 SPEC. ISS.), 287–291.

Mostaghimi, J., and Boulos, M. I. (1990). Effect of frequency on local thermodynamic equilibrium conditions in an inductively coupled argon plasma at atmospheric pressure. *Journal of Applied Physics*, *68*(6), 2643–2648.

Muta, A., Gejo, T., and Shiozawa, M. (1967). Method for producing boron carbide. Kabushiki Kaisha Hitachi Seisakusho.

Nair, K. U., Bose, D. K., and Gupta, C. K. (1992). The production of elemental boron by fused salt electrolysis. , 9(1-4), 283-291. *Mineral Procesing and Extractive Metallurgy Review*, *9*(1–4), 283–291.

Najafi, A., Golestani-Fard, F., Rezaie, H. R., and Ehsani, N. (2012). A novel route to obtain B4C nano powder via sol–gel method. *Ceramics International*, *38*(5), 3583–3589.

Oh, S.-M., and Ishigaki, T. (2004). Preparation of pure rutile and anatase TiO2 nanopowders using RF thermal plasma. *Thin Solid Films*, *457*(1), 186–191.

Ohno, S., and Uda, M. (1984). Generation Rate of Ultrafine Metal Particles in “Hydrogen Plasma-Metal” Reaction. *Journal of the Japan Institute of Metals*, *48*(6), 640–646.

Ostrikov, K., and Murphy, A. B. (2007). Plasma-aided nanofabrication: where is the cutting edge? *Journal of Physics D: Applied Physics*, *40*(8), 2223.

Pan, J. (2004). Solid-state diffusion under a large driving force and the sintering of nanosized particles. *Philosophical Magazine Letters*, *84*(5), 303–310.

Park, J. H., and Hong, S. H. (1997). Optimization analysis of an inductively coupled plasma torch for material processing by using local thermal equilibrium numerical models. *Journal of the Korean Physical Society*, *31*(5), 753–763.

Pierson, H. O. (1996). *Handbook of refractory carbides and nitrides: properties, characteristics, processing and applications*. William Andrew.

Poole, J. W., Freeman, M. P., Doak, K. W., and Thorpe, M. L. (1973). *Simulator Test to Study Hot-Flow Problems Related to a Gas Cooled Reactor*. Washington.

Pristavita, R., Mendoza-Gonzalez, N.-Y., Meunier, J.-L., and Berk, D. (2011). Carbon nanoparticle production by inductively coupled thermal plasmas: controlling the thermal history of particle nucleation. *Plasma Chemistry and Plasma Processing*, *31*(6), 851–866.

Punjabi-Vinoth, S., Joshi, N. K., Mangalvedekar, H., Lande, B., Das, A., and Kothari, D. C. (2012). *A comprehensive study of different gases in inductively coupled plasma torch operating at one atmosphere Related Articles A comprehensive study of different gases in inductively coupled plasma torch operating at one atmosphere*. *Physics of Plasmas* (Vol. 19).

Rafi-ud-din, Zahid, G. H., Asghar, Z., Maqbool, M., Ahmad, E., Azhar, T., … Shahzad, M. (2014). Ethylene glycol assisted low-temperature synthesis of boron carbide powder from borate citrate precursors. *Journal of Asian Ceramic Societies*, *2*(3), 268–274.

Rahmane, M., Soucy, G., and Boulos, M. I. (1995). Diffusion phenomena of a cold gas in a thermal plasma stream. *Plasma Chemistry and Plasma Processing*, *16*(1), S169–S189.

Ramachandran, M., and Reddy, R. G. (2013). Thermal plasma synthesis of SiC. *Advances in Manufacturing*, *1*(1), 50–61.

Ramos, A. S., Taguchi, S. P., Ramos, E. C. T., and Arantes, V. L. (2006). High-energy ball milling of powder B – C mixtures, *422*, 184–188.

Ridgway, R. R. (1934). Boron Carbide A New Crystalline Abrasive and Wear-Resisting Product. *Transactions of The Electrochemical Society*, *66*(1), 117–133.

Ridgway, R. R., and Bailey, B. L. (1936). *US2027786 (A). Method of making boron carbide articles*. Norton Company.

Rietveld, H. M. (1969). A profile refinement method for nuclear and magnetic structures. *Journal of Applied Crystallography*.

Sairam, K., Sonber, J. K., Murthy, T. S. R. C., Subramanian, C., Fotedar, R. K., Nanekar, P., and Hubli, R. C. (2014). Influence of spark plasma sintering parameters on densification and mechanical properties of boron carbide. *International Journal of Refractory Metals and Hard Materials*, *42*, 185–192.

Samuel, K., and Frank, S. (1955). *A Method for Determining the Composition of Methanol - Trimethyl Borate Mixtures*. Washington.

Schouler, M. C., Cheynet, M. C., Sestier, K., Garden, J., and Gadelle, P. (1997). New Filamentous Deposition in the Boron-Carbon System. *Carbon*, *35*(7), 993–1000.

Schroll, F., and Vogt, A. (1939). *US2163293 (A). Electrothermic production of boron carbide*. Dr. Alexander Wacker Gesellschaft Fur Elektrochemische Industrie, G.m.b.h.

Schwetz, K. A., and Grellner, W. (1981). The influence of carbon on the microstructure and mechanical properties of sintered boron carbide. *Journal of the Less Common Metals*, *82*, 37–47.

Schwetz, K. A., Sigl, L. S., and Pfau, L. (1997). Mechanical Properties of Injection Molded B4C–C Ceramics. *Journal of Solid State Chemistry*, *133*(1), 68–76.

Scott, J. J. (1964). *US3161471 (A). Arc furnace process for the production of boron carbide*. Norton Company.

Seo, J., and Hong, B. (2012). Thermal Plasma Synthesis of Nano-sized powders, *44*(1).

Shi, J.-L., Deguchi, Y., and Sakabe, Y. (2005). Relation between grain growth, densification and surface diffusion in solid state sintering—a direct observation. *Journal of Materials Science*, *40*(21), 5711–5719.

Shi, L., Gu, Y., Chen, L., Qian, Y., Yang, Z., and Ma, J. (2003). A low temperature synthesis of crystalline B4C ultrafine powders. *Solid State Communications*, *128*(1), 5–7.

Shi, X., Cao, J., Li, Z., and Yan, D. (2015). Effect of the Addition of Carbon on the Sintering Properties of Boron Carbide Ceramics Prepared by Pressureless Sintering.

Shu-Fang, M., Jian, L., Jun-Fu, Z., Xiao-Xia, S., and Bing-She, X. (2009). Effect on graphite substrate to formation of boron carbide/carbon composite nanoropes. *Chinese Journal of Inorganic Chemistry*, *25*(6), 1050–1054.

Sigl, L. (1998). Processing and mechanical properties of boron carbide sintered with TiC. *Journal of the European Ceramic Society*, *18*(11), 1521–1529.

Silver, K. G. (2007). Processing of nano-sized boron carbide powder. Georgia Institute of Technology.

Singh, P., Singh, B., Kumar, M., and Kumar, A. (2014). One step reduction of Boric Acid to boron carbide nanoparticles. *Ceramics International*, *40*(9), 15331–15334.

Sinha, A., Mahata, T., and Sharma, B. P. (2002). Carbothermal route for preparation of boron carbide powder from boric acid-citric acid gel precursor. *Journal of Nuclear Materials*, *301*(2–3), 165–169.

Soucy, G., Rahmane, M., Fan, X., and Ishigaki, T. (2001). Heat and mass transfer during in-flight nitridation of molybdenum disilicide powder in an induction plasma reactor. *Materials Science and Engineering: A*, *300*(1–2), 226–234.

Spohn, M. T. (1993). ANNUAL MINERALS REVIEW. BORON CARBIDE. *American Ceramic Society Bulletin*, *72*(6), 88–89.

Stein, H., Aselage, T., and Emin, D. (1991). Infrared absorption in boron carbides: Dependence on isotopes and carbon concentration. In *AIP Conference Proceedings* (Vol. 231, pp. 322–325). AIP.

Subramanian, C., and Suri, A. K. (2004). Development of boron based neutron absorber materials. *Met Mater Process*, *16*(1), 39–52.

Suri, A. K., Subramanian, C., Sonber, J. K., and Murthy, T. S. R. C. (2010). Synthesis and consolidation of boron carbide: a review. *International Materials Reviews*, *55*(1), 4–40.

Szépvölgyi, J., Marković, Z., Todorović-Marković, B., Nikolić, Z., Mohai, I., Farkas, Z., … Feil, S. (2006). *Effects of Precursors and Plasma Parameters on Fullerene Synthesis in RF Thermal Plasma Reactor*. *Plasma Chemistry and Plasma Processing* (Vol. 26).

Tanaka, T., Fan, X., Ishigaki, T., and Soucy, G. (1999). Compositional modification of boron carbide induced by induction plasma treatment. *Thin Solid Films*, *345*(1), 156–160.

Thakkar, N. R., and Reddy, R. G. (2014). Thermal Plasma Processing of Boron Carbide Fine Powders. In *Powder Materials: Current Research and Industrial Practices III* (pp. 47–60). Wiley-Blackwell.

Thevenot, F. (1991). A Review on Boron Carbide. *Key Engineering Materials*, *56–57*, 59–88.

Thévenot, F. (1990). Boron carbide—A comprehensive review. *Journal of the European Ceramic Society*, *6*(4), 205–225.

Tong, L., and Reddy, R. G. (2005). Synthesis of titanium carbide nano-powders by thermal plasma. *Scripta Materialia*, *52*(12), 1253–1258.

Uda, M., Ohno, S., and Hoshi, T. (1983). *US4376740. Process for Production Fine Metal Particles*. Japan.

Vanier, N. R., and Hung, C.-H. (2008). *US7438880B2. Production of High Purity Ultrafine Metal Carbide Particles*. Ppg Industries Ohio, Inc.

Venkatramani, N. (2002). Industrial plasma torches and applications. *Current Science*.

Verhoeven, J. D. (1975). *Fundamentals of physical metallurgy*. Wiley.

Wang, H., Zak Fang, Z., and Hwang, K. S. (2011). Kinetics of Initial Coarsening During Sintering of Nanosized Powders. *Metallurgical and Materials Transactions A*, *42*(11), 3534–3542.

Weimer, A. W. (1997). *Thermochemistry and kinetics. In Carbide, nitride and boride materials synthesis and processing*. London: Chapman & Hall.

Weimer, and Sotiris. (1976). Kinetics of Carbothermal Reduction Synthesis of Boron Carbide. *American Ceramic Society Bulletin*, (1), 2–7.

Widom, M., and Huhn, W. P. (2012). Prediction of orientational phase transition in boron carbide. *Solid State Sciences*, *14*(11–12), 1648–1652.

Xu, F.-F., and Bando, Y. (2004). Formation of two-dimensional nanomaterials of boron carbides. *The Journal of Physical Chemistry B*, *108*(23), 7651–7655.

Yang, D.-Y., Kim, Y., Hur, M., Lee, H. J., Kim, Y.-J., Lim, T.-S., … Yang, S. (2015). *Control of the Nano-Particle Weight Ratio in Stainless Steel Micro and Nano Powders by Radio Frequency Plasma Treatment*. *Metals* (Vol. 5).

Yang, W. Z., Huang, W. M., Zheng, Q., Huang, W., and Chen, Z. M. (2016). High Efficiency Preparation, Structure and Properties of Silicon Nano-Crystals by Induction Plasma Method. *NanoWorld J*, *2*(3), 63–68.

Yin, B., and Wang, L. (2003). Carbon-doping activated sintering of b4c powders obtained by jet milling. *Journal of Inorganic Materials*, *18*, 633–637.

Yin, B., and Wang, L. (2004). Study on mechanical strength of the hot-pressed sintered boron carbide ceramic. *Atomic Energy Science and Technology*, *38*(6), 522–525.

Yoo, S. H., Sethuram, M., and Sudarshan, S. (1999). *US5989487A. Apparatus for Bonding a Particle Material to Near Theoretical Density*.

Zeng, B., Feng, Z., Li, S., Liu, Y., Cheng, L., and Zhang, L. (2009). Microstructure and deposition mechanism of CVD amorphous boron carbide coatings deposited on SiC substrates at low temperature. *Ceramics International*, *35*(5), 1877–1882.

Zhai, W., Zhang, J., Sang, J., Cao, Z., and Liu, J. (2016). *CN105314636 (A). Method for preparing high-purity ultra-fine boron carbide powder from plasmas*. Dalian Jinma Boron Technology Group Co., Ltd.

Zhang, H., Bai, L., Hu, P., Yuan, F., and Li, J. (2012). Single-step pathway for the synthesis of tungsten nanosized powders by RF induction thermal plasma. *International Journal of Refractory Metals and Hard Materials*, *31*, 33–38.

Zielinski, J. M., and Kettle, L. (2013). Physical Characterization: Surface Area and Porosity. *No. April*, (April), 1–7.

APPENDIX

I. The Rietveld analysis of the experiment carried out with -45 mesh B_2O_3.

a. 0.35 CH_4 slpm (σ=1.63, R_w=7.95)

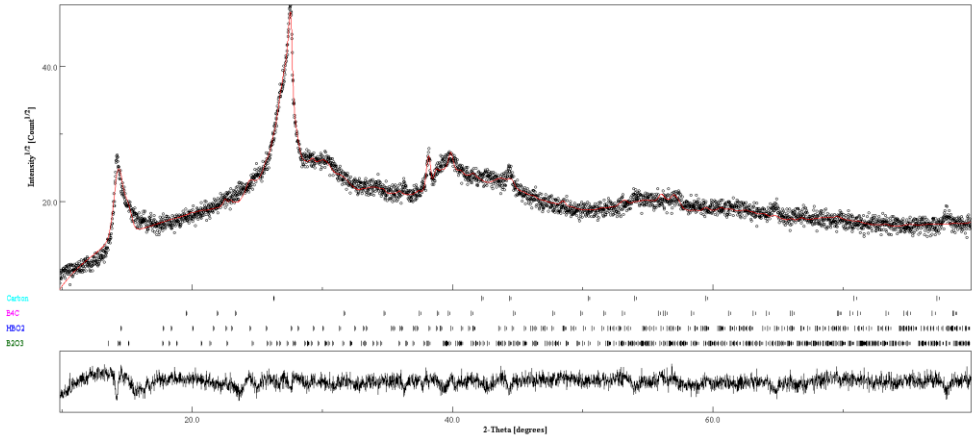

b. 1.4 CH_4 slpm (σ=1.67, R_w=9.65)

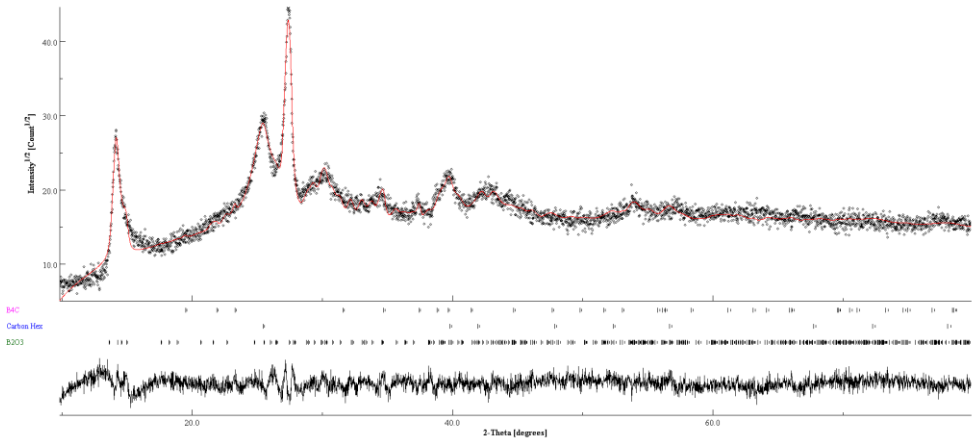

c. 2.5 CH_4 slpm (σ=1.73, R_w=10.5)

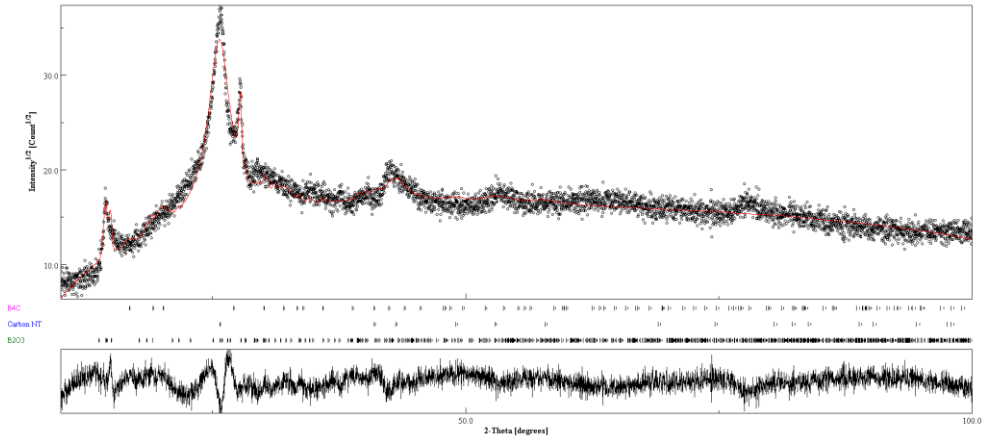

d. 3.6 CH_4 slpm (σ=1.82, R_w=10.34)

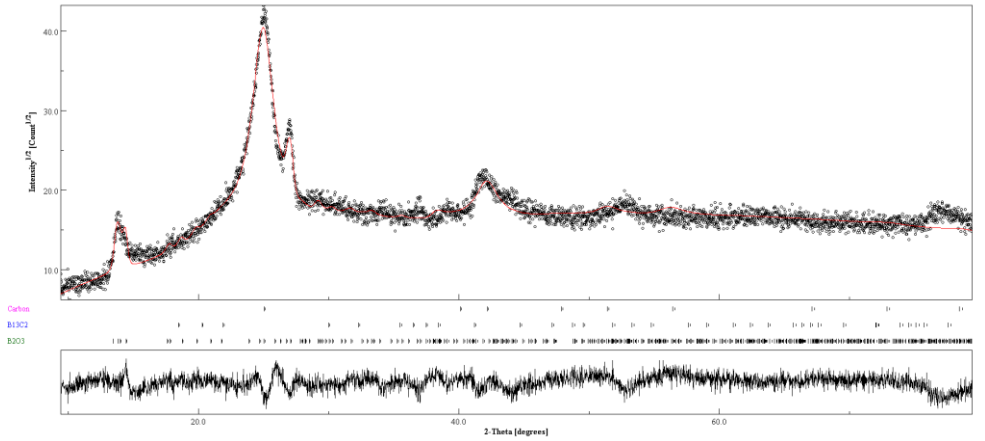

II. The Rietveld analysis of the experiment carried out with -325 mesh B_2O_3

a. 1 g/min B_2O_3 1.1 slpm CH_4 (σ=0.15, R_w=2.23)

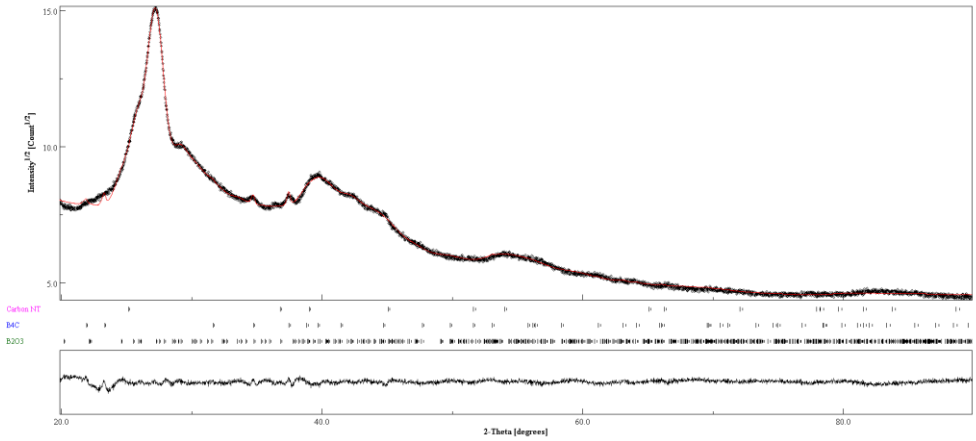

b. 1 g/min B_2O_3 1.5 slpm CH_4 (σ=0.32, R_w=4.29)

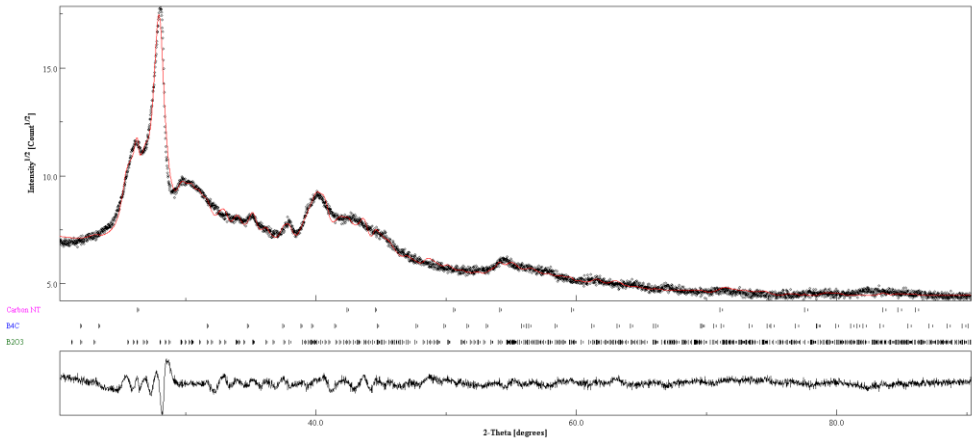

c. 1 g/min B_2O_3 2 slpm CH_4 (σ=0.42, R_w=5.2)

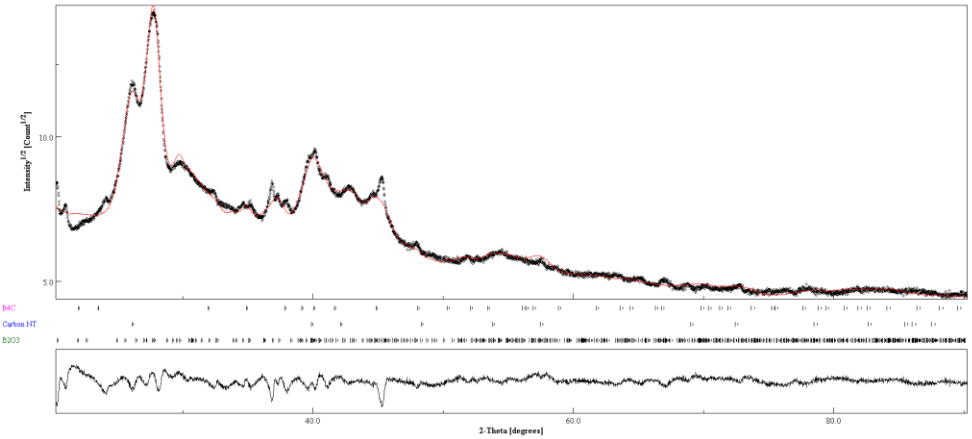

d. 2 g/min B_2O_3 1.5 slpm CH_4 (σ=0.35, R_w=5.95)

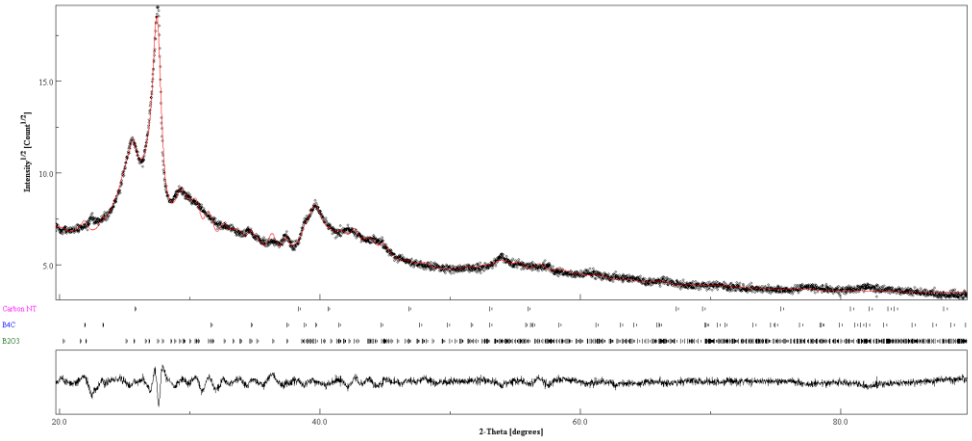

e. 2 g/min B_2O_3 2 slpm CH_4 (σ=0.39, R_w=6.01)

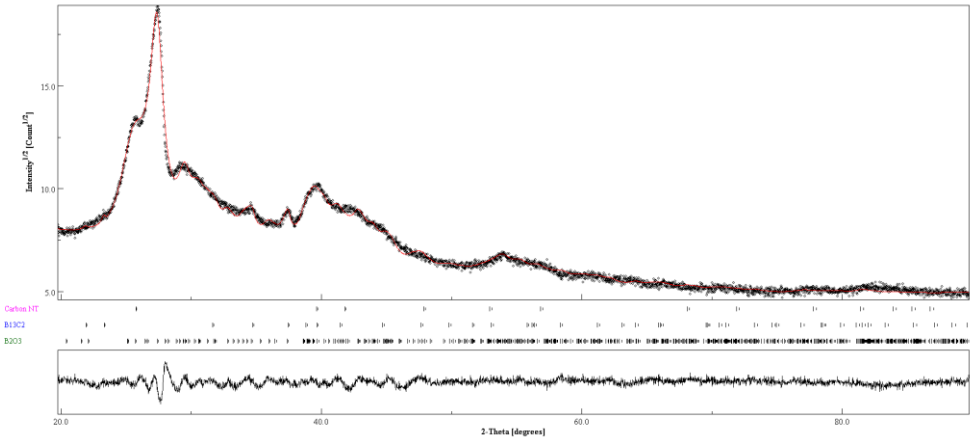

f. 2 g/min B_2O_3 2.2 slpm CH_4 (σ=0.46, R_w=6.32)

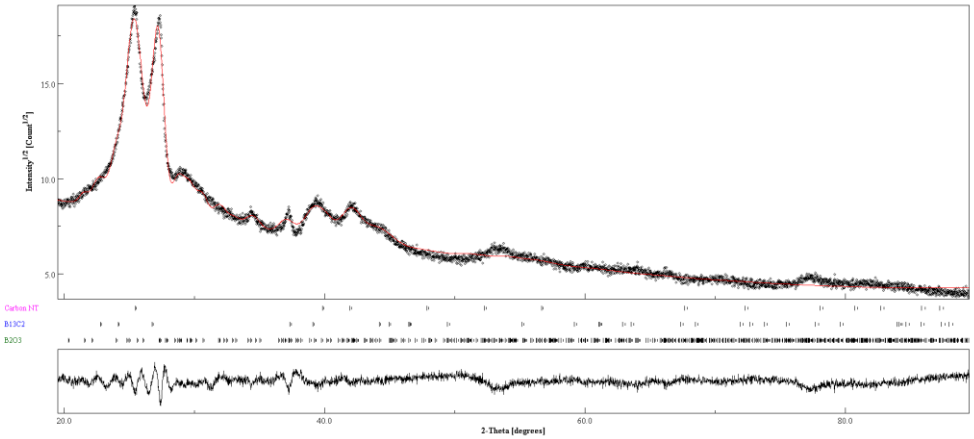

III. The Rietveld analysis of the experiment carried out with TMB-M

a. As-synthesized (σ=0.52, R_w=5.84)

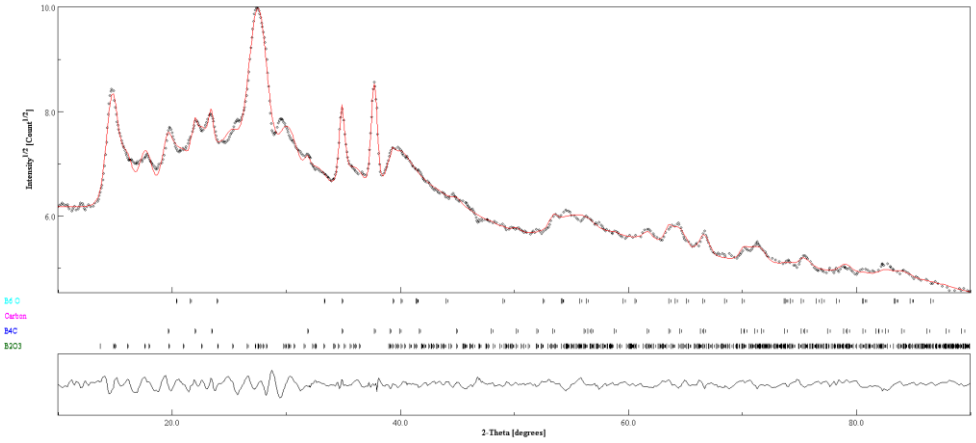

b. As-synthesized with 30 Hex (σ=0.71, R_w=7.1)

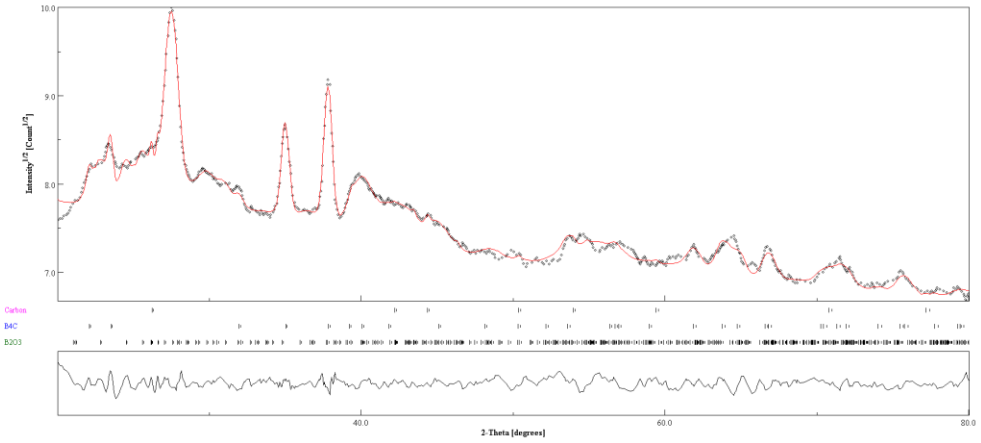

c. As-synthesized with 17 DIPA (σ=1.52, R_w=8.05)

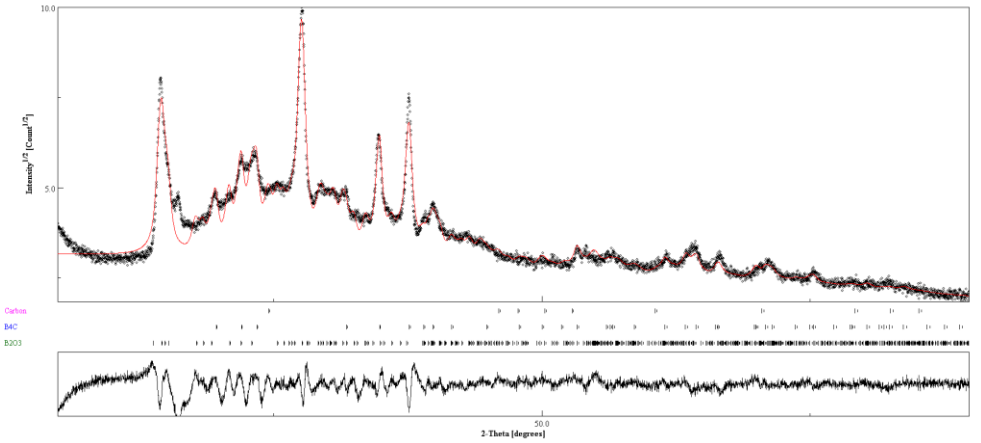

d. As-synthesized with 17 ml DIPA and 0.012 slpm N_2 (σ=0.46, R_w=10.06)

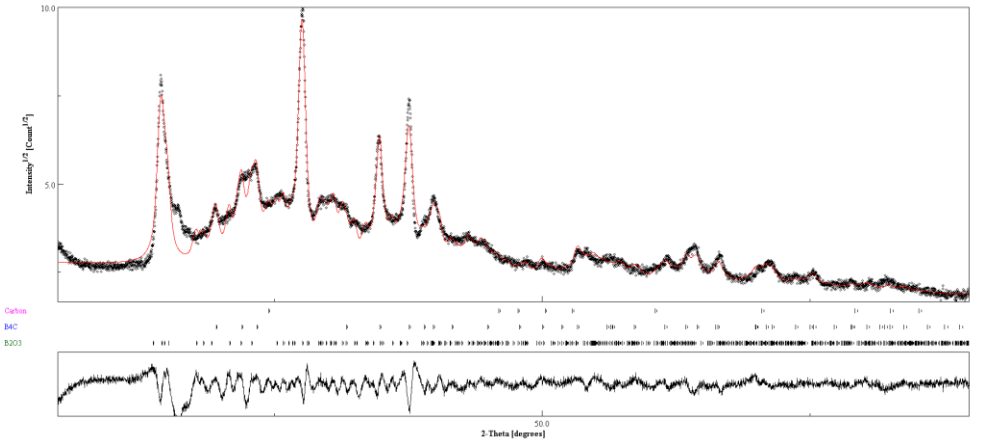

e. As-synthesized TMB-M with 17 ml DIPA and 5 slpm N_2 (σ=0.43, R_w=10.17)

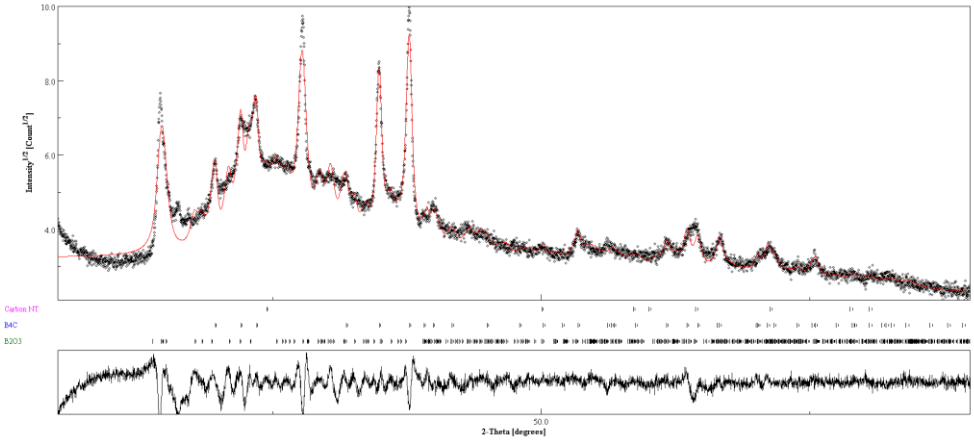

f. Methanol-washed with 17 ml DIPA and 5 slpm N_2 – methanol-washed (σ=0.37, R_w=6.03)